UNIVERSITY OF LATVIA
FACULTY OF CHEMISTRY

DOCTORAL THESIS

ELĪNA PAJUSTE

# TRITIUM BEHAVIOUR IN THE FUSION REACTOR MATERIALS

*Scientific supervisors*:
Dr. Chem. GUNTA ĶIZĀNE
Dr. Phys. J. PAUL COAD

Riga
2012

The doctoral thesis was carried out in the Laboratory of Radiation Chemistry of Solids of Institute of Chemical Physics and Faculty of Chemistry of the University of Latvia in period from 2007 to 2012.

Reviewers:

Dr.hab.chem. professor, **Valdis Kaļķis**

Dr.chem. asoc.professor, **Andris Actiņš**

Dr.chem. **Antonija Dindune**

Supervisors:

Dr. chem. **Gunta Ķizāne**

Dr. phys. professor **J. Paul Coad**

The thesis will be defended at the public session of the Doctoral committee of Chemistry, University of Latvia.

October 11, 2012

Faculty of Chemistry, University of Latvia

K. Valdemāra str. 48

The thesis is available at the Library of the University of Latvia, Kalpaka blvd. 4.

# ABSTRACT

**Tritium behaviour in fusion reactor materials**. Pajuste E., scientific supervisors Dr.chem., Ķizāne G., Dr. phys. Coad J.P. Doctoral thesis, 118 pages, 63 figures, 5 tables, 179 references, 1 appendix. In English.

NUCLEAR FUSION, TRITIUM, TRITIUM BREEDING BLANKET, BERYLLIUM, CARBON FIBRE COMPOSITE TILES, PLASMA FACING MATERIALS, DIFFUSION, MAGNETIC FIELD, IONIZING RADIATION.

Fusion reactor is very complex device and requires scrupulous selection of the materials to meet both technological and safety needs. These materials must resist the conditions of the reactor, at the same time perform their functions with high efficiency, retention of fusion fuel – radioactive hydrogen isotope tritium is also not acceptable.

The objective of this dissertation is to develop the knowledge base for fusion applications of two materials that are promising candidates for use in future fusion power reactors: beryllium and carbon fibre composites (CFC).

High radioactivity beryllium pebbles (neutron multiplayer) that have been exposed to neutron flux in the High Flux Reactor in Petten, the Netherlands, and carbon fibre composition tiles (plasma facing material) from the plasma chamber of the fusion device JET (Joint European Torus) in Culham, United Kingdom are analysed within this research.

Methods and techniques developed in the UL Institute of Chemical Physics Laboratory of Radiation Chemistry of Solids have been used in this study. Synergetic facilitating effect of accelerated electrons and high magnetic field on tritium release from materials has been found and its overall contribution estimated. Recommendations regarding the nuclear waste reduction based on the results on tritium behaviour studies have been provided.

# ANOTĀCIJA

**Tritija uzvedība kodolsintēzes reaktora materiālos**. Pajuste E., zinātniskie vadītāji Dr.ķīm. Ķizāne G., Dr. fiz. Coad J.P. Promocijas darbs. 118 lapaspuses 63 attēli, 5 tabulas, 179 literatūras atsauces, 1 pielikums. Angļu valodā.

KODOLSINTĒZE, TRITIJS, BERILIJS, OGLEKĻA KOMPOZĪTI, BLANKETA ZONA, PLASMAS KONTAKTMATERIĀLI, DIFŪZIJA, MAGNĒTISKAIS LAUKS, JONIZĒJOŠAIS STAROJUMS.

Viena no kodolsintēzes reaktora tehnoloģiskā risinājuma pamatproblēmām ir materiālu izvēle. Reaktora materiāliem jāspēj saglabāt savu funkciju izpilde reaktora darbības smagajos apstākļos, kā arī nav pieļaujama kodolsintēzes izejvielu uzkrāšanās materiālos, jo pretējā gadījumā tie būs pieskaitāmi radioaktīvajiem atkritumiem radioaktīvā ūdeņraža izotopa- tritija satura dēļ.

Disertācijas mērķis ir pilnveidot zināšanu bāzi par nākotnes kodolsintēzes enerģijas reaktoru divu daudzsološo materiālu - berilija un oglekļa šķiedru kompozītu, pielietojuma iespējām un ierobežojumiem.

Pētījumam izmantotas augstas radioaktivitātes berilija lodītes (reaktorā pilda neitronu pavairotāja funkciju), kas bijušas pakļautas neitronu starojumam Augstas plūsmas reaktorā (HFR) Pettenā, Nīderlandē, kā arī berilija un oglekļa šķiedru kompozītu ķieģeļi (plazmas kameras sienu aizsargmateriāls) no kodolsintēzes iekārtas JET (Joint European Toruss, Apvienotais Eiropas Torss) plazmas kameras Kalemā, Lielbritānijā.

Darbā izmantotas LU Ķīmiskās Fizikas Institūta Cietvielu Radiācijas Ķīmijas Laboratorijā izstrādātas metodes un iekārtas. Novērots sinerģētisks jonizējošā starojuma un magnētiskā lauka efekts tritija izdalīšanās veicināšanā un novērtēts tā kopējais ieguldījums. Balsoties uz iegūtajiem rezultātiem izstrādātas rekomendācijas attiecībā uz radioaktīvo atkritumu daudzuma mazināšanu kodolsintēzes reaktoros.

# CONTENTS

# ABBREVIATIONS

AEUL – Association EURATOM – University of Latvia

ANFIBE - ANalysis of Fusion Irradiated BEryllium

appm – atomic parts per million

CFC – Carbon Fibre Composite

CMT – Computer Aided Microtomography

DEMO – DEMOnstration reactor

dpa – displacement per atom

DTE-1 – First Deuterium Tritium Experiment

EURATOM – European Atomic Energy Community

EXOTIC – EXtraction Of Tritium In Ceramics

FRP – Fluoride Reduction Process

HCLL – Helium Cooled Liquid Lead

HCPB – Helium Cooled Pebble Bed

HFR – High Flux Reactor

HI – Hyperfine Interactions

HICU – High dose irradiation of Li-ceramic pebbles

HIDOBE – HIgh DOse irradiation of BEryllium

HIP – Hot Isostatic Pressing

IAEA – International Atomic Energy Agency

ICF – Inertial Confinement Fusion

IGA – Inert Gas Atomization

ILW – ITER Like Wall

ITER –International Thermonuclear Experimental Reactor

JET – Joint European Torus

LIBRETTO- Tritium production, extraction and release from liquid Pb-Li eutectic and tritium permeation under irradiation

M – Magnetic field

MCF – Magnetic Confinement Fusion

NIF – National Ignition Facility

PARIDE – Plasma facing material specimens, divertor and primary wall sub-assemblies

PBA – Pebble Bed Assembly

ppm – parts per million

PTE – Preliminary Tritium Experiment

R – Ionizing radiation

RAFM – Reduced Activation Ferritic Martensitic

REP – Rotating Electrode Process

SRP –Septum Replacement Plate

STP – Standard Temperature and Pressure

T – Temperature

TBM – Tritium Breeder Module

TDS – Thermo Desorption Spectra

TPD – Temperature programmed desorption

TTE – Trace Tritium experiment

WCSB – Water Cooled Solid Breeder

ZE – Zeeman Effect

# INTRODUCTION

Increasing energy demands, concerns over climate change and limited supplies of fossil fuels mean that the world needs to find new, ecologically safe and high efficiency energy source. Nuclear fusion of hydrogen isotopes, the process that powers the Sun, is one of the most perspective sources in the future that fulfils the condition described above. Research on solving fundamental and technological problems in development of fusion reactor is carried out worldwide.

Scientific organizations in Latvia are also taking part in this research since year 2000 and are coordinated by association AEUL (Association EURATOM – University of Latvia). Several organizations of the University of Latvia are included in this Association and among them - Laboratory of Radiation Chemistry of Solids of the Institute of Chemical Physics. This laboratory has carried out research on accumulation and release of tritium from fusion reactor blanket zone and plasma facing materials within frames of EURATOM.

Construction of the first experimental fusion reactor *ITER* has been commenced in Cadarache (France). *ITER* is a joint international research and development project that aims to demonstrate the scientific and technical feasibility of fusion power. The next step will be the demonstration reactor DEMO where energy will be obtained practically. Current expectations are that first industrial fusion reactors will be constructed in the years 2050 – 2060.

Fusion reactor is very complex device and requires scrupulous selection of the materials to meet both technological and safety needs. These materials must resist the conditions of the reactor; at the same time perform their functions with high efficiency. Retention of fusion fuel – radioactive hydrogen isotope tritium in these materials is also not acceptable. The majority of experimental systems in use up to now in the development of fusion have employed carbon as the plasma-facing material, either in the form of graphite tiles or CFC tiles for devices with higher power loads to the plasma-facing surfaces. The primary reasons for this are its durability under high thermal stress, and its low atomic number which limits the deleterious effects of atoms that may be eroded and enter the plasma. The other light metallic elements boron and beryllium are also used as additions to the plasma-facing surface and have been beneficial in controlling plasma density and stability, whilst beryllium has also been used for solid plasma-facing components in JET. The next generation experimental fusion device, ITER, plans to use both solid beryllium and CFC as plasma-facing components, and these materials are likely to continue as plasma-facing materials in the future development of power reactors. Beryllium, however will have an

additional new and crucially important role in the future. Fusion power reactors will have to breed tritium (probably by using the fusion reaction between lithium and neutrons) to provide fuel for the fusion process, in order to become self-sufficient in this scarce commodity: beryllium will be a key component of this breeding process as it is an extremely effective neutron multiplier.

**The objective** of this dissertation is to develop the knowledge base for fusion applications of two materials that are promising candidates for use in future fusion power reactors: beryllium and carbon fibre composites (CFC).

High radioactivity beryllium pebbles (neutron multiplayer) that have been exposed to neutron flux in the High Flux Reactor in Petten, Netherlands, beryllium and carbon fiber composition tiles (plasma facing material) from the plasma chamber of fusion device JET (Joint European Torus) in Culham, United Kingdom are analysed within this research.

The objectives of this dissertation are two-fold. Firstly, to pull together knowledge gained in other fields such as nuclear fission on neutron damage and on tritium retention in CFC and beryllium, especially on the very relevant experiences with beryllium pebbles used as neutron multipliers. Secondly, a programme of novel investigations and experiments has also been conducted that extend the knowledge of these materials under fusion power reactor relevant conditions, for example by studying the synergy of magnetic fields, fast electron bombardment and high temperature, and the results are described. Conclusions have then been drawn about the applicability of the materials for their fusion reactor roles.

**The tasks** carried out in the frameworks of this project are as follows:

- Develop and apply methods for tritium total amount, spatial distribution and chemical forms measurements in tritium containing materials;
- Estimate the role of the structure of the material and chemical impurities on tritium retention;
- Perform and analyze tritium thermal desorption experiments and estimate the role of the material properties and tritium initial chemical form on tritium desorption processes;
- Estimate effects of simultaneous and separate action of ionizing radiation and magnetic field on tritium desorption processes;
- Develop recommendations regarding the nuclear waste reduction based on the results on tritium behavior studies.

**Novelty:** Impact of ionizing radiation and magnetic field has been assessed on tritium containing materials regarding the problem of tritium retention. Tritium accumulation in structure and functional materials is limited to 350 g due to safety reasons. As soon as this limit will be reached reactor will be shut down for detritiation procedure. Many experiments have been performed worldwide for precise estimation of the tritium retention rates and most of the attention has been paid to the plasma facing materials and tritium breeding blanket materials since they will have either direct contact to tritium containing plasma or tritium will be produced within these materials (tritium breeder materials and neutron multipliers). Up to now there is no data on tritium behaviour under simultaneous action of ionizing radiation and magnetic field.

**Practical significance**: Although CFC and beryllium will have pivotal roles in the development of fusion power, the fusion community has no experience of these materials in the harsh environment that they will experience in a power reactor. Indeed, the database on beryllium is particularly sparse due to the hazardous nature of the material in some forms. Specifically, neutron damage will be many orders of magnitude greater than in any current fusion experiment, and there will also be synergistic effects of that damage with magnetic field, high temperature etc on tritium retention that have not be addressed by the fusion community heretofore. Results obtained in this work can be used to make corrections in tritium behaviour prediction and estimation of its overall retention in fusion devices as it provides information about tritium behaviour under simultaneous action of radiation and high magnetic field in beryllium and CFC materials. This study has been carried out within the EURATOM (European Atomic Energy Community) projects **JW10-FT-3.62 - EFDA Fusion Technology** "Post mortem analysis of tritium accumulated in selected plasma facing components", **TW5-TTBB-006-D08 - EFDA Fusion Technology "**Assessment of the effects of magnetic field, radiation and temperature on the tritium release from beryllium pebbles", **JW8-FT-1.12 "**Determination of tritium and analysis of carbon-based plasma-facing components before and after their detritiation with different methods", **JW6-FT-2.27 JET Task Fusion Technology "**Magnetic field effect on technologies for detritiation of beryllium materials" that demonstrates its scientific and practical relevance.

**Publicity:** Results of this research have been presented in 5 international conferences and 8 scientific papers have been published in international, cited journals.

**Acknowledgements:** I wish to express my sincere gratitude to my scientific supervisor Dr. chem. Gunta Kizane for guidance and support during these years. I would like to thank my

scientific supervisor Dr. phys. Paul Coad for introducing me to the tokamak science and supporting during my stay in Culham Science Center in 2010 as well as for the invaluable help with my first scientific manuscript. I wish to thank also Dr. chem. Aigars Vītiņš for performing technically sophisticated experiments to obtain tritium thermo desorption spectra that I have used in my work and for answering all my questions both scientific and technical. Many thanks to all my colleagues at Laboratory of Radiation Chemistry of Solids for always being there and supporting. I am also grateful to colleagues in Culham Science Centre and Karslruhe Institute of Technologies for advices and fruitful scientific discussions during my visits there.

My warm thanks go to my parents Valda and Antons and sister Agnese for supporting me for all the times. My special thanks go to my husband Kārlis and son Edvards for their love, patience and understanding.

In addition, I wish to thank those who may not find their names here, but who have contributed to this work.

This work has been financially supported by the European Social Fund within the project "Support for Doctoral Studies at University of Latvia" 2009/0138/IDP/1.1.2.1.2./09/IPIA/VIAA/004.

The support L'Oréal Latvian Fellowship for Women in Science 2010 with the support of the Latvian National Commission for UNESCO and the Latvian Academy of Sciences is also gratefully acknowledged.

# 1. LITERATURE REVIEW

## *1.1 Fusion Energy on Earth*

In 1920, British physicist and chemist F.W. Aston made an essential experimental observation that four hydrogen atoms are slightly heavier than one helium atom. Another British scientist, astrophysicist Sir A. Eddington immediately recognized importance of this discovery and realized that by converting hydrogen into helium the Sun releases about 0.7% of its mass into energy according to the famous Einstein's equation $E = mc^2$. In 1939, German physicist H. Bethe proposed a full quantitative theory explaining the generation of fusion energy in stars [1]. All these crucial discoveries led to an idea of controllable fusion energy here on Earth for practical purposes. Shortly after the World War II research in the field of fusion spread worldwide, but due to its military significance, most of experiments were secret. Situation changed in 1955 at the United Nations International Conference on the Peaceful Uses of Atomic Energy ("Atom for Peace") in Geneva where fusion research programs were declassified as secret and international scientific collaboration could be started. In Europe, associations were established between European Atomic Agency EURATOM and the scientific institutions of the member states.

Fusion reaction of hydrogen isotopes – deuterium $^2H$ and tritium $^3H$, is considered to be the most convenient for energy production due to its high energy yield (1.1)

$$^2H + ^3H \rightarrow ^4He + n + 17.6\ MeV \qquad 1.1$$

Deuterium is a stable isotope of hydrogen that can be extracted from sea water (its abundance is 0.0156% of all naturally occurring hydrogen) [2]. Whereas tritium is a radioactive isotope with relatively short half-life (12.3 years) and has to be produced artificially by interaction of neutrons with lithium isotopes, according to reactions (1.2, 1.3)

$$^6Li + n\ (thermal) \rightarrow ^4He + ^3H \qquad 940.4\ b \qquad 1.2$$

$$^7Li + n\ (E > 17MeV) \rightarrow ^3H + ^4He + n \qquad 0.026\ b \qquad 1.3$$

Tritium could be produced in reaction with $^6Li$ with low energy thermal neutrons, cross-section of the reaction - 940.4 barns. $^7Li$ can also take part in generation of tritium, but reaction requires neutrons with higher energy and its cross-section is considerably smaller - 0.3 barns [3].

For fusion reaction to occur the electrostatic repulsion between hydrogen isotopes must be overcome. In order to attain this, atoms must have a temperature of several tens of millions of degrees whereby they become completely ionized (turn into plasma state). In addition, sufficient density and energy confinement are required, as specified by the Lawson criterion [4]. Magnetic

confinement fusion (MCF) attempts to create the conditions needed for fusion energy production by using the electrical conductivity of the plasma to contain it with magnetic fields [5]. In 1968, at the third IAEA International Conference on Plasma Physics and Controlled Nuclear Fusion Research at Novosibirsk, Soviet scientists A. D. Sakharov and I. E. Tamm announced that they had achieved unprecedented results with a *tokamak*[1] magnetic confinement device with a special geometry in a shape of torus [6]. Nowadays, *tokamak*s are the dominant experimental technique for studying fusion. The largest present-day *tokamak* device, The Joint European Torus (JET), located near Oxford in United Kingdom, was put into operation in 1983 (more information in chapter 1.4) [7]. Nevertheless, another type of magnetic confinement device *stellarator* invented by American physicist L.Spitzer should also be mentioned since it is still considered as an alternative for a *tokamak* [8]. The largest *stellarator* device Wendelstein 7-X is currently under construction in Greifswald, Germany [9]. List of major toroidal confinement devices, their location, approximate years of operation and used materials can be found in the review article provided by G. Frederici et al [10].

Alternative technique to the magnetic confinement fusion (MCF) is an inertial confinement fusion (ICF) that is based on a process where nuclear fusion reactions are initiated by heating (usually by lasers) and compressing a fuel target, typically in the form of a pellet that contains a mixture of deuterium and tritium. The largest inertial confinement device National Ignition Facility (NDF) is located in Livermore, California (United States) and it was put into operation in 2009 [11].

Currently one of the World's most expensive scientific experimental devices – *tokamak* device *ITER* is already under construction in South of France. This will be followed by an exploitation phase lasting about 20 years, afterwards demonstration reactor DEMO will be built where energy will be obtained practically. Current expectations are that first industrial *tokamak* type fusion reactors will be constructed in the years 2050 – 2060 [12]. More detailed information is given in the following chapter 1.2.

Public acceptance of a new energy source is also an important problem and probably not less crucial than technological issues for its implementation in industry. Recent events in Japan (leakage of radioactive material from the Fukushima Daiichi power plant caused by the magnitude - 9 earthquake and following tsunami in March 2011) have made society more aware of everything related to the nuclear energy [13]. Estimation of the radioactive waste production

[1] *From Russian: **то**роидальная **ка**мера в **ма**гнитных **к**атушках*

and overall safety during the fusion reactor operation has been performed with a high accuracy. Main advantage of fusion energy is the total absence of high level radioactive spent fuel as produced in fission reactors [14]. As mentioned above the product of fusion reaction is inert helium gas. Nevertheless, some amount of radioactive materials will be produced as a result of neutron induced activation of structural materials and tritium inventory [15]. Therefore lot of effort is put to develop low-activation materials and methods for sufficient material detritiation (see chapter 1.7). Moreover, it must be mentioned that combustion of coal introduces more radioactive long living isotopes in the atmosphere than any nuclear facility if normalized to the energy output [16].

### *1.2 ITER and beyond*

*ITER* (International Thermonuclear Experimental Reactor) is a joint international research and development project that aims to demonstrate the scientific and technical feasibility of fusion power. It will be equipped with complete deuterium-tritium fuel cycle [17]. Its construction was begun in 2008 in Cadarache, France, whereas the first plasma is expected in 2018. The project's members are the European Union, Japan, China, the United States, South Korea, India and Russia. EU as a host party for ITER will contribute 45% of the cost, with the other parties contributing 9% each. The fusion reactor itself has been designed to produce 500 MW of output power for 50 MW of input power, or ten times the amount of energy put in. Hereby the machine is expected to demonstrate the principle of getting more energy out of the fusion process than is used to initiate it, something that has not been achieved with previous fusion reactors [12, 18].

Schematic view of ITER machine is demonstrated in Figure 1.1. Main components of a *tokamak* are magnets, vaccum vessel, blanket, divertor, diagnostics, external heating and cryostat. Also the external systems are of great importance – vaccum and cryogenics, remote handling, powere supply, hot cells, cooling water and tritium breding. Short description of each component of a *tokamak* taken from the official ITER web page (www.iter.org) is given below.

Magnet System comprises 18 superconducting Toroidal Field and 6 Poloidal Field coils, a Central Solenoid, and a set of Correction coils that magnetically confine, shape and control the plasma inside the Vacuum Vessel.

Vacuum Vessel is a hermetically-sealed steel container inside the Cryostat that houses the fusion reaction and acts as a first safety containment barrier. In its doughnut-shaped chamber, or torus, the plasma particles spiral around continuously without touching the walls.

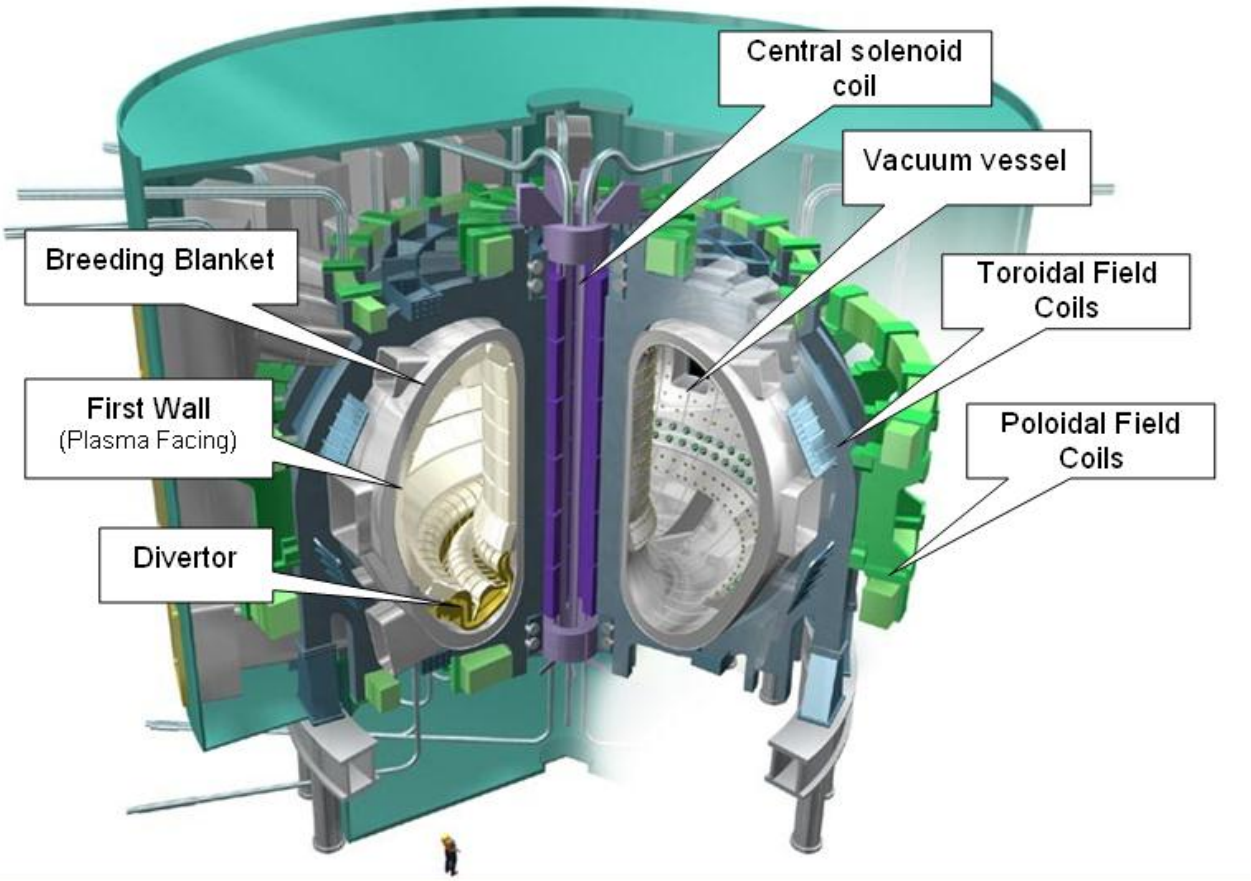


*Figure 1.1* **International Thermonuclear Experimental Reactor [www.iter.org]**

Blanket covers the interior surfaces of the Vacuum Vessel, providing shielding to the Vessel and the superconducting Magnets from the heat and neutron fluxes of the fusion reaction. The neutrons are slowed down in the Blanket where their kinetic energy is transformed into heat energy and collected by the coolants. In a fusion power plant, this energy will be used for electrical power production. Also tritium production will be realized within the blanket.

Divertor is situated along the bottom of the Vacuum Vessel, its function is to extract heat and Helium ash — both products of the fusion reaction — and other impurities from the plasma, in effect acting like a giant exhaust system. It will comprise two main parts: a supporting structure made primarily from stainless steel, and the plasma-facing components (either carbon or tungsten), weighing about 700 tons.

An extensive diagnostic system will be installed on the ITER machine to provide the measurements necessary to control, evaluate and optimize plasma performance in ITER and to

further the understanding of plasma physics. These include measurements of temperature, density, impurity concentration, and particle and energy confinement times.

Heating System: ITER *Tokamak* will rely on three sources of external heating that work in concert to provide the input heating power of 50 MW required to bring the plasma to the temperature necessary for fusion. These are neutral beam injection and two sources of high-frequency electromagnetic waves.

Cryostat is a large, stainless steel structure surrounding the Vacuum Vessel and superconducting Magnets, providing a super-cool, vacuum environment. It is made up of a single wall cylindrical construction, reinforced by horizontal and vertical ribs. The Cryostat is 29.3 metres tall and 28.6 metres wide [19].

Significant information and technologies provided by ITER will be crucial for development of a demonstration reactor DEMO (DEMOnstration Power Plant). DEMO's goal is to produce 25 times as much power as introduced and its 2 to 4 gigawatts of thermal output will be on the scale of a modern electric power plant [12]. DEMO's linear dimensions will be about 15% larger than ITER and a plasma density about 30% greater. A very optimistic report on the official ITER website states that a prototype commercial fusion reactor DEMO could make fusion energy available within 20 years, based on a conceptual design for DEMO machine being completed by 2017, and "if everything goes well, DEMO will lead fusion into its industrial era, beginning operations in the early 2030s, and putting fusion power into the grid as early as 2040" [19].

In this study, more attention will be paid on the progress related to development of the functional materials used in a blanket and as a plasma facing. Therefore overview of the European Union concept and research activities of blanket design and development of plasma facing material combination will be given in more detail in the following chapters.

### *1.3 The EU blanket design, research and development (R&D) activities prior to installation in ITER*

Dominating fraction (about 80%) of the power generated by fusion will be captured by neutron moderation in the breeding blanket surrounding the plasma where tritium production and energy extraction take place. Due to its exceptional relevance, the question on the right breeding blanket concept has frequently been discussed in literature [20-26].

European Union proposes two concepts of helium cooled tritium breeding blanket modules for testing in ITER: Helium - Cooled Lithium - Lead (HCLL) blanket which uses the eutectic Pb-

15.7 Li at 90% $^{6}$Li enrichment as both breeder and neutron multiplier, and Helium - Cooled Pebble Bed (HCPB) blanket where lithium ceramic pebbles ($Li_4SiO_4$ or $Li_2TiO_3$, $^{6}$Li enrichment 40% or 70%, respectively) are used as a breeder and beryllium pebbles as a neutron multiplier. HCPB concept is demonstrated in Figure 1.2. Both blankets will use pressurized helium technology for the power conversation cycle (8MPa, inlet/outlet temperature 300$^{o}$C/500$^{o}$C) and Reduced Activation Ferritic Martensitic (RAFM) steel as structural material, the EUROFER [25, 27, 28]. The EU Testing programme foresees several TBMs (Tritium Breeding Module) during the first 10 years of ITER operation [22]. Also other partners are planning to test their blanket concepts in ITER, for example, Water Cooled Solid Breeder blanket concept WCSB proposed by Japan [29].

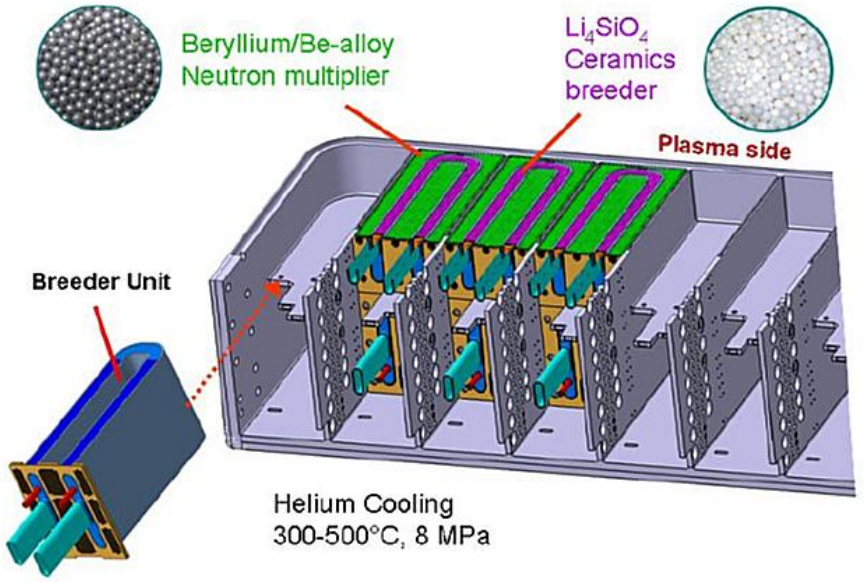


*Figure 1.2* **Helium Cooled Pebble Bed concept of a blanket module [30]**

The choice of breeding blanket concepts has been based on the following issues: overall system and development cost, risks including all related sub-system outside the reactor like tritium extraction, heat exchangers and power conversation, tritium control, technical feasibility, reliability, ease of manufacture, maintainability, compatibility with advanced reactor layouts and safety [20]. A lot of effort has been concentrated on the functional material testing under relevant conditions of the reactor to ensure requirements regarding the issues mentioned above.

Neutron irradiation is one of the main obstacles complicating the material choice due to the problems it causes; e.g., neutron-induced transmutations (long - term activation, tritium inventory in beryllium materials) and structure degradation (brittleness, swelling, etc) [31, 32]. A wide

variety of neutron irradiation projects for breeding blanket materials have been undertaken or are in progress. The major facility in Europe providing irradiation of blanket relevant materials is the High Flux Reactor (HFR), located in Petten, the Netherlands. The following experiments has been or is going to be performed: EXOTIC - Tritium production and release from Li-ceramics [33], Pebble-Bed Assemblies (PBA) - thermo-mechanical behaviour of breeder pebble-beds [34], HICU- High dose irradiation of Li-ceramic pebbles, effect of tailored neutron-spectrum on pebble (stack) integrity [35], HIDOBE - High Dose Beryllium, effect of He-bubbles on tritium-inventory and pebble-bed behaviour [36, 37], LIBRETTO [38]: Tritium production, extraction and release from liquid Pb-Li eutectic and tritium permeation under irradiation, PARIDE - Plasma facing material specimens, divertor and primary wall sub-assemblies [39]. All of these experiments give a possibility to do both in-pile and out-pile or post irradiation measurements.

Great input in blanket development has been provided by Karlsruhe Institute of Technologies. Lot of investigations performed by this scientific institution are related to understanding and predicting release of gaseous neutron transmutation products from materials irradiated under fusion conditions (in collaboration with HFR), as well as detailed structure analysis [27, 40-42]. Calculations and experiments related to tritium breeding self - sufficiency based on neutronic analysis are also of great importance and have been done by number of institutions all across the Europe and Asia [43-45]. Issues related to fabrication technologies of blanket modules are also under discussion [23].

### *1.4 Research and development activities related to Tokamak performance - the Joint European Torus*

In order to solve fundamental and technological problems related to *tokamak* system performance under complex conditions of fusion reactors, research is carried out worldwide and plenty of experiments are performed on the *tokamak* devices such as *DIII-D* (USA), *EAST* (China), *KSTAR* (South Korea), *TFTR* (USA), *Joint European Torus* (UK), *JT-60* (Japan), *Tore Supra* (France), *T-15* (Russia), etc [10].

The largest current experiment is the Joint European Torus (JET) – *tokamak* device with unique scientific and technical features (Figure 1.3) [46]. Comparison of JET and ITER technical parameters is given in Table 1.1.

JET is equipped with a sophisticated diagnostics system that gives possibility to obtain crucial information about the plasma behaviour and material compatibility with real reactor

conditions. Remote handling system developed and used at JET is also an essential step towards safe maintenance of the reactors.

*Table 1.1* **Technical data on JET and ITER**

| **Parameters** | **JET[7]** | **ITER [19]** |
|---|---|---|
| Plasma major radius, m | 3.0 | 6.2 |
| Plasma minor radius, m | 1.25 | 2,00 |
| Plasma current, MA | 7.0 | 15.0 |
| Plasma volume, $m^3$ | 200 | 840 |
| Toroidal magnetic on axes, T | 4.0 | 5.3 |
| Burn flat top, seconds | 60 | >400 |
| Fusion power, MW | 16 | 500 |

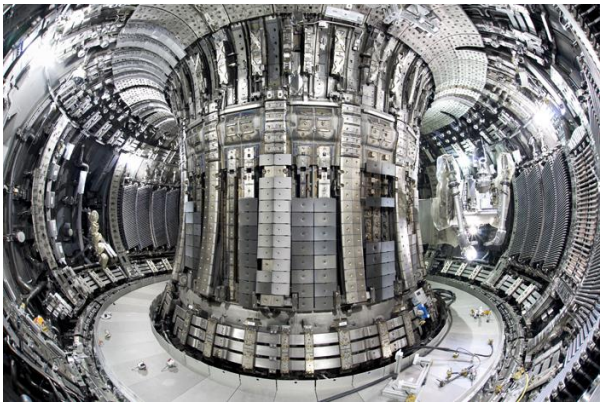

*Figure 1.3* **The photograph of the JET vessel interior taken in September 2010 [www.efda.jet.org]**

In 1997, during the deuterium – tritium campaign DTE1, JET produced a peak of 16.1 MW of fusion power (65% of input power), with fusion power of over 10 MW sustained for over 0.5 seconds [47]. There have been several deuterium–tritium experiments in JET. First of them was performed in the end of the year 1991 and it was called The Preliminary tritium experiment PTE, where total amount of tritium injected into torous was 53 (±4) Ci or 1,96 TBq [48]. Plasma containing 11% of tritium in deuterium produced a peak fusion power of 1.7 MW for 2 seconds and a fusion gain 0.12 [47]. The most recent experiment involving tritium was Trace Tritium Experiment TTE in 2003, where the fraction of tritium was kept at "trace" level, i.e. <1-2% of the deuterium majority fuel [49, 50]. Though in the TTE type experiments trace levels of tritium have been used the differences between requirements for TTE and full DT operations are relatively small [49, 51-53].

Currently JET *tokamak* is operating within the ITER Like Wall (ILW) project. The aim of this project is to test plasma facing materials relevant to ITER. Carbon tiles had been removed and combination of beryllium (Be), tungsten (W), W-coated carbon fibre composites (CFC) and Be-coated inconel[2] tiles are introduced into the vessel instead [46, 54-56]. Up to now ITER relevant materials have been tested only in isolation in *tokamaks*, plasma simulators, ion beams and high flux test beds. An integrated test demonstrating both acceptable tritium retention and ability to operate ITER-relevant plasmas with high power input within the limits set by these materials will be demonstrated for the first time [55].

### *1.5 Issues related to tritium accumulation in fusion reactor materials*

Tritium is produced in the process of fusion reaction, in nuclear reactions of neutrons with lithium in the blanket zone. To guarantee uninterrupted operation of reactor it is necessary to ensure sufficient tritium is bred in the blanket, extracted and delivered to the tritium storage unit to replace the tritium consumed by fusion reactions and lost in the fuel cycle. As mentioned in T. Nishitami et al review on fusion reactor materials development "a basic tritium behaviour database must be developed containing information such as solubility, diffusivity, permeability, characteristics of trapping, release, replacement, reactions etc. for advanced materials for DEMO" [26]. Schematic view of fuel (deuterium and tritium) cycle is given in Figure 1.4.

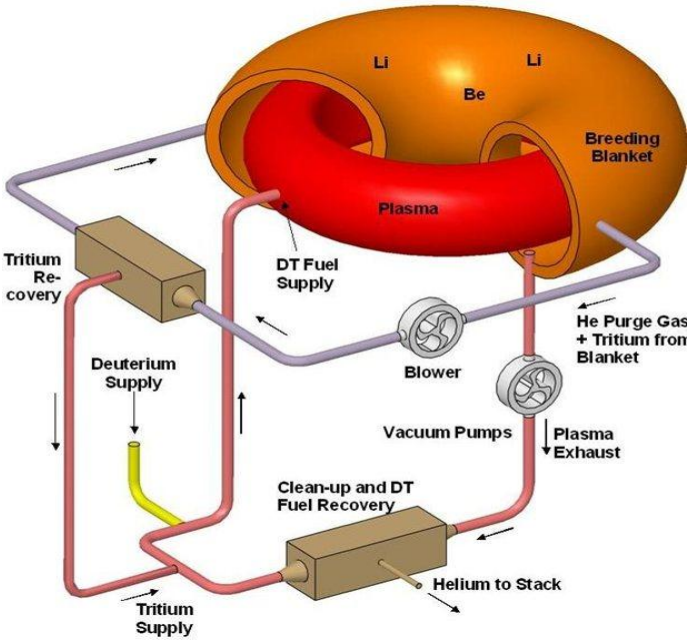


*Figure 1.4* **Fuel cycle in ITER [www.iter.org]**

[2] *A registered trademark of Special Metals Corporation that refers to a family of austenitic nickel-chromium-based super alloys. Inconel alloys are typically used in high temperature applications.*

From blanket, where it is produced, tritium is carried by the helium purge gas (+0.1% $H_2$ as an isotope swamping) to a tritium recovery system and then introduced into plasma chamber by a combination of gas and pellet (ice) injection [57]. In case of ITER tritium will be mostly procured from the worlds inventories, whereas DEMO will demonstrate full tritium breeding self-sufficiency [19].

Tritium accumulation in fusion reactor materials is a significant safety issue. Tritium control in a breeding blanket and vacuum vessel is a key issue in terms of both tritium breeding self-sufficiency and safety of the fusion plant. Estimations of tritium inventory in the reactor materials have been done both experimentally and by theoretical modelling by a number of scientific institutions [57-59]. Safety requirements limit the in-vessel inventory to the total of 350 g of tritium; this is due to risk of its release at accidental heat transients.

Tritium retention is especially critical for solid breeding blanket materials and plasma facing materials; therefore further in this work focus will be put on these materials.

## *1.6 Functional material development and research for fusion applications*

In this work main focus will be put on beryllium as a neutron multipliers and plasma facing component and on carbon based material that is considered as a divertor material in a high flux areas. Therefore literature about these materials will be reviewed in more detail.

### 1.6.1 Beryllium and its alloys

Beryllium is a light metal with unique properties that makes it attractive for the nuclear applications, including fusion. It is a hard, low Z metal, and excellent ability to moderate and multiply neutrons. However, its melting point (1285$^{o}$C) is not particularly high. In the EU Helium Cooled Pebble Bed breeder blanket concept beryllium is used as a neutron multiplier. Reference material is chosen to be 1 mm pebbles fabricated by NGK Inc by Rotating electrode process (REP). For a tritium breeding ratio above 1, the volume taken up by the Be pebble bed has to be approximately four times larger than for the Li-ceramic pebbles. In the vacuum vessel of ITER it is foreseen also as a plasma facing material due to its good mechanical properties and low impact on plasma performance. The ITER reference design has a nearly continuous actively cooled Be wall surface [56].

Beryllium performance under neutron irradiation is an important issue and has been studied widely.

- *Swelling, embrittlement and hardening*

Beryllium swelling, embrittlement and hardening as a result of the neutron irradiation are important issues regarding its mechanical performance. Swelling in neutron-irradiated materials is interpreted in two general mechanisms. First is a direct consequence of the crystal lattice radiation damage. High energy neutrons knock out the atoms in the lattice and generate defects such as vacancies and interstitials[60]. In beryllium irradiated at low temperatures (below 200$^{o}$C) dislocations loops have been observed experimentally by several authors. Moreover, the accumulation of the dislocations in different lattice planes depends on the type of the dislocation; vacancy loops are located on the basal planes, whereas interstitials on the prismatic ones [61, 62]. Another observation made by the same authors is that in the case of beryllium, amount of neutron created vacancies are larger by several orders than interstitials [63]. Through the classical mechanism of vacancy accumulation, voids are formed. Accumulation of these voids on the grain boundaries leads to the embrittlement of a polycrystalline beryllium [61]. Therefore it might be assumed that large grains are more desirable regarding the mechanical durability of beryllium. Second type of swelling is a consequence of the gaseous nuclear reaction products. The second mechanism is dominant in the limiting of the lifetime of the beryllium pebbles [60]. Mathematical approach of swelling model has been provided by several authors. The parameters used in these calculations are the neutron flux, initial porosity, amount of impurities, grain size [64]. Neutron induced hardening caused by the produced helium has also been described by number of authors [63]. Production of the gaseous species as a result of neutron irradiation is a one of the main problems of beryllium performance; therefore plenty of investigations on their behaviour in the solid beryllium have been done worldwide.

- *Gaseous products of nuclear reactions*

As a result of neutron induced transmutations of beryllium helium and tritium gas is produced in considerable amounts. In the frame of the European Power Plant Conceptual Study, the peak integral gas production in beryllium, at the End-Of-Life of HCPB modules (40 000 h operation), has been assessed as 25 700 appm helium and 640 appm tritium, taking account in-pile tritium decay. The global tritium production in the whole of the blanket (390 tons of beryllium) is 23.8 kg [40]. Neutron reactions with beryllium are demonstrated below (1.4-1.8) [65].

*Chain 1*

$$^{9}Be + n(th) \xrightarrow{9.5mb} {}^{10}Be^{*} \longrightarrow {}^{10}Be + \gamma + 6.8\ MeV$$

$$\downarrow\ 2.7 \cdot 10^{6} yr$$

$$^{10}B + \beta^{-}$$

$$\downarrow$$

$$^{10}B + n(th) \xrightarrow{3843b} {}^{7}Li + {}^{4}He$$

*1.4*

*Chain 2*

$$^{9}Be + n(4 - 10MeV) \xrightarrow{10mb}$$

$$^{9}Be + n(2 - 4MeV) \xrightarrow{85mb} {}^{10}Be^{*} \longrightarrow {}^{4}He + {}^{6}He - 0.64MeV$$

$$^{9}Be + n(1 - 2MeV) \xrightarrow{20mb} \qquad \downarrow 0.8\ s$$

$$^{6}Li + \beta^{-}$$

$$\downarrow$$

$$^{6}Li + n(th) \xrightarrow{950b} {}^{3}H + {}^{4}He + 4.7MeV$$

$$\downarrow\ 12.3\ yr$$

$$^{3}He + \beta^{-}$$

$$\swarrow\ 12.3\ yr$$

$$^{3}He + n(th) \xrightarrow{5237b} {}^{3}H + p$$

*1.5*

*1.6*

*1.7*

*Chain 3*

$$^{9}Be + n(> 2\ MeV) \xrightarrow{580mb} 2\ {}^{4}He + 2n - 1.7\ MeV$$

*1.8*

Tritium and helium production and accumulation under different irradiation conditions (temperature, neutron flux, and time) has been investigated by a number of authors.

It is assumed that initially helium and tritium form a dynamic solution throughout the entire lattice. Due to low solubility, helium tends to form gas clusters that performs as a nucleation site for further formation of bubbles [66]. In fact, grain boundaries are a strong sinks for such defects, therefore large fraction of these clusters could be formed nearby them. Nevertheless, it must be noted that formation of these clusters is only a theoretical assumption - it has never been observed experimentally due to the extremely small size. Process of the bubble formation occurs via gas precipitation and a vacancy capture and this process is strongly temperature dependent [60]. After irradiation at temperatures below 200$^{o}$C no bubbles can be observed, whereas at the temperatures above this level - bubbles of few nanometres start to appear [61, 67]. Interesting fact is that this tendency remains even at very long exposure time and large helium amount. In the low temperature (70$^{o}$C) irradiation experiment of beryllium that lasted for 15 years (helium

content reached 2.2 at%), no bubbles were observed although significant swelling of the sample was obvious. Bubbles appeared only during post irradiation thermo annealing of the sample [68]. Another phenomena described in the literature is a specific crystallographic form of the bubbles inside the grains - it was found to be a hexagonal prism and more likely it is related to beryllium lattice parameters [66].

Tritium is assumed not to form its own gas inclusions since its overall concentration is very low if compared with helium. It is believed to accumulate as an interstitial atom or to be trapped by the structural or chemical traps. In contrast to helium tritium has a high chemical reactivity and it can form chemical bonds with impurities, mostly with beryllium oxide forming the hydroxide. It has been found that besides oxide layer on the surface BeO inclusions have a tendency to accumulate on the grain boundaries [61], therefore it can be expected that chemically bonded tritium can be found either on grain boundaries or in the surface layer. However, it is assumed that most of the tritium resides mostly in the helium gas inclusions as a molecule [69]. Direct measurements of the tritium chemical state in a beryllium bulk have not been done. All the assumptions are based on the measurements of tritium released at the thermo desorption experiments and cannot be precisely interpreted for the real situation in a solid matrix.

For modelling tritium behaviour in beryllium it is necessary to know such parameters as solubility, trapping energies and diffusivity. Some properties might be extrapolated from available data about protium or deuterieum, however, isotopic effects must be taken into account [70]. Ratio of diffusivities of the isotopes is equivalent to the inverse ratio of the square root of the masses of the isotopes and can be described by the equation 1.9:

$$\frac{D_T}{D_H} = \sqrt{\frac{m_H}{m_T}} \qquad 1.9$$

In fact, it should be mentioned that in one of the first successful attempts to measure hydrogen solubility in beryllium tritium was used instead due to its simple detection based on its radioactivity [71]. Comprehensive overview of the experimentally obtained data on hydrogen solubility, diffusivity and permeation has been provided by R. A. Causey in 2002 [72]. Graphical view of the diffusion coefficients (in a logarithmic scale) from different authors are presented in Figure 1.5. There is a large discrepancy in the data obtained by different authors. This might be explained both by the differences of beryllium grades used in the experiment and different technique. In this work diffusion coefficients are attempted to be classified according to the source of hydrogen isotope: (I) hydrogen sorption in a material as a result of exposure to its gas at

a given pressure and temperature (H, D and T) [71, 73], (II) tritium formed as a result of exposure to a neutron irradiation (only tritium) [74, 75] and (III) implantation of the energetic ions (usually deuterium) [76, 77].

It is clear that diffusion is not the single mechanisms of tritium transport in beryllium. Trapping phenomena and influence of oxide layer have a crucial role. M. G. Ganchenkova has provided a theoretical model of tritium trapping on the imperfections of the lattice, such as vacancies, grain boundaries, etc. [78]. Reported diffusion coefficients might be better considered as an effective ones due to fact that classical diffusion approach cannot be applied (beryllium lattice is not an ideal one, especially after neutron irradiation or ion implantation). Gaseous sorption of hydrogen isotopes has been used in work of P.M.S. Jones and R. Giboson [71] and E. Abramov et al [73]. In the work of E. Abramov et al deuterium diffusivity in two grades of beryllium (high and extra grade beryllium, with 99% and 99.8% beryllium content, respectively) has been measured, whereas P.M.S. Jones and R. Gibson have used tritium. Differences in diffusion results of these two author groups could be explained by the fact that E. Abramov et al have taken into account contribution of beryllium oxide. It is well known that hydrogen diffusion in BeO is much lower than that in pure beryllium [79-82]. In 2011, V. Chakin et al [83] published work about possibility to simulate neutron irradiation by loading beryllium with hydrogen/tritium gas mixture at high temperatures with the aspect of hydrogen isotopes accumulation in beryllium pebbles. An intense oxidation of beryllium during thermo sorption at high temperatures limits application of this method, whereas low temperature sorption ($<700^{o}C$) might be used as a simulation tool for a low tritium concentrations [83]. However, neutron induced lattice damage and helium production in real irradiation conditions have a crucial role in tritium behaviour. Diffusion coefficient of neutron produced tritium has been measured by I. Tazhibaeva et al [84], D.L Baldwin and M.C. Billone [75] and S. Cho et al [74]. Whereas transport mechanisms and overall behaviour of tritium in neutron irradiated beryllium has been studied by a number of authors, even a special codes or models have been developed [40, 43, 74, 80, 85-88].

D.L. Baldwin and M.C. Billone have studied tritium diffusion process dependency on the beryllium density. An interesting phenomenon was revealed within this study- tritium diffusivity in a low density beryllium (81%TD) is lower than that for 100% or 99% theoretical density (TD) beryllium. It could be related to larger free surface within beryllium material where tritium could be trapped.

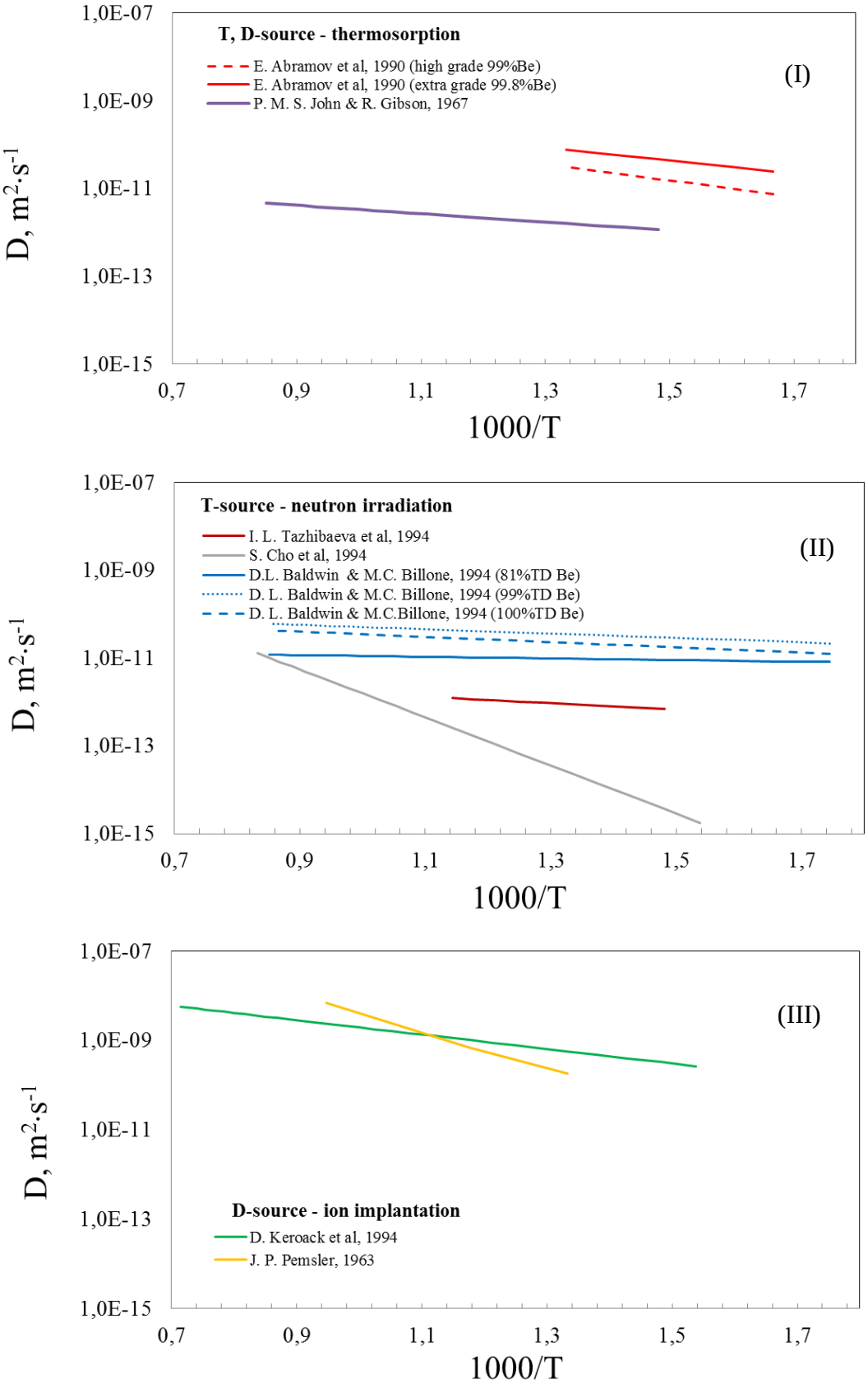


*Figure 1.5* **Diffusion coefficients of hydrogen isotopes in beryllium (in logarithmic scale) by different authors**

Great effort in explaining tritium behaviour in irradiated beryllium is given by F. Scaffidi - Argentina and his colleagues. In their work tritium and helium release during thermo-annealing of irradiated beryllium pebbles has been analysed in detail and a computer code for its prediction ANFIBE (Analysis of Fusion Irradiated Beryllium) has been developed. This code further was improved by E. Rabaglino. ANFIBE provides comprehensive model describing tritium trapping mechanisms in presence of both pressurized traps and chemical traps. This code includes a number of physical properties and the equations describing them.

Tritium and helium thermo-desorption spectra had been analysed widely in order to get comprehensive overview of the processes occurring during thermo annealing of irradiated beryllium [40, 60, 87, 89-91]. It is believed that most of tritium releases together with helium, whereas helium can be released at temperatures close to the melting point of beryllium. Nevertheless, low temperature peaks of tritium release have been observed in several experiments. Some authors believe that it is a tritium located close to the surface and is escaping through the micro cracks created by the irradiation [91]. Other associates it with the diffusion of the tritium existing as an interstitial [40, 89]. Beryllium microstructure after the irradiation and also after thermo annealing of the tritium has been also studied by number of authors [61, 66, 68, 89, 92]. Micro structural analysis gave an understanding about processes regarding helium bubble behaviour during thermo – annealing; bubbles tend to grow and coalescence that results in a venting process when all the gaseous products are released [40, 41, 92]. High quality visualization of the porosity is provided by A. Möslang et al by using a computer aided microtomography (Figure 1.6).

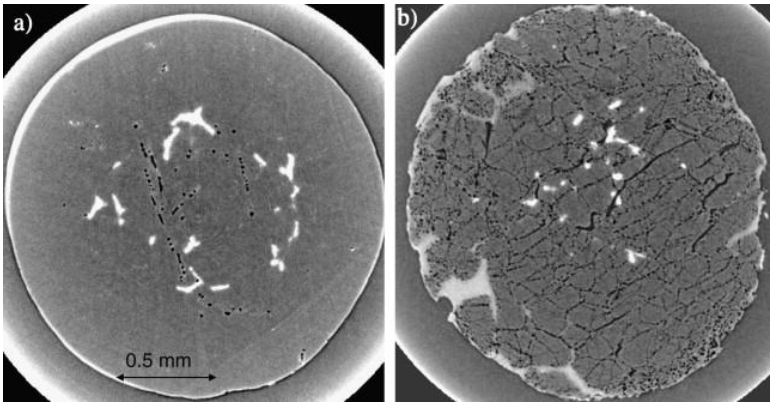


*Figure 1.6* **Evolution of pores and cracks during thermo-annealing published by A. Möslang et al in 2009. Method of computer aided microtomography CMT. Horizontal CMT cross sections of a Be pebble before (a) and after (b) neutron irradiation at 770 K and annealing at 1500 K. [41]**

Studies of the ion implantation in the surface of beryllium are particularly important for prediction its durability as a plasma facing material. Ion implantation as a loading method has been use in works of D. Keroack et al [77] and J.P. Pemlser et al [93]. The values of diffusion coefficients are comparably close, but the activation energy differs (graphically it can be observed as a slope angle). Ion implementation process results in lattice damage and therefore formation of the traps for hydrogen. Ion induced damage can be observed physically as a blisters and pores on the surface. It could be assumed that in the beryllium used in this two studies different amount of traps were formed due to differences in implantation temperature, ion energies, beryllium grade, etc.

- *Interaction with plasma*

Since beryllium tiles are planned to be used as a plasma facing material its interaction with plasma is a significant field of studies. Great input in beryllium and plasma compatibility studies had been provided by JET. 1989 to 2009 beryllium was evaporated periodically within the main chamber onto the carbon plasma-facing tiles. Experiments were also carried out with solid Be tiles as plasma-facing surfaces in certain areas, such as a limiter (1989-92), lower dump plate (1991-2) or divertor (1995) [94, 95]. In 2010-2011 all the carbon plasma-facing tiles were removed, and in 2011 JET began operating with the ITER like wall which uses beryllium as one of the main components. Main problems regarding beryllium use as a plasma facing material is its low melting point and high electrical conductivity, also tritium inventory is a significant issue [96, 97]. Comprehensive overview of research activities related to plasma wall interactions is given by J. Roth in 2009 [98]. Plasma caused beryllium melting, erosion and re-deposition have been described widely by number of authors [10, 56, 72, 95, 97, 99, 100]. In this work, main focus is put on tritium, therefore studies about plasma – beryllium interaction effect on the tritium accumulation will be reviewed. There is more pathways of tritium accumulation besides neutron induced transmutations in beryllium used as plasma facing, such as direct implantation of ions, diffusion and migration into the bulk and co-deposition [31]. Plasma driven accumulation of tritium has been described by A.A. Pisarev et al in 1996 [101]. Tritium permeation through beryllium wall coating has also been studied since it is a safety issue [102].

- *Thermomechanical behaviour*

Besides behaviour under neutron irradiation and plasma exposure other beryllium properties has been investigated regarding its performance in fusion reactor. Thermo mechanical

properties of the beryllium pebble beds is also an issue to be taken in account and has been described in the literature. Maximum temperature of Be pebble bed is supposed to be approx. 650$^{o}$C in the HCPB design (a strong upper limit does not exist but the decreasing of mechanical properties and swelling suggest to limit the max temperature below 700$^{o}$C) [27]. Temperature differences and different thermal expansion coefficients between pebble beds and structural materials result in constrained strains, which cause elastic and plastic pebble deformations. These deformations is also an important issue for prediction of the pebble bed behaviour [103].

- *Impurities*

An important issue is the impurity level in beryllium used for fusion applications. Impurities could act as a parasitic thermal neutron absorbents and therefore decreasing tritium breeding self-sufficiency. Some of the impurities could cause induced radioactivity of the material. The impact on tritium breeding has been studied by Y. Verzilov el al. They found that such impurities as Li, B, Cd and other can affect tritium breeding ratio even if their content is less than 10ppm [104]. Comprehensive overview on issues related to a long – term activation has been given by N.P.Tailor et al in 2000 [32]. In case of beryllium, $^{59}$Co is a significant problem due to its transmutation into $^{60}$Co that is an emitter of high energy gamma rays.

- *Compatibility*

Compatibility issues are also still under discussion. Beryllium reactivity with steel and lithium compounds could be a problem in real reactor conditions [105].

- *Alternative to beryllium - beryllides*

Currently beryllium pebbles is the main reference material for the HCPB, nevertheless titanium beryllide must be mentioned since it is considered as an alternative due to its higher melting point and smaller reactivity with other blanket components [106].

- *Toxicity*

Safety issues regarding toxicity of beryllium itself are also of great importance and studies related to it have been carried out [94, 107].

### 1.6.2 Carbon based materials

Carbon fibre composites (CFC) or carbon fibre reinforced carbons are a candidate material for divertor areas near the plasma strike points in future fusion devices. This choice is based on the ability of carbon to handle off–normal heat loads without melting and its low Z.

Carbon fibre reinforced carbon is a composite material consisting of carbon fibre reinforcement in a matrix of graphite. The atomic structure of carbon fibre is similar to that of graphite and consists of sheets of carbon atoms (graphene sheets) arranged in a regular hexagonal pattern. The difference lies in the way these sheets interlock. Graphite is a crystalline material in which the sheets are stacked parallel to one another regularly. Whereas carbon fibre may be turbostratic[3] or graphitic depending upon the precursor to make the fibre, or have a hybrid structure with both graphitic and turbostratic parts present (Figure 1.7) [108].

In the EU divertor concept for ITER the Carbon Fibre Reinforced Carbon Material of SNECMA NB41 Grade (Manufactured by SNECMA PROPULSION SOLIDE, Public Limited Company, France) has been chosen [109].

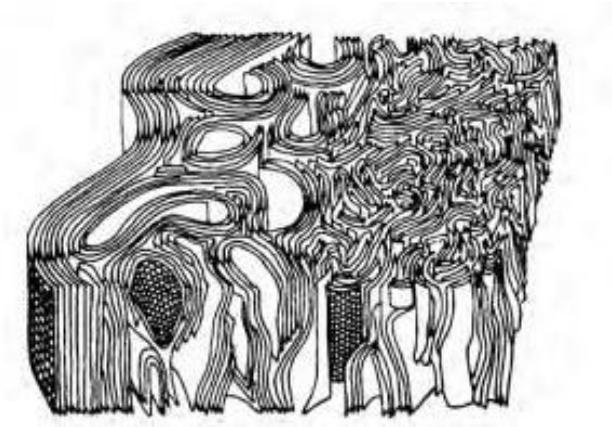

*Figure 1.7* **Turbostratic arrangement of graphene sheets[108]**

The SNECMA NB41 grade is a 3D material with the fibres oriented in the 3 orthogonal spatial directions. With regard to fusion applications the fibres oriented in the high heat flux direction are made of pitch precursors while in the other two directions the fibres used are PAN-fibres In particular the fibres are forming a 2D laminar structure consisting of ex-pitch and ex-PAN fibres layers which is then reinforced in the third direction by a so-called needling process.

[3] A type of crystalline structure where the basal planes have slipped sideways relative to each other, causing the spacing between planes to be greater than ideal

This is causing the reorientation of a part of the ex-PAN fibres, which provide a higher flexibility than the ex-pitch fibres [109].

In the plasma chamber the first wall materials are exposed to the severe conditions, such as bombardment by energetic ions and neutrals, plasma exposure, neutron irradiation. Experimental data on CFC behaviour in similar conditions are obtained mainly from testing in *tokamak* devices (JET, TFTR etc), plasma devices and simulations in the laboratory conditions.

- *Dimensional stability*

There have been several studies on CFC performance under neutron irradiation [62, 110-113]. Neutron irradiation mainly affects the dimensional stability of these materials as a result of carbon atom displacements (Figure 1.8) [111]. If one compares with beryllium, the carbon application in fusion devices is not limited by the neutron irradiation. However, the increase of the traps for hydrogen adsorption as a result of neutron exposure must be emphasized (this topic will be in more detail discussed below).

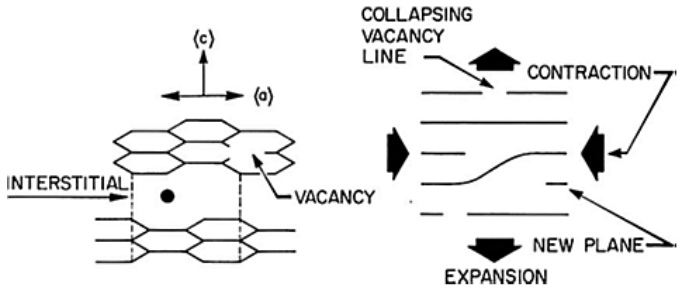


*Figure 1.8* **Neutron damage mechanism in graphite according to Snead et al [111]**

- *Erosion and re-deposition*

High physical and chemical erosion yields leads to a limit to the lifetime of the plasma-facing component, whereas build-up of tritium inventory is an important safety issue [114]. As a result of plasma induced erosion large amounts of carbon are introduced into the plasma edge and then re-deposited at different locations of the chamber together with the hydrogen isotopes. This co-deposition is considered the dominant fuel retention mechanism in fusion devices. Deposited layer mostly consist of so called hydrogenated amorphous carbon or amorphous hydrocarbon, denoted as a-C:H, with some metals species (mostly beryllium since it has been introduced into plasma chamber and used as oxygen scavenger and wall conditioner) and oxygen. Hydrogenated amorphous carbon films have been investigated widely beyond the fusion studies due to interesting mechanical and optical properties and therefore possible application in different areas

[115, 116]. The a-C:H has been found even in interstellar media in the carbonaceous dust and therefore is an investigation object also in astrophysics [117]. In the plasma chamber of fusion reactor such films form as unwanted by-product on the first wall as a re-deposited layers from previously eroded carbon and abundantly available hydrogen [118]. The film consists of a cross-linked three dimensional network in which the small graphite clusters are embedded and are usually obtained by plasma deposition. Crosslinking is possible due to tetrahedrally coordinated carbon atoms ($sp^3$ hybrids), whereas graphite clusters are composed of threefold coordinated $sp^2$ hybrids (Figure 1.9).

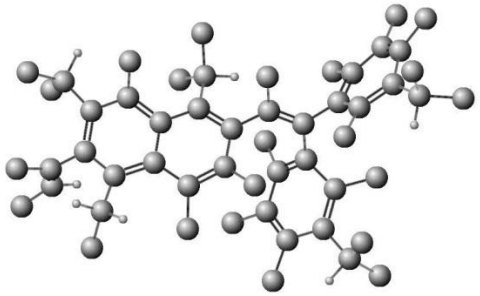

*Figure 1.9* **Structure of hydrogenated amorphous carbon (fragment)**

Different forms of hydrogenated amorphous carbon films can be distinguished by the content of $sp^3$ and $sp^2$ carbon and hydrogen. F. W. Smith in 1991 [119] introduced a ternary phase diagram for such films based on experimental and theoretical data (Figure 1.10).

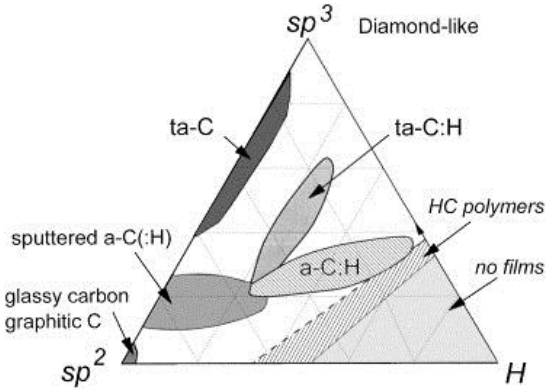


*Figure 1.10* **Ternary phase diagram of bonding in amorphous hydrogenated carbon films, where a-C:H is an amorphous hydrocarbon, ta-C:H - tetrahedral amorphous hydrocarbon, ta-C - tetrahedral carbon (also called diamond like carbon). The area close to the hydrogen rich corner marks the region where no stable film can be formed (volatile hydrocarbons), this region is limited by long chain polymers**

Diagram was later used and improved by W. Jacob and W. Moller in 1993 [116]. Three components are included in this diagram– carbon in $sp^3$ and $sp^2$ hybridization and hydrogen (in atomic % units) [116].

Critical dependency of the energy of incident hydrogen flux has been found by group of authors. Energetic ions lead to the deposition of hard films with hydrogen concentrations H/C of about 0.4 (~30%), while low energy thermal hydrogen leads to the formation of soft films, with H/C concentration exceeding 1 (>50%) [120]. In the ternary phase diagram it is the region of a-C:H type material. In the deposition layers from JET plasma chamber the ratio D/C (D-deuterium) has been found to be ~0.75 (~40% of deuterium) [121].

There is lot of experimental data and theoretical assumptions about pure a-C:H films, however deposition layer in the fusion reactor plasma chamber is presumably more complex systems due to presence of other elements, such as beryllium, boron, oxygen and impurities from the Inconel. All these factors more likely have an impact also on hydrogen isotope (including tritium) bonding and behaviour in the deposits and must be taken into account. The chemical composition and structure of the deposition layer on the surfaces of sampler exposed in the plasma chamber of the fusion devices have been studied by different methods in number of institutions [122-129]. A comprehensive overview on the re-deposition of hydrocarbon layers in fusion devices has been given by W. Jacob in 2005 [130].

Certainly, there are more mechanisms responsible for the hydrogen isotope retention in the carbon based materials beyond co-deposition with eroded particles. These mechanisms include implantation of energetic ions in the near surface layers, absorption on internal porosity, and transgranular diffusion into the bulk. All of them can make significant contributions to the fuel immobilization [72].

- *Ion implantation*

In the fusion devices, plasma facing materials are bombarded by energetic ions and neutrals from the plasma with energies of up to a few keV [10]. Ion-solid interactions include such processes as backscattering, sputtering and displacement, as well as implantation of the impinging species in the surface layer. Since ions are immediately neutralized upon approaching the surface, the interaction of ions and neutrals with solid surface might be considered as identical [118]. Interaction depends on the energy of the incident particle. Energies, slightly higher than thermal (few tens of an eV), allow overcoming the activation barriers to surface adsorption. At energies in the range of several eV of the particles is sufficient to break bonds at the surface, therefor new reaction channels might be open and surface diffusion increased. At higher energies (above few tens of eV), impinging species may penetrate the surface and be

trapped in the bulk. The last can be referred to an implantation [118]. R. B. Wright et al had carried out study on ion implantation in graphite by bombardment it with 15 keV protons and deuterons. They found out that conjugated acetylenic bonds were formed in the near surface layer [131]. The thickness of the saturated layer is limited to only about 0.1 μm and therefore has a limited effect on the tritium inventory for D-T burning devices [72].

In contrast to fine grain graphite no saturation of implantation layer has been observed for the carbon fibre composites which is a more porous material. Instead, the retained amount of hydrogen increases close to square root of the ion fluence due to diffusion deep in the bulk [120].

- *Hydrogen isotope transport, interaction with carbon*

Several explanations of the hydrogen migration within the bulk of carbon based materials have been proposed by a number of scientists. According to M. Warrier et al hydrogen transport in the bulk of the carbon based materials is contributed by following processes:

- Trapping – detrapping;
- Recombination, dissociation and molecule formation;
- Transgranular diffusion;
- Diffusion along voids [132].

In their work M. Warrier et al have studied hydrogen transport mechanism at different temperatures. At the temperature below 900 K transport of hydrogen is assumed to be due to surface diffusion of atoms on the void – granule surface (activation energy ~0.9 eV). At higher temperature adsorption - desorption mechanisms starts to dominate (activation energy ~1.9 eV) due to larger jump size (surface diffusion is constrained to jumps on the surface, whereas desorbed particle might jump across voids) [132]. Trapping –detrapping mechanism requires even more energy determined by the type of the trap (in this work traps of 4.3 eV energy has been studied). An interesting study on hydrogen trapping mechanisms has been performed by S. L. Kanashenko et al in 1996 [133]. They proposed that hydrogen – graphite interaction is based on its adsorption on three different types of sites in the lattice:

- Un-relaxed dangling bonds on edge carbon atoms of carbon interstitial loops (cluster) with the hydrogen adsorption energy of – 4.4 eV/$H_2$ (trap 1);
- Relaxed dangling bonds on grain surfaces of the carbon lattice with the hydrogen adsorption enthalpy of -2.3 eV/$H_2$ (trap 2);

- Basal plane adsorption sites with the hydrogen adsorption enthalpy of +2.43 eV/$H_2$ (trap 3). This adsorption might be thought also as the true solution [133].

Returning to the work of M. Warrier et al it might be assumed that trap 3 proposed by S.L. Kanashenko is responsible for the adsorption –desorption mechanism, whereas traps 1 and 2 for trapping –detrapping mechanism.

H. Atsumi el al have studied hydrogen adsorption in carbon materials regarding the possibilities of hydrogen storage [134]. They have studied different trapping sites in their work in 2003. Schematic illustration of the trapping mechanisms proposed by H. Atsumi et al (according to S. L. Kanashenko) is given in Figure 1.11.

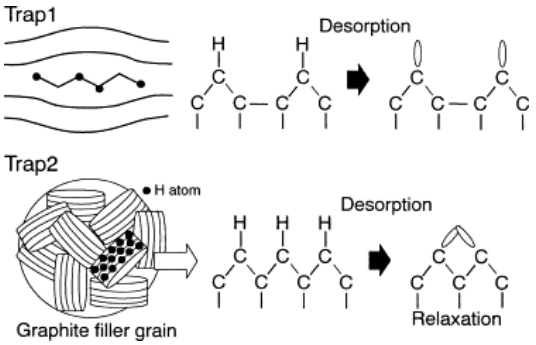


*Figure 1.11* **Schematic illustration of the hydrogen trapping in a graphite material [134]**

Different types of carbon based materials contain different concentration of the traps due to differences in microstructure. Atomic displacements produced by neutron irradiation increases the number of traps 1 and 2 while number of trap 3 remains constant. At the damage levels of 1dpa (at room temperature) concentration of traps 1 and 2 was found to increase to 1500 and 3000 appm, respectively [133].

The effect of the free surface within the carbon fibre composites on tritium inventory has also been studied by group of authors [132, 135].

Due to complex characteristics of hydrogen transport it cannot be considered as a classical diffusion, however it is possible to though on effective diffusion parameters. R. A. Causey has made an overview of the experimentally obtained coefficients of effective diffusion of hydrogen isotopes in carbon based materials (Figure 1.12) [72].

Comprehensive studies on hydrogen isotope behaviour in the carbon based materials by taking into account all transport and retention mechanisms are of great importance. Experimental data for such studies can be obtained merely in the real *tokamak* devices, such as JET, Tora Supra, TRFR etc. Fuel retention and liberation characteristics in the materials exposed in plasma

chambers in a *tokamak* devices both in-situ and post-mortem has been performed by number of scientists and gives a possibility to extrapolate the results to the larger devices such as ITER or DEMO.

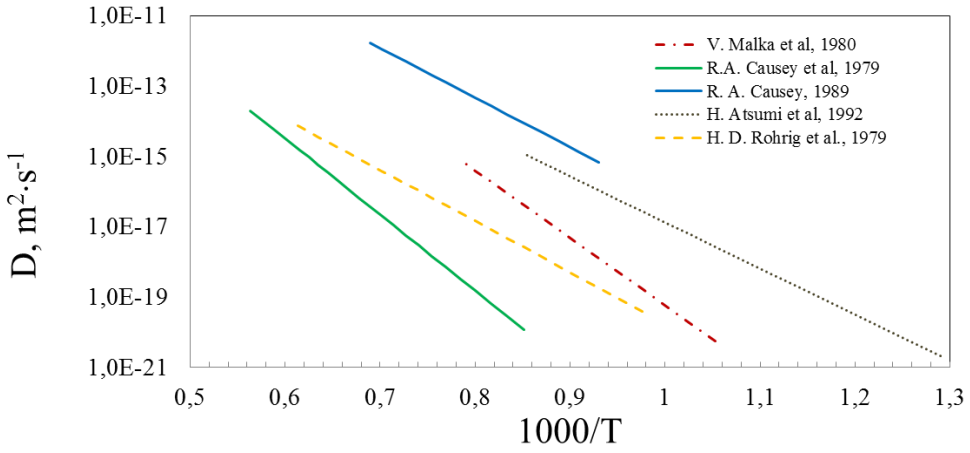


*Figure 1.12* **Diffusion coefficients of hydrogen isotopes in carbon (in logarithmic scale) by different authors**

Most of performed experiments regarding the fuel retention include deuterium (or in some cases tritium) depth profile measurement and its release during the temperature programmed desorption process. For the depth profile of tritium in the JET CFC tiles full combustion has been used both by R.-D. Penzhorn et al in 2001 [136] and N. Bekris in 2003 [137]. Both authors have observed that tritium can be found throughout all of the bulk of the tiles, indicating to the significance of bulk diffusion and trapping. Another important data can be obtained by determination of gaseous species releases during the thermal treatment. Such work has also been performed by N. Bekris et al. By the masspectrometry method they have recorded methanated species such as $CH_xQ_y$ (where Q is D and/or T, x+y = 4) [138].

An interesting study has been published by A. Pisarev et al in 2011. They have compared the thermal desorption spectra of deuterium from carbon fibre composite exposed to deuterium plasma, deuterium gas and after deuterium ion implantation [139]. Such experimental data provides material for interpretation of the TDS spectra of materials exposed to less predictable conditions such as those in a *tokamak*.

It must be emphasized that most of the experiments have been performed with deuterium and results later extrapolated to tritium. However, it has been proven experimentally by R. D. Penzhorn et al that more energy is required to liberate tritium than deuterium in the similar conditions. Authors explain it with stronger bonding of tritium to the graphite matrix caused by the damage resulting from radiation-induced gas/solid interactions [136]. Wherewith, it could be

concluded that there are lot of uncertainties and more experimental data on tritium behaviour in carbon materials is needed.

### *1.7 Detritiation methods*

Tritium accumulation in the fusion reactor is a problem that ought to be solved. First approach is an appropriate choice of materials and mitigation of its retention during operation. To mitigate tritium inventory several approaches have been provided, for instance, minimizing tritium introduced, tailoring isotope ratio, ending every shot in deuterium-only phase with sweeping of the divertor strike points, seeding the plasma with nitrogen, ammonia, etc [120, 140, 141]. Nevertheless it is not possible to achieve no inventory at all. Therefore lot of work is devoted to development of an efficient and low-cost detritation method both in-situ and after exploitation in a reactor. Detritiation of the materials would give an option to reclassify these materials for disposal from intermediate-level waste to low level wastes. Low-level wastes are much easier and less expensive to dispose [142] .

There have been different detritiation methods and their combination considered:

- Superficial cleaning and washing;
- Vacuuming, purging;
- Thermal desorption;
- Isotopic exchange;
- Chemical or electrochemical etching;
- Plasma discharge methods;
- Radiofrequency heating;
- Laser scanning and ablation (laser induced desorption of tritium [143] and laser ablation as a method for removing co-deposited material [144]);
- Flash lamps (photon cleaning) [145];
- Destructive techniques such as melting and dissolution [146].

Regarding the detritiation alternatives distinction must be made between surface tritium (co-deposited) and bulk tritium. Tritium-rich deposited films on plasma facing materials might be removed by in-reactor techniques, such as treatment with argon plasma, an open flame (nitrous oxide-acetylene), radio frequency heating and scanning laser, etc. [147-151]. To remove tritium from the bulk the high-temperature annealing or methods including full destruction (melting, dissolution) might be considered as appropriate options.

### *1.8 Magnetic field effects on physical and chemical processes*

In physics, magnetic field is defined as a field of a force associated with electric charge in motion, having both electric and magnetic components and containing a definite amount of electromagnetic energy.

Magnetic field can be described by following quantities: magnetic field strength H ($A \cdot m^{-1} = J \cdot T^{-1} \cdot m^{-3}$), magnetic flux density B ($T = Wb \cdot m^{-2}$) and magnetization M ($A \cdot m^{-1} = J \cdot T^{-1} \cdot m^{-3}$) that are correlated mutually by the following equation:

$$B = \mu_0 H + \mu_0 M \qquad 1.10$$

where $\mu_0$ is the permeability of a vacuum ($4\pi \cdot 10^{-7}$ $H \cdot m^{-1}$).

For characterizing the substance regarding the magnetic field the main quantities are magnetic susceptibility $\chi$ (dimensionless) and permeability $\mu$ ($H \cdot m^{-1}$). Magnetic susceptibility indicates the degree of magnetization of a material and is defined by the equation:

$$M = \chi H \qquad 1.11$$

Permeability is defined by the following equation:

$$B = \mu H \qquad 1.12$$

Magnetic field energy is considerably smaller than thermal energy or electrical energy; nevertheless it could have a great effect on processes by utilizing appropriate mechanisms based on quantum mechanics, electromagnetism and magnetic properties of materials. Magnetic field effects can be classified according to the properties of fields (steady or time varying, homogenous of gradient). Classification is given in a [152] and some of the effects described below.

*Table 1.2* **Summary of magnetic field effects**

| Magnetic field properties | | Effect |
|---|---|---|
| Time properties | Space properties | |
| Steady field | homogenous | Quantum effect (Zeeman effect) |
| | | Magneto-thermodynamic effect |
| | | Magnetic torque |
| | | Lorentz force |
| Time-varying field | Gradient field | Magnetic force (Faraday force) |
| | Alternating field | Eddy current |
| | High-frequency field | Energy injection |

- *Magneto-thermodynamic effect*

In the early stage of the studies on the role of magnetic field in chemical processes, main theoretical assumptions were based on thermodynamics.

Every substance has its magnetic free energy under the influence of a magnetic field. If this energy is considerably different for a reactant and a product, the reaction tends to proceed towards the lower magnetic free energy. The magnetic contribution $\Delta G_m$ to the free enthalpy of a reaction in a magnetic field of strength $B^0$ in a vacuum can be expressed by the following equation:

$$\Delta G_m = -{}^1/_2 \, \Delta\chi_M B_0^2 \qquad 1.13$$

Where $\Delta\chi_M$ is a change of the magnetic susceptibility during the reaction [153].

The value of $\Delta G_m$ is usually much smaller than that for a thermal energy even at high magnetic fields. However, if the ferromagnetic components take part in a reaction, the change in magnetic free energy might reach up to several tens of a percent of the thermal energy [152].

- *Lorentz force*

When charged particle moves in a magnetic field, it receives a Lorentz force that is proportional to the charge and velocity of the particle and the magnetic flux density according to the equation.

$$F_L = qvB \qquad 1.14$$

where q – an electric charge, v – velocity of charged particle and B applied magnetic field. In solutions, ions and charged particles cannot move alone due to the collisions with the solvent. As a result, Lorentz forces cause a convection of the solutions. This phenomena is on a basis of magnetohydrodynamics [152].

- *Magnetic force*

Magnetic force, called the Faraday force, is acting on a magnetic substance if it is positioned in a gradient field. This force is usually very weak for diamagnetic substances, however, some diamagnetic substances, such as water and organic compounds, can be levitated in air by applied fields up to 20 T and more. In contrast to Lorentz force where interacting quantity is an electrical charge, magnetic force is determined by the magnetic susceptibility of a substance.

$$F_{mag} = \mu_0 \chi H \frac{\delta H}{\delta z} \quad 1.15$$

where $\chi$ – isotropic magnetic susceptibility, $\delta H/\delta z$ the gradient of H (magnetic field strength) in the z-direction.

- *Quantum effects and dynamic spin chemistry*

In quantum theory, the particle having a spin is accompanied by a magnetic moment and can interact with a magnetic field. Nowadays, the magnetic field effects on the chemical reactions are mainly explained by these interactions and specific sub-field called *spin chemistry* has been developed. Spin chemistry can be regarded as a modern magnetochemistry. Dynamic aspects, such as chemical reactivity, dynamics and kinetics of magnetic phenomena in chemistry, may be called *dynamic spin chemistry* [152].

In contrast to thermodynamic and kinetic effects, the effects of external magnetic fields on a reaction involving a radical pair can be substantial [153]. Effects of magnetic field on the processes where radicals are involved can be explained by so called *radical pair mechanism*.

The radical has an unpaired electron and its spin can interact with a magnetic field. The spin can be described by the spin angular momentum operator $\hat{S}$.

$$\hat{S} = \hat{r} \times \hat{p} \quad 1.16$$

Where $\hat{r}$ is a position vector operator and $\hat{p}$ momentum operator. The most used operators are $\hat{S}^z$ and $\hat{S}^2 = \hat{S}^x + \hat{S}^y + \hat{S}^z$. The eigenstates of these operators are as follows:

$$\hat{S}^z|l,m\rangle = m\hbar|l,m\rangle \quad 1.17$$

$$\hat{S}^2|l,m\rangle = l(l+1)\hbar|l,m\rangle \quad 1.18$$

For a single spin $\frac{1}{2}$ (spin of the electron) the value of $l$ is $\frac{1}{2}$. The value of $m$ may be $\frac{1}{2}$ or - $\frac{1}{2}$, so there are two eigenstates of $\hat{S}^z$:

$$|l,m\rangle = \left|\frac{1}{2},\frac{1}{2}\right\rangle \text{ or } |l,m\rangle = \left|\frac{1}{2},-\frac{1}{2}\right\rangle \quad 1.19$$

Following alternative abbreviation for these will be used further in the text:

$$\left|\frac{1}{2},\frac{1}{2}\right\rangle \equiv \left|\frac{1}{2}\right\rangle \equiv |+\rangle \quad 1.20$$

$$\left|\frac{1}{2},\frac{1}{2}\right\rangle \equiv \left|-\frac{1}{2}\right\rangle \equiv |-\rangle \quad 1.21$$

If two electron spins interact there can be four combinations:$\{|++\rangle,|+-\rangle,|-+\rangle,|--\rangle\}$, where $|++\rangle$ means $|+\rangle_1$, $|+\rangle_2$, etc. The corresponding Hamiltonians are as follows:

$$\mathcal{H}|++\rangle = \frac{1}{4}J|++\rangle \quad 1.22$$

$$\mathcal{H}|-+\rangle = -\frac{1}{4}J|-+\rangle + \frac{1}{2}J|+-\rangle \quad 1.23$$

$$\mathcal{H}|--\rangle = \frac{1}{4}J|--\rangle \quad 1.24$$

$$\mathcal{H}|+-\rangle = -\frac{1}{4}J|+-\rangle + \frac{1}{2}J|-+\rangle \quad 1.25$$

Where $J$ is an isotropic exchange coupling parameter. The eigenstates of these four configurations are E = $J$/4 (3 times) and E =- 3$J$/4. The first three form a triplet and the last one a singlet. These configurations might be rewritten as follows:

$$|T_+\rangle = |\alpha_1\alpha_2\rangle \quad 1.26$$

$$|T_0\rangle = \frac{1}{\sqrt{2}}\{|\alpha_1\beta_2\rangle + |\alpha_2\beta_1\rangle\} \quad 1.27$$

$$|T_-\rangle = |\beta_1\beta_2\rangle \quad 1.28$$

$$|S\rangle = \frac{1}{\sqrt{2}}\{|\alpha_1\beta_2\rangle - |\alpha_2\beta_1\rangle\} \quad 1.29$$

Where α and β correspond to $|+\rangle$ and $|-\rangle$, respectively. The eigenvectors of these configurations are written below.

$$\psi_1 \equiv \begin{pmatrix}1\\0\\0\\0\end{pmatrix}\ \psi_2 \equiv \begin{pmatrix}0\\\frac{1}{\sqrt{2}}\\\frac{1}{\sqrt{2}}\\0\end{pmatrix}\ \psi_3 \equiv \begin{pmatrix}0\\0\\0\\1\end{pmatrix}\ \psi_4 \equiv \begin{pmatrix}0\\\frac{1}{\sqrt{2}}\\-\frac{1}{\sqrt{2}}\\0\end{pmatrix} \quad 1.30$$

Where $\Psi_1$, $\Psi_1$, $\Psi_1$ corresponds to a triplet state $T_+$, $T_o$ and $T_-$, respectively. Whereas $\Psi_4$ to a singlet. The four possible configurations are illustrated in Figure 1.13 [154].

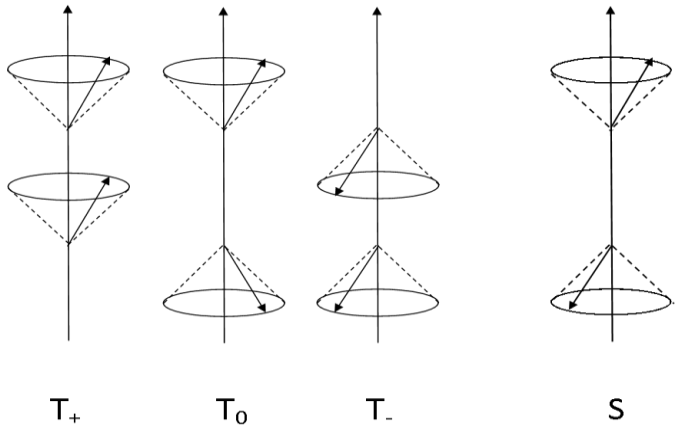


*Figure 1.13* **Configuration of triplet and singlet states or electron pair**

However, the spin state of the radical pair is not stationary. A pair of spins in singlet configuration can be induced into a triplet if their individual precession frequencies differ. If the frequencies differ by $\Delta\omega$, complete conversation will occur in a time $\pi/\Delta\varpi$. A difference of frequencies about the z-direction depends on the two spins experienced different fields along z. It is also possible for spins to experience different local field along the x and y directions. In this case twist of $\alpha$ into $\beta$ and vice versa is possible, therefore S can be evolved into $T_-$ or $T_+$.

These transitions are the result of magnetic interactions that are included in the Hamiltonian of a radical pair. The Hamiltonian of radical pair AB could be written as follows:

$$\mathcal{H}_{AB} = -J(2\boldsymbol{S_1}\boldsymbol{S_2} + 1/2) + g_A\beta BS_1^z + \sum_i^A \boldsymbol{S}_1 A_i \boldsymbol{I_i} + g_B\beta BS_2^z + \sum_k^B \boldsymbol{S_2} A_k \boldsymbol{I_k} \qquad 1.31$$

Where $\boldsymbol{S_1}$, $\boldsymbol{S_2}$ and $g_A$, $g_B$ are the angular spin momentum operators and the g-tensors of unpaired electrons on radicals A and B, $J$ is an isotropic exchange coupling parameter, $\beta_e$- Bohr magneton ($5.78\cdot10^{-5}$ eV/T), B- the flux density of applied external magnetic field, $A_i$, $A_k$ and $I_i$, $I_k$ are the isotropic hyperfine coupling tensors and nuclear spins in radicals A and B, respectively. Term - $J(2S_1S_2 + 1/2)$ corresponds to exchange interaction between electrons (Heisenberg exchange), $g_A\beta BS_1^z$ and $g_B\beta BS_2^z$ Zeeman interactions (direction of external field is taken as the z axis) and $\sum_i^A A_i I_i S_1$ and $\sum_k^B A_k I_k S_2$ electron -nuclear hyperfine interactions [155].

The hyperfine interaction (HI) is based on the interaction between spins of electron and nucleus. The hyperfine Hamiltonian has components of magnetic field in all three directions and therefore can induce transitions between the electronic singlet and all three triplet states. The rate of interconversations under the influence of HI depends on nuclear spin states of the radicals and therefore chemical reactions could be used for isotope separation on the basis of their spins rather

than masses [156]. This interactions leads also to a such phenomenon as magnetic polarization of both nuclei and electrons (CIDNP and CIDEP - chemically induced dynamic nuclear (electron) polarization) [155, 157].

Zeeman Effect (ZE) is based on the increase difference between $g_1$ and $g_2$ that is proportional to the applied magnetic field. This difference corresponds to a relative re-phasing of two spins around z- direction. It means that only $S \rightarrow T_0$ transition is possible. If the external field is >0.1T then Zeeman effect is dominant and $S \rightarrow T_{\pm}$ transitions are negligible.

Radiolysis of a molecule ($T_2$ or a-C:H, for example) leads to a formation of a singlet radical pair. The components of the radical pair diffuse apart, but they have a significant probability of re-encountering each other. If they re-encounter they may form a bond: this is geminate recombination and the product is called cage product. The bond will form, however, only if the radicals have single-phased electron spins when they re-encounter: if the electrons are triplet phased (parallel) the bond will not form and the encounter will be unproductive. If a singlet phasing of the radical pair is transferred into triplet, it follows that the probability of geminate recombination is reduced. In this case proportion of cage products declines relative to the escape products. Therefore the magnetic field will affect the proportions of cage and escape products [156].

### *1.9 Summary*

The World is on its way to a new, efficient and safe energy source – nuclear fusion. Scientists and engineers worldwide have done a great work to make this a near future reality. But still there is a lot of work ahead.

A lot of effort has been put into studies on tritium behaviour in the fusion reactor materials. Pathways of its accumulation and release have been studied both experimentally and theoretically. Several modelling codes have been developed. Mechanism of tritium transport in the lattice of beryllium has been estimated, but there is a lack measurement that would prove these assumptions. Initial and post - annealing chemical forms of tritium within the material lattice have not been analysed, only its chemical state in the purge gas. There is a lack of information of tritium behaviour in a real reactor conditions. Up to now tritium release experiments have been done by heating the sample, whereas influence of other factors present in the reactor has not been taking into account. It is well known that ionizing radiation can have a great impact of the physical and chemical processes, for example, radiation enhanced diffusion.

Effectd of the magnetic field that is an obligated component of the reactors also should be considered. The crucial effects of the magnetic field on the chemical and radiolysis processes has been described widely, but there is no data about its impact on tritium behaviour accumulated in the functional materials. Another important point is the detritiation of the fusion reactor materials; there are a number of proposed methods, but all of them have their advantages and disadvantages. If the use of the already existing factors in the reactor purposefully as a dertitiation tools would be possible it would be an excellent way to decrease detritiation expenses.

Methods and equipment developed in the UL Laboratory of Radiation Chemistry of Solids can attempt to solve these unanswered questions and give a input in further explanation and prediction of tritium behaviour in a real reactor conditions. These studies could also give a possibility to introduce corrections into the estimations of total tritium inventory in reactor materials. Estimation of the use of magnetic field and radiation as a potential detritiation tool also is possible with the equipment available in our laboratory.

# 2. EXPERIMENTAL

In this chapter studied samples are described, including the production methods and irradiation conditions, as well as experimental methods applied both to obtain information on the initial properties of the samples and accumulated tritium and to study tritium behaviour at different conditions. Some of these methods are developed in the laboratory of Radiation Chemistry of Solids, University of Latvia.

## *2.1 Samples*

In this study, several types of tritium containing materials have been investigated:

(1) *neutron multipliers* - neutron irradiated beryllium pebbles,

(2) *plasma facing materials* - beryllium and carbon fibre tiles exposed in plasma chamber of the fusion device *Joint European Torus (JET*).

Specification of these samples (production method, dimensions, etc) and the exposure, irradiation condition are described below.

### 2.1.1 Neutron multiplier – neutron irradiate beryllium samples

Two types of beryllium samples that have been irradiated in the experiments EXOTIC 8/3 (Extraction Of Tritium In Ceramics) and PBA (Pebble Bed Assembly) have been studied. All these irradiation programs have been performed in the *High Flux Reactor (HFR)* in Petten, the Netherlands. Description of the samples is given below.

- *Production*

Beryllium pebbles types have been produced by different methods. Metallic beryllium is obtained from the betrandite and beryl ores by the methods of chemical extraction, where the last step is beryllium fluoride reduction by magnesium metal. At this stage beryllium metal is obtained as spherical pebbles of (of ~2 mm in diameter) [158]. Further these pebbles can be processed by vacuum melting to eliminate impurities. Spherical beryllium powder (of 0.1-0.5 mm in diameter) that has been used in the experiment EXOTIC 8/3 is obtained by the Inert Gas Atomization method (IGA, manufacturer Brush Wellman, Inc, USA) [159], whereas pebbles of 0.9-1.1 mm used in PBA experiment by the Rotating Electrode Method (REP, manufacturer NGK, Inc, Japan) [160]. IGA is a commonly used technique for the production of metal powders requiring low oxygen content and spherically shaped particles. A high pressure (0.6 to 1.4 MPa at

BrushWellman, Inc), high velocity gas stream is used to break up a molten metal stream to form powder particles. The particles cool as they fall to the base of chamber where the powder is collected.

Pebbles for PBA experiment have been produced by the improved REP method that has been patented in 1999 by NGK, Inc [160, 161]. Production method is based on making an arc between plasma dissoluble electrode and a cylindrical column-like metal beryllium consumable electrode, both of which being disposed in a closed container filled with an inert gas as an atmosphere. While rotating, the beryllium electrode is melting and splashing droplets due to the centrifugal force. These droplets cool and solidify during their flight in helium. This method produces coarser material than the IGA method [160].

Pebbles have always a coarse grain microstructure, with much larger grains than beryllium materials produced by Hot Isostatic Pressing (40-200μm compared to 10μm) [162].

- *Irradiation conditions*

*EXOTIC 8/3–Tritium production and release from Li-ceramics*. End of irradiation 2000. This irradiation experiment was mainly foreseen to test lithium ceramics, nevertheless some beryllium samples were also included to study compatibility with structure materials.

Experiment EXOTIC 8/3 were designed to reach relatively high lithium burnup, >10%. For that purpose pebbles with 50% Li-6 enrichment were enclosed in a three coaxial annular beds: two beds with lithium containing pebbles separated by a bed with beryllium pebbles. These beryllium pebbles are used in this study. Annular beds were made of stainless steel and purged with helium and 0.1% $H_2$ mixture. Temperature of the beryllium was assumed to be 520-620$^{o}$C. EXOTIC 8/3 was in irradiation for 8 cycles, 449.8 full power days. The irradiation was performed in the core position with the typical neutron fluence rate of about $9\times10^{17}m^{-2}s^{-1}$ (fast, En > 0.1 MeV) and $5\times10^{17}$ $m^{-2}s^{-1}$ (thermal). Total flux of fast neutrons - $2.70 \times 10^{25}$ $m^{-2}$. [163].

*PBA – Pebble Bed Assembly - thermo-mechanical behaviour of breeder pebble-beds* End of irradiation 2004. The aim of this experiment was to test breeder pebble beds.

The basic tests elements were EUROFER-97 cylinders with a horizontal bed of ceramic breeder pebbles, either $Li_4SiO_4$ or $Li_2TiO_3$ (with a natural Li-6 abundance, 7%), sandwiched between two beryllium pebble beds from where samples for this study were obtained. The breeder and beryllium pebble beds were separated by EUROFER-97 steel plates (14 mm) and purged with helium and 0.1% $H_2$ mixture. Temperature of beryllium was in range of 150-550$^{o}$C

depending on the position. Total flux of fast neutrons - 3-4 × $10^{25}$ $m^{-2}$ (En>0.1 MeV) and 1.5-2× $10^{25}$ $m^{-2}$ (En>1 MeV) [34].

Basic description of the samples and irradiation conditions are summarized in the Table 2.1

*Table 2.1* **Description of the samples**

| | **PBA** | **EXOTIC 8/3-13** |
|---|---|---|
| ***Manufacturer*** | NGK Insulators Ltd., Handa City, Japan | Brush Wellman Inc., Cleveland, Ohio, USA |
| ***Production process*** | Rotating Electrode Process (REP) | Inert Gas Atomization (IGA) |
| ***Pebble diameter, mm*** | 0.9-1.1 | 0.1-0.2 |
| ***Main impurities*** | 2300 ppm BeO,<br>300 ppm Mg | 3400 ppm BeO,<br>100 ppm Mg |
| ***Irradiation time*** | 294 days | 449.8 days |
| ***Neutron fluence (E>0.1 MeV)*** | 3-4 × $10^{25}$ $m^{-2}$ | 2.70 × $10^{25}$ $m^{-2}$ |
| ***Irradiation temp.*** | 150-550 $^{o}$C | 520 -620$^{o}$C |
| ***$^{4}$He content*** | 300-600 appm | 285 appm |
| ***Year of end of irradiation*** | 2004 | 2000 |

- *Sample preparation*

These samples did not require any specific preparation since they were in a form of small pebbles. In case of PBA in each experiment one pebble per test were used. Each pebble were weighed with the analytical balance (d=0.00001 g). In case of EXOTIC 8/3 2-4 mg of the pebbles in each test were used (due to very small size of a separate pebble).

### 2.1.2 Plasma facing materials (limiters) - beryllium tiles exposed in JET plasma chamber

The analysed samples were beryllium belt-limiters that protected the main plasma chamber wall during the campaigns in 1989-1992 operation period of JET. In this study two exposed tiles and one unexposed tiles were used (Figure 2.1).

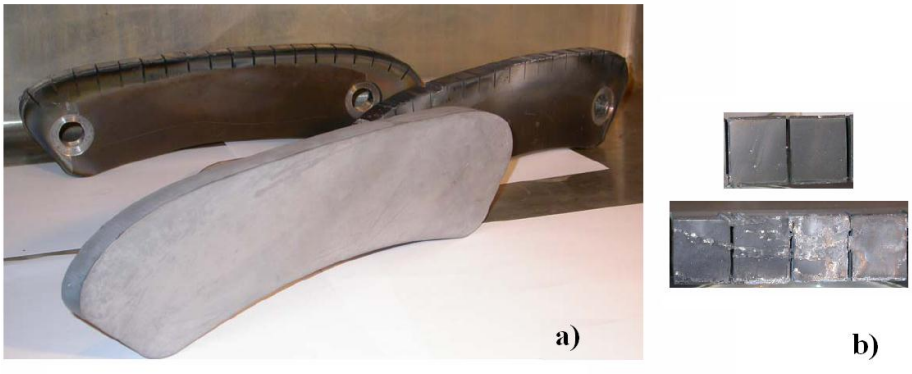


*Figure 2.1* **Beryllium tiles: a) overall view of two exposed and one unexposed tiles, b) castellated plasma facing surface with deposition layer (above) and melted parts (below)**

- *Production*

Analysed tiles were manufactured to near net shape by a (JET-developed) HIP (Hot Isostatic pressed) method from the S65b powder with addition sinter and cold-pressing process [95]. At the HIP process loose beryllium powder are placed in a steel can which is welded shut after degassing at elevated temperature. The sealed can is then placed into a pressure vessel where it is heated and then pressed from all directions simultaneously (isostatically) by argon gas. Simple shapes made by HIP have minimal anisotropy in mechanical properties [159]. Castellation and plasma-facing surface of the tiles were machined after fabrication [95].

- *Exposure conditions*

Analysed tiles have been placed in a plasma chamber with the castellated surface facing the plasma. Tiles were separated by 4-5 mm wide gaps with inconel plates as spacers. All castellated groves were toroidal, whereas the gaps between tiles were in poloidal direction. Beryllium belt-limiter tiles had operated for approximately 56,000 s in the plasma chamber. In the 1990-1992 JET configurations, limiter plasmas were obtained up to a maximum plasma current of 7 MA. In the end of the year 1991 The Preliminary tritium experiment (PTE) has been performed with a total amount of tritium injected into torous of 53 (±4) Ci or 1,96 TBq [164] Plasma containing 11% of tritium in deuterium produced a peak fusion power of 1.7 MW for 2 s and a fusion gain 0.12 [47]. Both the plasma facing surface and the inner surface of castellation have a visible deposition layer or melted areas.

- *Preparation of samples*

The exposed beryllium tiles investigated were denoted as tiles "A" and "B". Samples having a defined surface area about 0.5 $cm^2$ and thickness of 2–3 mm were cut from separate "teeth" (area between castellation) of the operating surface. Activities with beryllium materials were performed in a special beryllium workshop developed in the laboratory according to the European safety standards on the work with beryllium (due to its high toxicity).

### 2.1.3 Plasma facing materials (divertor) - CFC tiles exposed in JET plasma chamber

The analysed tile was from the MkII Septum Replacement Plate (MkII SRP) divertor used in the 2001-2004 operation period of JET: a cross-sectional view is shown in Figure 2.2.

- *Production*

The analysed tile is made of Carbon Fibre Composite, Concept I manufactured by Dunlop Ltd (CFC) [165]. It is manufactured from fibre reinforced graphite by chemical vapour deposition (graphitization) with methane and it has a 2D woven fibre sheets arrangment.

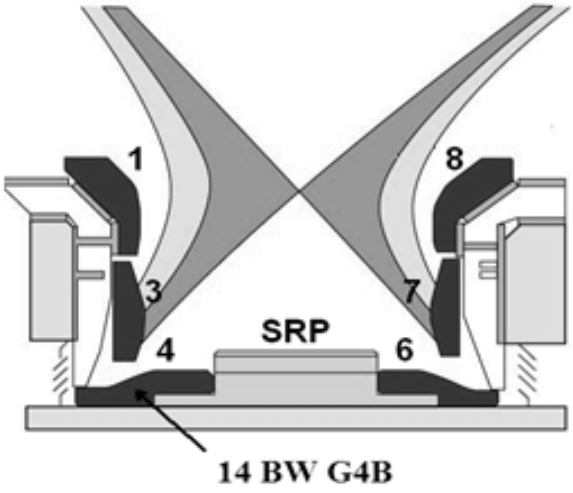


*Figure 2.2* ***Cross -section of the JET MkII Septum Replacement Plate divertor (SRP)***

- Exposure conditions

Tile were placed in the plasma chamber with the weave planes normal to the plasma facing surface [137]. The divertor tiles are bolted to carriers connected to a water cooled structure, so the backs of the tiles are indirectly cooled following plasma heating of the front surfaces: bulk temperature between pulses is ~100$^{o}$C.

Since the greatest tritium accumulation occurs on the inner divertor shadowed areas [166], tile 4 (14BWG4B) has been selected for this investigation (Figure 2.2). During the operation period no full D-T mixture discharges were made, however in the year 2003 the Trace Tritium Experiment had been performed with an introduction of 380 mg tritium (133.5 TBq) into the vacuum chamber. Tritium was introduced by the methods of gas puffing and neutral beam injection; therefore, both the thermalised $T^+$ and fast $T^+$ (~100 kV) were present in the plasma chamber. During the exploitation period tritium ions with energy up to 1 MeV had also been produced as a result of D + D reactions [167].

Plasma interaction was essentially limited to the sloping part of tile 4, since the rest of the tile was shadowed. During the SRP campaign the inner strike point was on tile 4 for a total of $\sim 4 \cdot 10^4$ seconds, and, assuming a similar distribution of ion fluxes per second for pulses with strike points on tile 3 (which can be measured by Langmuir probes ), the integrated ion flux for the campaign would be of the order $10^{27}$ ions$\cdot m^{-2}$ [145].

- *Preparation of samples*

Samples for the analysis of tritium and structure were made by a core-drilling method. Cylinders (ø 1 cm and 1.5 cm) were cut from the CFC tiles normal to the plasma exposed surface (and thus parallel to the tile planes, including a number of such planes) and sliced into separate slices of thickness 1 mm. From tile 14BWG4B 66 cylinders were core- drilled (11 rows in poloidal and 6 rows in toroidal directions) in order to give a comprehensive picture of the tile (see below) and each sliced into 11 – 23 slices depending on the thickness of the tile at the particular position. In Figure 2.3 the labelling and positions of the 1st row cylinders drilled out of the tile is shown. Because of the differences in exposure conditions, the tile was divided virtually in three parts (Figure 2.2 and Figure 2.3):

I "SRP part" - horizontal part of tile nearest the SRP that has some exposure to plasma and some shadowing from SRP tile. Deposition layer about 10μm or less [165].

II "Sloping part" – sloping part of the tile that has been exposed to plasma and is the furthest part into the corner of the divertor that can be reached by the plasma. Deposition layer can reach thickness up to 300 μm, dusty in nature and of low density [165].

III "Shadowed part" – horizontal part of tile shadowed from the plasma by tile 3, deposition layer up to 250 μm in form of a smooth, dense film with high H/C ratio [145].

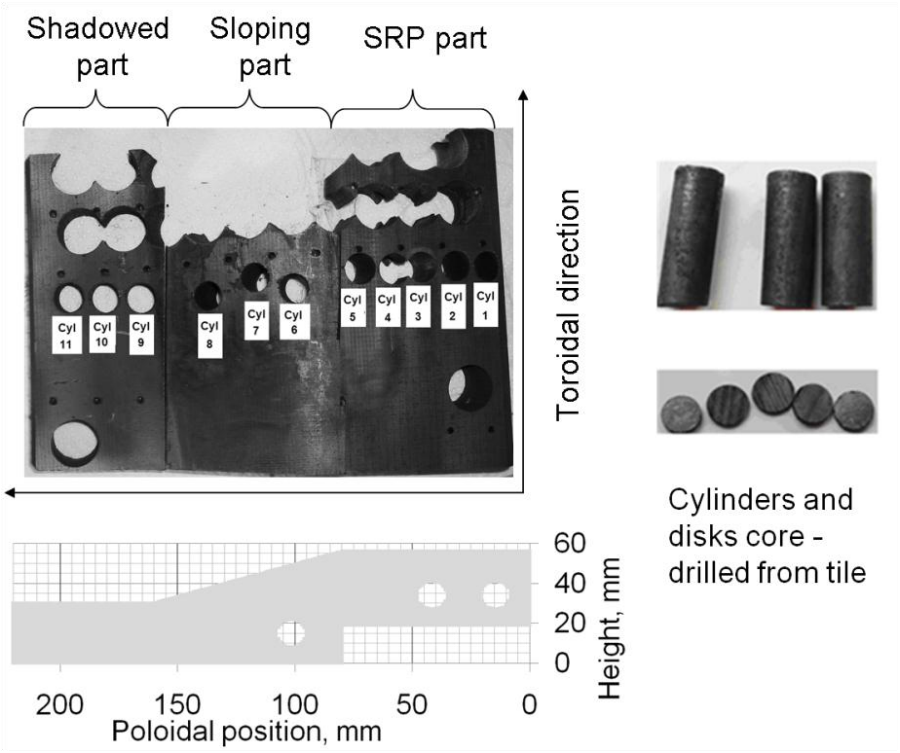


*Figure 2.3* ***Preparation and labelling of the carbon tile samples***

## *2.2 Methods*

Both destructive and non-destructive methods have been used in this study.

### 2.2.1 Structure and chemical composition

Methods used for structure and chemical composition analysis were scanning electron microscopy SEM, energy dispersive X-ray analysis EDX and X-ray diffraction analysis XRD. Structure of the materials could have a crucial role both in the durability of a material in the reactor condition and in the tritium inventory processes. Evaluation of the chemical impurities in the fusion reactor materials is an important issue due to several reasons. The main of them are:

- chemical interactions with tritium (especially in case of oxygen);
- activation as a result of neutron induced transmutation (cobalt, etc);
- creep phenomena in the beryllium materials due to impurities with low melting point [168].

Analysis of the neutron irradiated beryllium samples is quite complicated due to their gamma activity (even in high purity beryllium there is appm level of $^{59}$Co that transforms into unstable $^{60}$Co as a result of neutron irradiation). This radioactivity leads to significant restrictions

on the sample handling. Chemical analysis of the beryllium pebbles is complicated also due to the beryllium transparency to x-rays (EDX and other methods based on detection of the X-rays).

SEM method has been used for the structure analysis of both beryllium and CFC samples. Metallic samples were prepared by the polishing with SiC sandpaper and then by diamond pastes of 6, 3, 1 and 0.05 μm. CFC samples were prepared by cutting slices and then cleaning from the dust mechanically (possible impact of the mechanical cleaning on the structure were controlled). Two Scanning electron microscope devices were used in this study - Hitachi S-4800 and Zeiss EVO-50. The latter was equipped with an EDX detector and gave a possibility to obtain information on the chemical composition of the sites of interest of the samples. For the structure analysis beam energy 2 kV and beam current 15 μA were chosen, whereas for the chemical composition up to 22 kV was used. XRD analysis has been used to assess BeO content in the samples from the plasma facing materials and tile structure itself in case of CFC. X-ray diffraction analysis device Bruker D8 Advanced has been used.

SEM and BSE images have been analysed by the *ImageJ* program [Developed by W. Rasband, National Institute of Health].

### 2.2.2 Tritium distribution and chemical forms

In order to determine total tritium activity, bulk distribution and abundance ratios of chemical forms ($T_2$,$T^0$,$T^+$) in irradiated beryllium samples, chemical scavenger and dissolution method has been used. This method had been originally developed in the UL Laboratory of Radiation Chemistry of Solids within this study.

Samples are dissolved in the solutions of $2\,mol\cdot L^{-1}\,H_2SO_4$ and $2\,mol\cdot L^{-1}\,H_2SO_4 + 0.5\,mol\cdot L^{-1}\,Na_2Cr_2O_7$ in a special setup (Figure 2.4) [169].

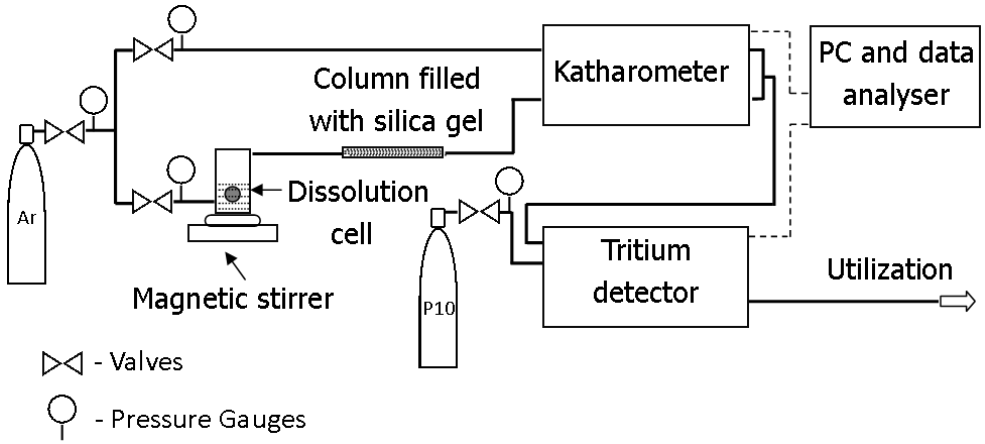


*Figure 2.4* **Scheme of a setup for dissolution of beryllium samples**

Following processes are taking place during the dissolution:

$$Be^0 + 2H^+ \rightarrow Be^{2+} + 2H^0 \qquad 2.1$$

$$H^0 + H^0 \rightarrow H_{2\,(gass\,ph.)} \;\; K \approx 1 \times 10^{10} L \cdot mol^{-1} s^{-1} \qquad 2.2$$

$$H^0 + T^0 \rightarrow HT_{(gass\,ph.)} \;\; K \approx 1 \times 10^{10} L \cdot mol^{-1} s^{-1} \qquad 2.3$$

$$6H^0(T^0) + Cr_2O_7{}^{2-} + 8H^+ \rightarrow 2Cr^{3+} + 7H_2O_{liquid\,ph.} \qquad 2.4$$

$$K \approx 2.6 \times 10^{10} L \cdot mol^{-1} s^{-1}$$

$$T_{2\,(solid\,ph.)} \rightarrow T_{2\,(gass\,ph.)} \qquad 2.5$$

$$T^+{}_{(solid\,ph.)} \rightarrow T^+{}_{(liquid\,ph.)} \qquad 2.6$$

In the solution of $2\,mol \cdot L^{-1}\,H_2SO_4$ molecular and atomic tritium ($T_2$ and $T^0$) of the activities $\underline{A_{T2}}$ and $A_T{}^0$ respectively, present in a Be sample transfer as $T_2$+$HT$ into a flow of carrier gas, where the tritium activity released (1) was measured with tritium monitor TEM 2100A with a proportional gas flow-through detector DDH 32. Detector has been calibrated with tritiated water of definite activity (calibration factor $K_D$, Bq·cps$^{-1}$·m$^{-3}$).

$$A_{T,gas.,acid} = A_{T_2} + A_{T^0} \qquad 2.7$$

$T^+$ localized in a Be layer remains in the solution and the tritium activity $A_{T\_sol\_acid}$ was measured with liquid scintillation method. Solution containing tritium was distilled and 1 or 5 mL (depending of a tritium activity, in case of 1mL of sample solution 4mL of distilled water added) aliquot mixed with 15 mL of *Ultima Gold* scintillation cocktail and analysed for total tritium with a TRi-Carb 2910TR counter [PerkinElmer, Inc].

90% of $H^0$ ($T^0$) reacts with the scavenger $Na_2Cr_2O_7$ in the solution of $2\,mol \cdot L^{-1}\,H_2SO_4 + 0.5\,mol \cdot L^{-1}\;Na_2Cr_2O_7$ and remains in the solution. Activity of the tritium released into a gas phase and retained in the solution are the respective sums:

$$A_{T,gas.,Cr(VI)} = A_{T_2} + xA_{T^0} \qquad 2.8$$

$$A_{T,sol.,Cr(VI)} = A_{T^+} + (1-x)A_{T^0} \qquad 2.9$$

Where value x was found experimentally to be 0.1 (10%). The contents of $T^0$,$T_2$, $T^+$(Bq g$^{-1}$) in a sample were determined separately from the corresponding differences in the activities by following equations:

$$A_{T^0} = \frac{A_{T,gas.,acid} - A_{T,gas.,Cr(VI)}}{(1-x)} \qquad 2.10$$

$$A_{T_2} = A_{T,gas.,acid} - A_{T^0} \qquad 2.11$$

$$A_{T^+} = A_{T,sol.,acid} \qquad 2.12$$

Activity of tritium in a gas flow is calculated by the following Equation 2.13

$$A_T = \frac{vK_D\Delta t}{3600 \cdot 1000} \cdot R_T \qquad 2.13$$

where, $A_T$ – the released tritium activity, Bq;

$v$ –gas flow, $L \cdot h^{-1}$;

$K_D$ – calibration factor, $Bq \cdot cps^{-1} \cdot m^{-3}$;

$\Delta t$ – experiment time, s;

$R_T$ – mean anticoincidence value, cps.

Amount of released tritium atoms can be calculated by means of the tritium decay constant $\lambda = 1{,}75\ 10^{-9}\ s^{-1}$ (Equation 2.14)

$$N_T = \frac{A_T}{\lambda} \qquad 2.14$$

where, $N_T$ – detected quantity of tritium atoms;

$A_T$ – the released tritium activity, Bq;

$\lambda$ – tritium decay constant, $s^{-1}$.

Calculations on tritium distribution in the bulk of the pebble are based on the controlled dissolution process of pebble and simultaneous tritium measurements. One hydrogen molecule corresponds to one beryllium atom (1) and the dissolution rate of beryllium (and hereby also the thickness of dissolved layer for the estimation of tritium bulk distribution) can be calculated from the hydrogen measurements. The rate of hydrogen evolution was measured with a katharometer

If dissolution process of the beryllium pebble starts at $t = t_0$ and radius of the pebble in this moment is $r_0$, it could be calculated as follows (Figure *2.5*):

$$r_0 = \sqrt[3]{\frac{3m_0}{4\pi\rho_{Be}}} \qquad 2.15$$

where, $r_0$ – theoretical radius of the pebble, cm;

$m_0$ – mass of the pebble, g;

$\rho_{Be}$ – beryllium density, $g/cm^3$.

Radius of the pebble in the moment t therefore is calculated as follows:

$$r_t = \sqrt[3]{\frac{3(m_0 - \Delta m_t)}{4\pi\rho_{Be}}} \qquad 2.16$$

Where $\Delta m_t$ is a mass of dissolved beryllium at the moment *t* and can be calculated from the released hydrogen amount (tritium gas contribution is negligible and therefore is not taken into account).

$$\Delta m_t = \frac{N_{H_2}}{N_A \cdot M_{Be}} \qquad 2.17$$

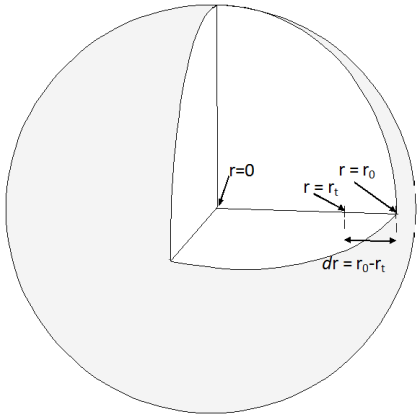


*Figure 2.5* **Estimation of dissolved layer**

Specific mass tritium activity of beryllium pebble:

$$A = \frac{\int_{t_0}^{t_b} A_T dt}{m_0} \qquad 2.18$$

where, A - relative tritium activity in the beryllium, $Bq \cdot g^{-1}$;

$A_T$ – the released tritium activity, Bq;

$m_0$ – mass of pebble, g.

In this method pebble is regarded as a perfect sphere and assumed that tritium concentrations in all points of a sphere with radius $r_t$ is equal. Therefore only the overall tendency of tritium distribution is obtained.

- *Wet oxidation method (carbon based materials)*

In order to determine tritium content in carbon fibre samples wet oxidation (combustion) technique proposed by Vance et al. [170] and employed in study JET-P(99)53 [171] was used. A scheme of the glass experimental apparatus used is shown in Figure 2.6. Combustion of a separate carbon disc was normally performed at a temperature of 850-870$^{o}$C in a flow rate of

moistened air of 15-20 mL/min. Tritium was collected in two bubblers (volumes of distilled water 100-200 mL and 100 mL respectively); 98-99% of tritium was collected in the first bubbler. The time for complete combustion, 4-6 h, depends on the mass of the sample being combusted. After each combustion 5 mL water aliquots were taken from each of the two bubblers. Each of these aliquots was mixed with 15 mL of *Ultima Gold* scintillation cocktail and analysed for total tritium with a TRi-Carb 2910TR counter [PerkinElmer, Inc].

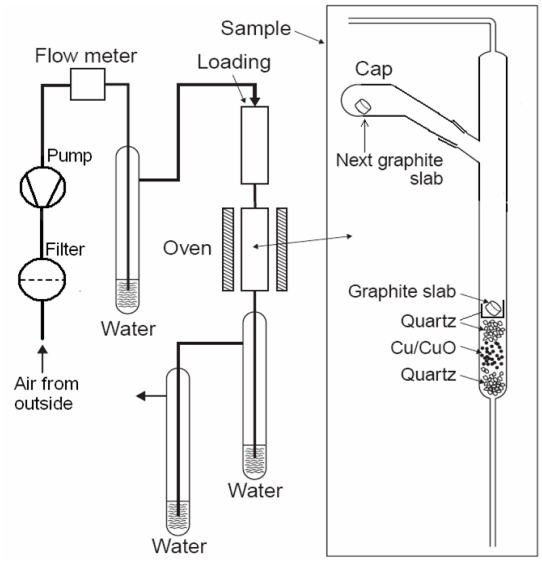


*Figure 2.6* **Scheme of a modified Vance apparatus for the combustion of carbon samples**

### 2.2.3 Tritium thermo desorption

Tritium release experiments were performed in a setup enabling annealing at temperatures up to 1040-1280$^{o}$C with and without exposure to the fast electrons (5 MeV) and magnetic field (1.7 T). So called Thermo-magnetic rig has been developed in the Laboratory of Radiation Chemistry of Solids (UL) and is based on the electron accelerator LINAC-4. Schematic view of this original experiment setup is given in Figure 2.7.

Tritium release from beryllium samples was performed in a quartz tube of 156 cm$^3$, consisting of two compartments – one for the sample and one for a bed of granulated zinc. The tritium release was performed in a continuous flow of the purge gas He + 0.1% $H_2$ of the rate 14.5-14.9 L/h. The sample temperature was initially increased linearly with time at a constant rate of 2.3-4.8$^{o}$C/min from room temperature up to an end temperature (varies in different experiments from 280$^{o}$C up to 1280$^{o}$C), which was kept constant for a determined time (from 1 h up to 5 h).

Temperature of the sample (thermo-emfs of the type S and K thermocouples) and the Zn bed (thermo-emf of the type K thermocouple) were continuously measured. Tritium activity in the purge gas, which was derived from the count rate of proportional detector DDH 32 of the operating volume 300 $cm^3$, was continuously measured with tritium monitor TEM 2102A

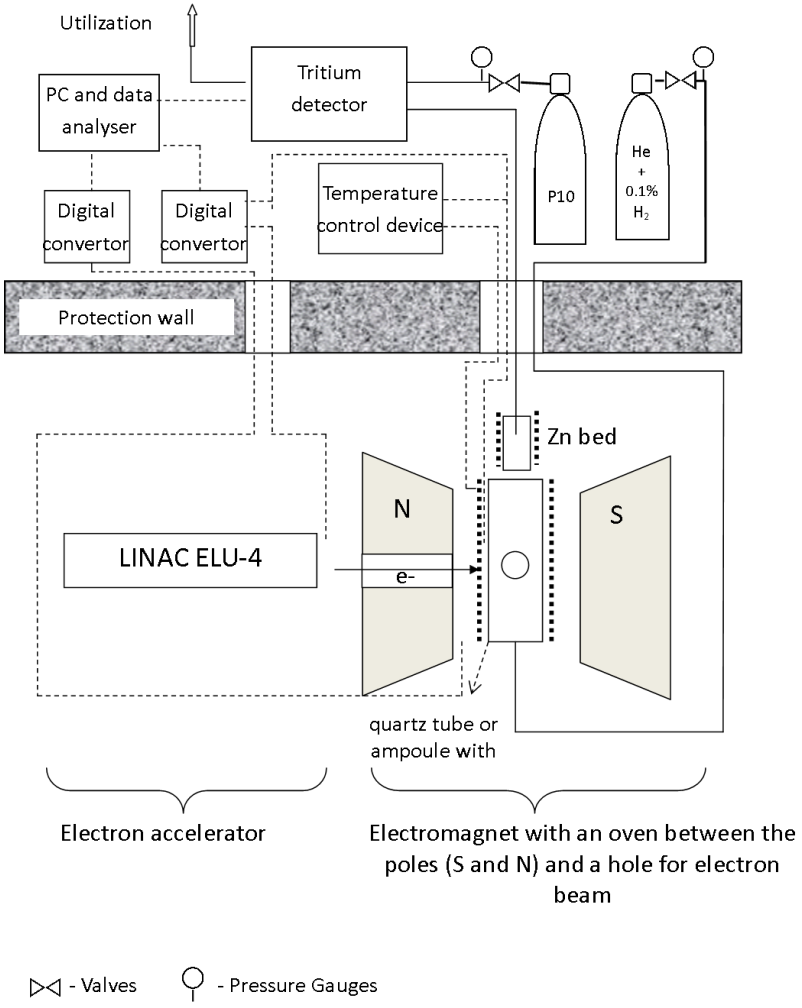


*Figure 2.7* **Schematic view of a Thermo-magnetic rig**

Energy transfer of the external fields in the desorption experiments has been calculated for better interpretation of the results later.

- *Thermal heating*

Absorbed energy by the sample during thermal treatment can be calculated based on thermal properties of the material (thermal capacity) according to the following equation.

$$E_{absorbed} = a \cdot (T_2 - T_1) + \frac{b}{2} \cdot (T_2^2 - T_1^2) - c \cdot \left(\frac{1}{T_2} - \frac{1}{T_1}\right) \qquad 2.19$$

Where $T_1$ and $T_2$ are the start and the end temperature, respectively, whereas values of a, b, c are the constants. For beryllium, in the temperature range of 25-1283$^{o}$C these constants are:

$a$ = 19.16; $b$ = 0.00887; $c$ = -477000.

According to the equation above, in the experiment where 1 mg beryllium pebbles is heated up to 280$^{o}$C the absorbed energy is 0.567 J per pebble

- *Fast electron flux*

Fast electrons carries considerable amount of energy that is transferred to the sample during exposure.

$$\Phi_e = \frac{I}{e \cdot S} \qquad 2.20$$

where

$I$ - current (in the irradiation experiments - 6μA)

$e$ - elementary charge ($1.602 \cdot 10^{-19}$C)

$S$ - electron beam cross section (0.000314 m$^2$).

The calculated value of electron flux is $1.19 \cdot 10^{17}$electrons$\cdot$m$^{-2}\cdot$s$^{-1}$. Energy flux therefore is electron flux multiplied with energy of one electron, in this case 5 MeV. That gives the value of energy flux carried by electrons $5.96 \cdot 10^{23} eV \cdot m^{-2} \cdot s^{-1}$ or 95.5 $kJ \cdot m^{-2} \cdot s^{-1}$.

Total energy of electrons exposing the sample during experiment can be calculated as follows:

$$E_0 =\cdot \Phi_e \cdot S \cdot t \qquad 2.21$$

where

$S$ – exposed area of a sample, m$^2$;

$t$ – time of the exposure, s.

Energy absorbed by a sample:

$$E_{absorbed} = E_0 \cdot e^{-\frac{\mu}{\rho} l} \qquad 2.22$$

where

μ/ρ – mass attenuation coefficient, m$^2$kg$^{-1}$;

$l$ – thickness of a sample, m.

Absorbed energy by a beryllium tile sample of the size 0.5×0.5×0.5 cm (dimensions of the samples cut from the beryllium tiles, Figure 2.8) is 4.7 J$\cdot$s$^{-1}$. If experiment lasts for one hour, then total absorbed energy is about 17,13 kJ.

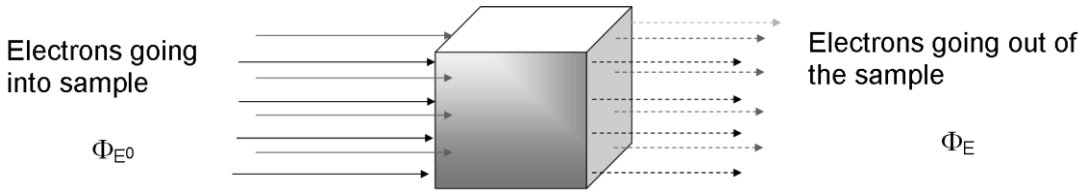


*Figure 2.8* **Schematic view of electrons penetrating the cubic beryllium sample**

For the samples of different shape these calculations are more complicated. Calculations for a beryllium pebble are given below (Figure 2.9).

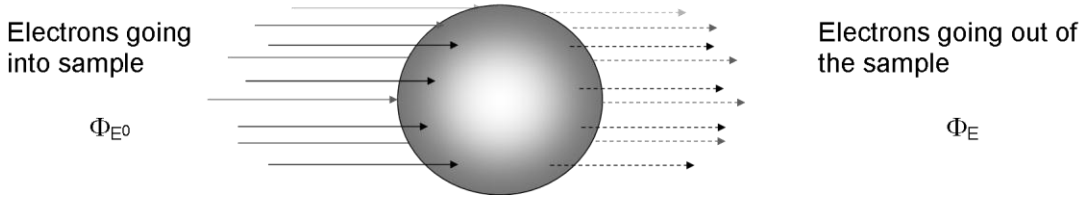


*Figure 2.9* **Schematic view of electrons penetrating beryllium pebble**

The average thickness of a sample is calculated by transferring mathematically sphere into cylinder by dividing its volume by cross section, $V \cdot S^{-1}$, m.

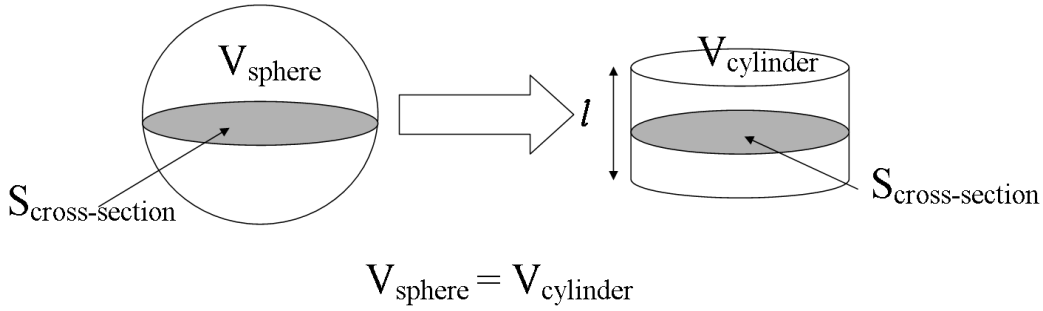


*Figure 2.10* **Mathematical transfer of sphere into cylinder**

If to assumed that pebble is 1 mg of mass and ideally spherical the absorbed energy in experiment 1h long is 0.85 kJ

- *Fast electron flux in a magnetic field*

To ensure that magnetic field effect is correctly estimated, its impact on the electron beam and transferred energy has been measured experimentally and calculation done. It was found that electron beam is focused.

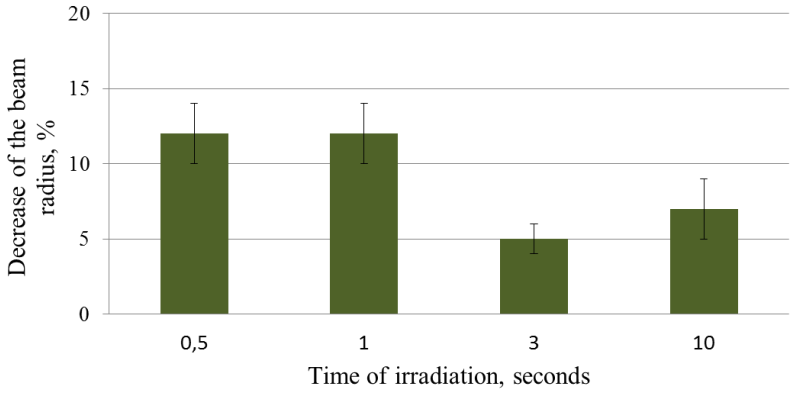


*Figure 2.11* **Focusing of the electron beam in the magnetic field**

If to compare absorbed energy by one 1 mg beryllium pebble in all three experiments then it can be found that at treatment in temperature it is 0.6 J, radiation - 848.1 J, radiation in the presence of magnetic field - 932.9 J (due to the focusing of the beam).

### 2.2.4 Tritium effective diffusion coefficient

Tritium effective diffusion coefficient has been calculated from the thermo desorption data. Calculation method has been developed by A. Vitins and it is based on an equation for diffusion in a sphere in non-steady state. Tritium distribution in a pebble is assumed to be uniform and a surface concentration - constant. Total amount of diffusing substance leaving a sphere of radius $r_0$ is given as a function of time, t:

$$f = 1 - \frac{6}{\pi^2}\sum_{n=1}^{\infty}\frac{1}{n^2}e^{-\frac{n^2\pi^2 Dt}{r_0^2}} \qquad 2.23$$

where $f$ is a fraction of released tritium and $D$-its diffusion coefficient. For approximation when f>0.4, only the first term of the series may be used and then the equation 2.23 can be reduced to a linear equation 2.24.

$$ln(1-f) = -\frac{\pi^2 Dt}{r_0^2} - ln\frac{\pi^2}{6} \qquad 2.24$$

### 2.2.5 Tritium thermo sorption

Tritium sorption experiments have been performed to study mechanisms of tritium accumulation in beryllium materials in plasma chamber. For investigations of tritium sorption, 5mm×5mm×5mm cube-shaped Be samples from the non-irradiated limiter tile were used. A Be pebble irradiated in the BERYLLIUM experiment was used as a tritium source in an ampoule

(one Be pebble in each ampoule for three Be samples). Quartz ampoules 50cm in length were degassed to pressure 0.13 Pa and sealed. The Be pebble placed apart from Be samples was heated at 1030$^{o}$C for 3 h. After that thermal sorption of gaseous tritium $T_2$ in the cube-shaped Be samples was performed at 500$^{o}$C for 3 h both without and with electron radiation and/or MF. The partial pressure of tritium in the ampoules after the tritium sorption was determined in the following way. A single ampoule was broken with flat nose pliers in a bendable plastic tube with flowing moistened air (15 L/h) inside. The airflow was maintained by a built-in air pump WISA 300 of a tritium monitor TEM 2100A. The tritium activity in the airflow was measured with a tritium monitor TEM 2100A with a detector DDH 32. The total activity of tritium in the ampoule was determined. Taking the volume of the ampoule (9–13 cm$^3$) into account, the partial pressure of tritium in the ampoule was calculated according to the rule of ideal gases (Equation 2.25):

$$pV = NkT, \qquad 2.25$$

where $p$ is the pressure, $V$ is the volume, $N$ is the number of molecules, $k$ is the Boltzmann constant and $T$ is the temperature. 2.8–6.2MBq of tritium had been released into gaseous phase corresponding to the partial pressure of $T_2$ 0.8–1.7 Pa at 500$^{o}$C. The concentration of $T_2$ in ampoules was $8\times10^{13}$ to $2\times10^{14}$ molecules·cm$^{-3}$, which corresponds to the conditions of JET.

# 3. RESULTS AND DISCUSSION

In this study, materials foreseen for the application in two conceptually different fusion reactor components, blanket modules and vacuum vessel, has been investigated. Due to large differences in application and exposure conditions these two groups of materials are discussed separately. First part of the results and discussion section is devoted to neutron multipliers - beryllium pebbles, second - to the plasma facing materials - solid beryllium and carbon fibre composite tiles. In the third part the main tendencies of tritium behaviour under the specific conditions of fusion reactor materials are discussed.

One of the most efficient methods for behaviour studies of tritium accumulated in solid materials is the temperature programmed desorption (TPD). Tritium desorption from the materials has been studied also under action of such external energetic factors as fast electron irradiation and high magnetic field. Results of these experiments provide better understanding on tritium behaviour in the conditions similar to the magnetic confinement fusion (MCF) devices and give possibility to compare material reliability for fusion applications regarding the detritiation options. In order to describe and predict tritium behaviour during desorption from neutron irradiated or tritium containing plasma exposed samples, it is necessary to estimate factors that may affect transport mechanisms. Therefore preliminary examination of the samples has been performed before the tritium release measurements for each group of the materials. Such crucial properties as structure, chemical impurities of the samples as well as tritium initial bulk distribution and chemical forms have been assessed.

## *3.1 Neutron multipliers – neutron irradiated beryllium pebbles*

As a result of neutron irradiation helium and tritium generate in the bulk of beryllium pebbles. Accumulation of these gaseous species depends highly on the structure of the pebble and the chemical impurities.

### 3.1.1 Preliminary examination

- *Structure and chemical composition*

Structure and chemical composition analysis has been performed for the samples irradiated with neutrons in the PBA and EXOTIC 8/3 experiments. If one compares the surface morphology and overall shape of pebbles it is obvious that pebbles irradiated in PBA experiment and produced by REP method are more spherical and the surfaces are smoother than that for pebbles

produced by IGA method from EXOTIC 8/3 irradiation. Pebbles from EXOTIC 8/3 are irregular, several of them stacked together and the surface seems to have layers (Figure 3.1).

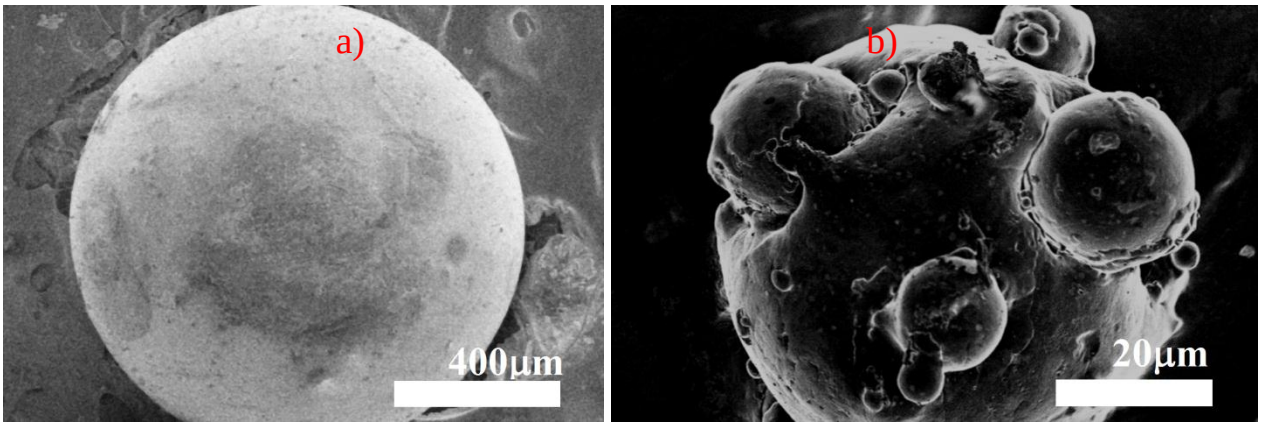


*Figure 3.1* **Beryllium pebbles from PBA and EXOTIC 8/3 experiments. a) PBA pebble, b) EXOTIC 8/3 pebbles**

Pebbles from the EXOTIC 8/3 experiment can be classified into three groups according to the structure: spherical pebbles with a smooth surface (I), pebbles with layers on a surface (II) and pebbles with porous structure reminding a strawberry (III) (Figure 3.2).

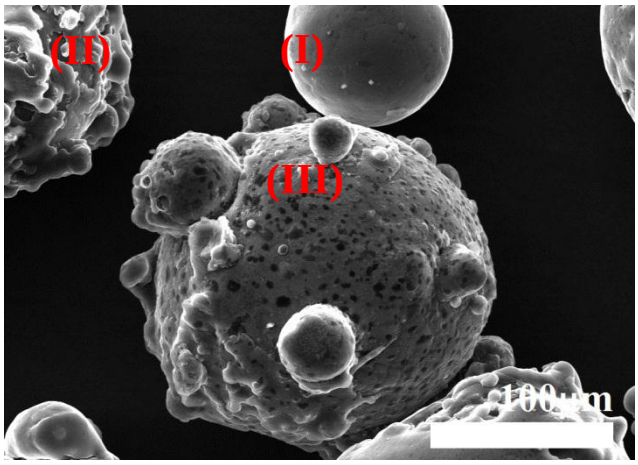


*Figure 3.2* **Three types of the beryllium pebbles form EXOTIC8/8 experiment: (I) smooth and spherical, (II) layered, (III) porous ("strawberry" structure)**

There is also significant size diversity of the pebbles form experiment EXOTIC 8/3. Size distribution of the pebbles has been also studied to ease the interpretation of data on tritium diffusion (Figure 3.3).

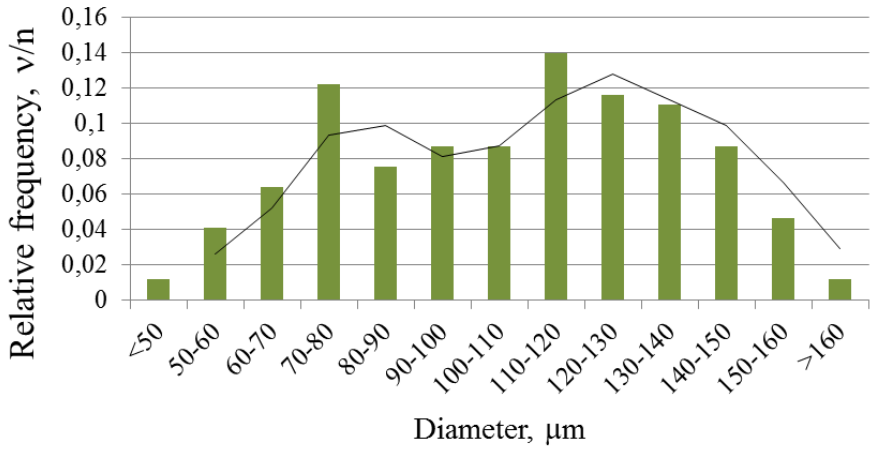


*Figure 3.3* **Distribution of the EXOTIC 8/3 pebbles size**

Chemical composition of the pebbles from experiments EXOTIC 8/3 and PBA were analysed and compared by the EDX method in the Institute of Solid State Physics. Analyses revealed that fraction of EXOTIC 8/3 pebbles is strongly oxidized (pebbles type 3, porous – "strawberry" structure) (Figure 3.4), whereas PBA pebbles have comparably small content of oxygen (thin oxide layer on the surface). Description given by the manufactures (see chapter 2.1.1) did not show significant differences in oxide content, therefore it might be assumed that oxidation of beryllium pebbles took place during the irradiation. That could be a result of interaction with lithium silicates. Although the experimental setup of irradiation beryllium and silicate samples are separated by the annular steel tubes [163], some signs of Si were found on the surface of beryllium pebbles that might prove the fact of direct contact during the irradiation. One example of the chemical interactions between lithium orthosilicate and beryllium during neutron irradiation is shown below ($T_2$ and He in the right side of the reaction come from neutron induced transmutations, one Be atom might be transformed into one helium plus one tritium atom):

$$100Li_4SiO_4 + 36Be \rightarrow 64Li_4SiO_4 + 36Li_2SiO_3 + 72He + 36T_2 + 36BeO \qquad 3.1\ [172]$$

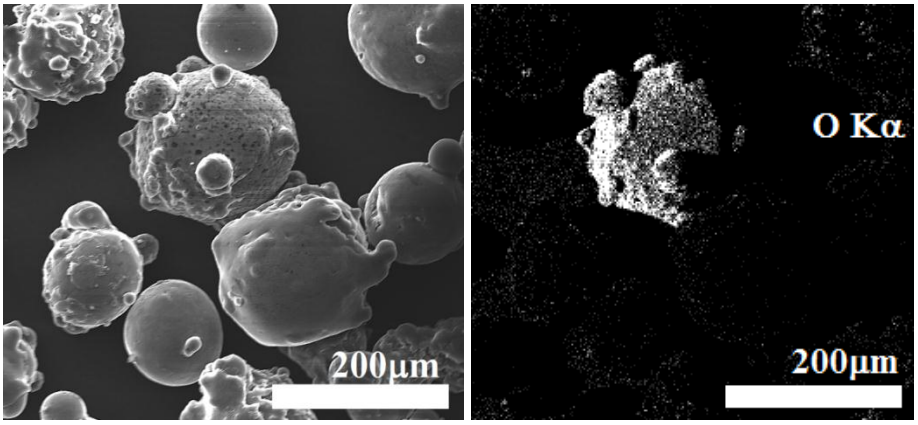


*Figure 3.4* **(I) SEM image of EXOTIC 8/3 pebbles and (II) oxygen map of the same pebbles showing the oxidized pebble (white pattern shows the concentration of the oxygen)**

Another reason for higher oxide content is the difference in irradiation conditions. Beryllium tends to oxidize at the temperature above 400$^{o}$C (even if the oxygen concentration is very small). Since the data of irradiation temperature in experiment EXOTIC is given in a large range it is possible that some fraction was exposed to that high temperature.

Chemical composition of the PBA pebbles has been analysed by two different equipment to ensure reliability of the results. Pebbles were analysed also in the Ion Implantation Laboratory of Sussex University by the method of Particle Induced X-ray emission (PIXE). With both methods such elements as Cr, Fe, Ni, Cu were determined. These elements could come from the stainless steel that has been also irradiated in PBA experiment. Ca could appear from sample preparation process (C tape could be touched by fingers before using). It was not possible to see signs of Co and Mg since their concentration in these samples are very low.

Inner structure and chemical impurities of the bulk was studied both for the pebbles from the PBA and EXOTIC 8/3 experiments, nevertheless more measurements were done for the PBA pebbles since it was technically easier than that for pebbles form EXOTIC 8/3 due to size differences.

Large voids became visible in the bulk of most of the examined PBA pebbles after polishing (Figure 3.5).

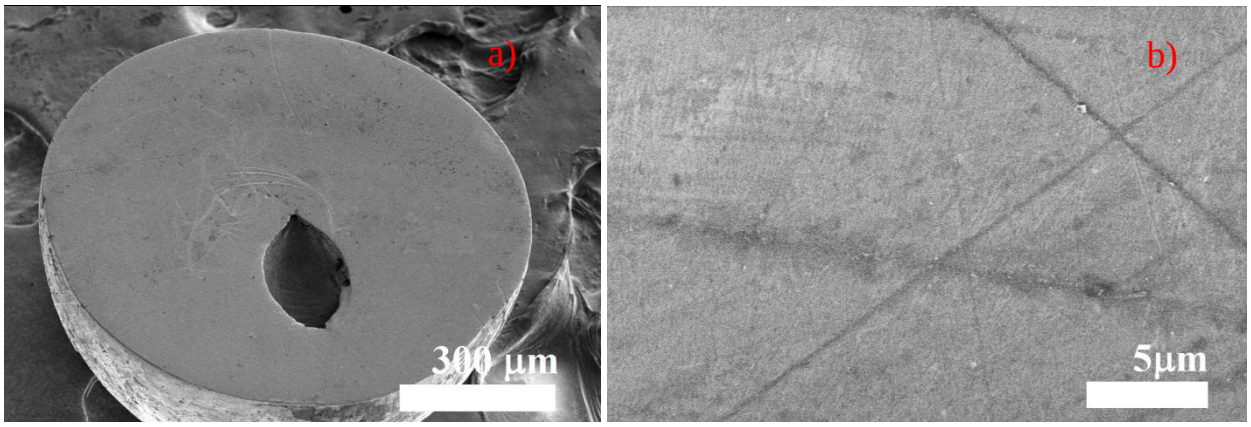


*Figure 3.5* **SEM image of polished cross-section of PBA pebble: a) large void , b) absence of visible pores (lines comes from the polishing)**

These voids are generated during the cooling phase of the fabrication process and might be called "technical voids". Contents and purpose of the technical void are described in the patent of the Rotating Electrode Process method for beryllium pebble production [160]. This void also has its own patent where it is said that it is developed to prevent beryllium swelling and failure when irradiated with neutrons - helium produced in the nuclear reactions is stored in this void instead of beryllium lattice [161]. Nevertheless, existence of such technical void increases tritium retention since it may act as a sink for tritium trapping [90]. Inventors of the REP method also admit the disadvantage of this technology regarding the tritium retention together with helium. Cross-section diameter of these voids ranges from 100 – 250 µm that corresponds to approximately 0.5 % of the pebble volume.

According to the chemical composition of the bulk both pebbles were found to be very clean (amount and type of the impurities do not exceed those given by the manufacturers). An interesting phenomenon has been observed regarding the BeO localization. The backscattered electron images shows that beryllium oxide tends to accumulate on the boundaries of poly crystals; therefore it works also as "decorator" of their boundaries. It could be assumed that grains consist of small crystals that are having the same orientations within one grain.

Porosity of the PBA pebbles before thermal treatment was found to insignificant – few pores with the size several tens of nanometers. This corresponds also to the information found in literature [62, 67] - at the irradiation temperatures below ~400$^0$C size of helium inclusions are less than several tens of nm.

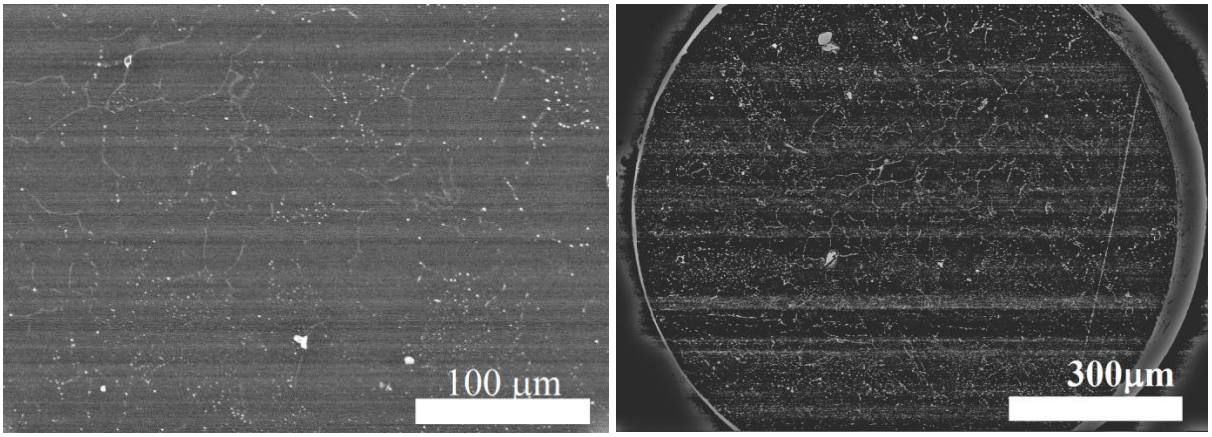


*Figure 3.6* **Backscattered electron image of PBA pebble cross section showing the oxygen on the poly crystal boundaries (elemental composition of these lines measured by EDX showed high content of oxygen)**

In the bulk of pebbles from EXOTIC 8/3 experiment technical void was not observed, nevertheless some small pores were present in a fraction of pebbles. In the areas where two pebbles have stacked together interlayer has been observed (Figure 3.7).

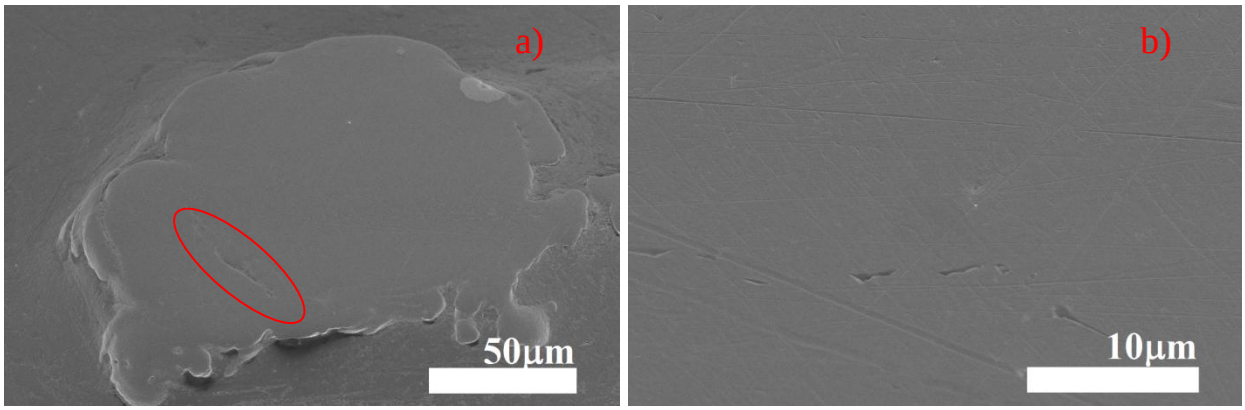


*Figure 3.7* **SEM image of polished cross-section of EXOTIC8/3 pebble: a) cross section of a pebble, interlayer between stacked pebbles(marked with red), b) separate pores in the bulk of the pebble**

- *Initial tritium content, chemical forms and distribution*

Initial tritium content and chemical forms have been analysed for all samples, whereas bulk distribution only for the pebbles from PBA experiments since pebbles from EXOTIC 8/3 were too small for such measurements. Methods for distinguishing chemical forms and measuring the bulk distribution in beryllium have been developed within this work in the UL Laboratory of Radiation Chemistry of Solids.

Tritium content of the beryllium pebbles was different due to different irradiation conditions (irradiation length, neutron flux, temperature, etc.) and the properties of the samples

(diameter, structure, impurities). Content of tritium in the pebbles experiments by the time of measurements was as follows:

- PBA: (2-4) GBq·g$^{-1}$
- EXOTIC 8/3: (0.002-0.02) GBq·g$^{-1}$

Tritium produced in the neutron induced transmutation of beryllium can diffuse into the lattice or can be trapped by structure traps (such as intragranular He bubbles, closed porosity, grain boundaries, etc.) or it may react with *BeO* to form $Be(OT)_2$ (3.2) with the formation energy of -0.7 eV at the standard temperature, pressure(STP) [87].

$$2BeO + 2T \rightarrow Be(OT)_2 + Be \qquad 3.2$$

The abundance ratio of tritium chemical forms in the beryllium pebbles was measured for samples from both irradiation experiments (Figure 3.8).

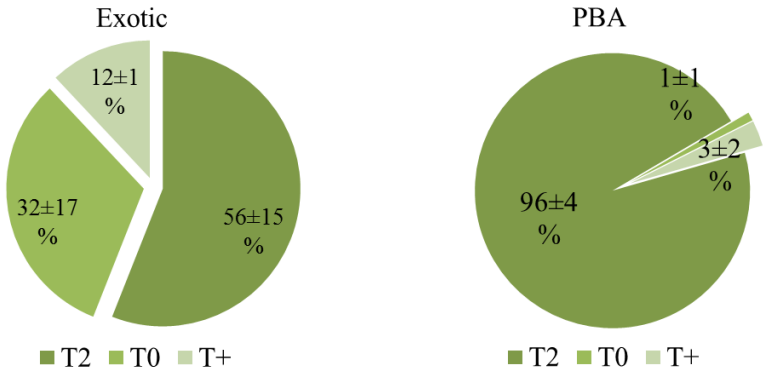


*Figure 3.8* **Abundance ratios of tritium chemical forms in the beryllium pebbles irradiated in experiments EXOTIC 8/3 and PBA**

Large fraction (up to 96%) of the tritium accumulated in irradiated beryllium pebbles was found to be in the molecular form. It can coexist with the helium in the gas inclusions. Large fraction of gaseous species very likely is trapped also in the technical void in the bulk of the pebbles that might explain the highest $T_2$ content in the pebbles from the PBA experiment (fabricated by the REP method). Presence of molecular tritium in the pebbles is undesirable. In order to extract $T_2$ from the metallic matrix it is required $T_2$ to dissociate into $T^0$ (dissociation energy for hydrogen - 4.52 eV).

In the investigated samples fraction of atomic tritium was in range from 1 – 32%. Atomic tritium can either exist as interstitial or can be trapped in the vacancy–based defect of the beryllium [173]. Atomic tritium can diffuse without any transformation - energy is required only

for passing through the diffusion energy barrier. The role of molecular and atomic tritium ratio is obvious if one compares the tritium release from EXOTIC 8/3 and PBA pebbles (see chapter 3.1.2).

Chemically bonded tritium $T^+$ was found to be in range from 3-12%. Highest concentration of $T^+$ was in the pebbles from the experiment EXOTIC 8/3. According to the chemical analysis these pebbles have the highest beryllium oxide content. Tritium retained in the form of beryllium hydroxide stays immobile unless temperature required for dehydration of $Be(OT)_2$ is reached (complete dehydration is reached at temperatures above 950$^o$C) [158]. Tritium possible states are shown schematically in Figure 3.9.

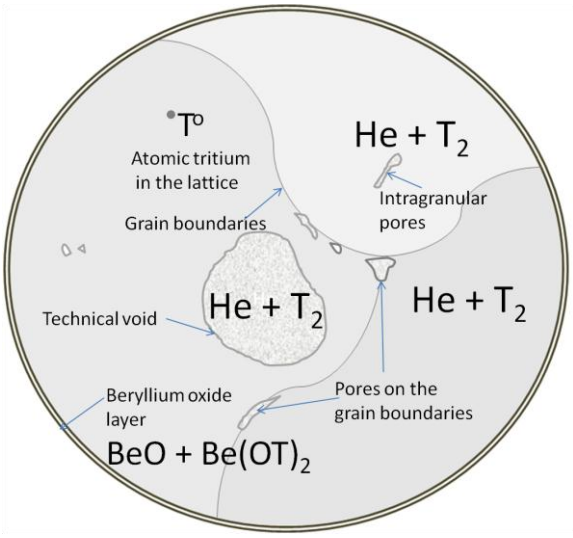


*Figure 3.9* **Schematic view of possible tritium states in the neutron irradiated beryllium pebble**

Bulk distribution of tritium in the pebbles has been determined for the pebbles of PBA experiments (Figure 3.10). Distribution was calculated by measuring tritium activity in the gas phase released during the dissolution, therefore distribution of chemically bonded tritium $T^+$ was not determined (more likely most of it is in the surface oxide layer and in the oxide inclusions in the bulk). For both types of samples distribution of tritium was similar – low concentration in the first micrometers from the surface, more or less uniform distribution in the bulk and in some pebbles a sharp peak somewhere in the bulk. The peak might indicate the position of the large void that was found during the structure investigations. Whereas low concentration in the first micrometers from surface indicates tritium desorption during storage in the ambient conditions.

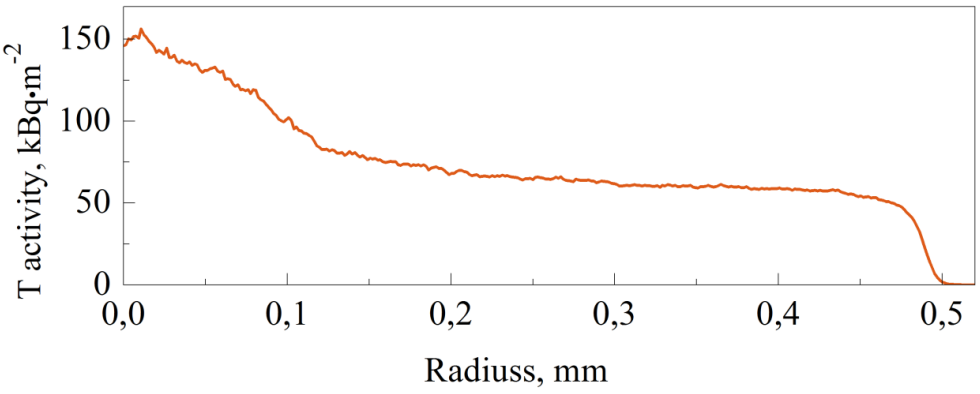


*Figure 3.10* **Tritium distributions in the bulk of pebbles irradiated in PBA**

*Summary*

In neutron irradiated beryllium tritium can be accumulated as an interstitial atom ($T^o$), a molecule in gas inclusions ($T_2$) or it can be chemically bonded to impurities ($T^+$). Total content of tritium and fractional distribution of chemical forms depend both on beryllium material itself (existence of voids where gaseous species might accumulate, oxygen content that might form chemical bond with tritium) and irradiation conditions (temperature, length, etc).

### 3.1.2 Tritium desorption

Tritium thermo desorption experiments has been performed at a constant temperature increase rate of ~2.5$^o$C·min$^{-1}$ and ~5.0$^o$C·min$^{-1}$ up to 280$^o$C, 500$^o$C, 850$^o$C, 1050 and 1250$^o$C and then held for 1 to 4 h in a constant temperature in a flow of purge gas (He with 0.1% $H_2$). Maximum temperature of thermal treatment was chosen based on the experimental results and correspond to the temperature where tritium desorption maximum peak starts to decrease. Radiation facilitated diffusion and radiolysis in a high magnetic field condition must have a significant role in the desorption process of tritium. Therefore, tritium thermo desorption has been studied also with the presence of magnetic field and ionizing radiation. After desorption experiments remaining tritium has been determined by the method of dissolution.

In Figure 3.11 tritium thermo desorption spectra (TDS) from EXOTIC 8/3 and PBA pebbles has been compared at similar conditions (5$^o$C·min$^{-1}$, 850$^o$C, 3 h). Tritium amount units are per cents of its total amount in particular samples.

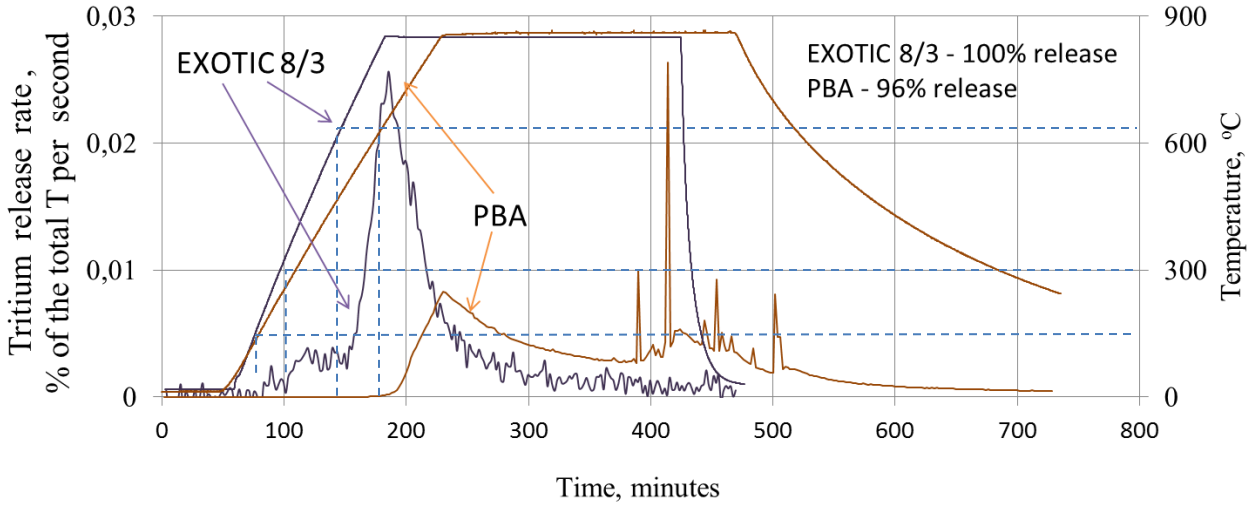


*Figure 3.11* **Tritium thermo desorption from pebbles irradiated in EXOTIC 8/3 and PBA experiments (heating rate ~5°C·min$^{-1}$ up to 850°C, held at constant temperature for 3 h)**

Heating at 850°C is sufficient to release all tritium from the pebbles irradiated in EXOTIC 8/3 experiment, whereas in pebbles from PBA experiment there is still some tritium remaining. Moreover, tritium desorption from the EXOTIC 8/3 pebbles starts at considerably lower temperature ((90±10)°C at a temperature increase rate of 5°C/min) than that for PBA pebbles ((682±25) °C at a temperature increase rate of 5°C/min and (628 ± 12)°C at the increase rate of 2.4°C/min). In tritium TDS for EXOTIC 8/3 at the conditions described above two small and one large peak can be observed that might indicate presence of three desorption mechanisms where one of them is dominant. PBA tritium desorption starts at the approximately the same temperature where the dominant peak of EXOTIC TDS start to appear that follows by a second peak that is not observed for EXOTIC 8/3.

This significant difference might be caused by several factors; main of them are assumed to be as follows:

- size of the pebble(diffusion length);
- structure (accumulation in the pores, grain boundaries, transportation along the cracks, etc);
- concentration of the helium gas inclusions, size of the gas bubbles (tritium accumulation together with helium);
- chemical impurities, oxide content (tritium chemical bonding).

First of all size differences must be emphasized - pebbles used in the EXOTIC 8/3 experiment have much smaller diameter (0.1 mm in average, see Figure 3.3) than that for PBA

(1mm). Therefore tritium diffusion length from the bulk of the pebble to the surface for EXOTIC 8/3 pebbles are smaller up to a factor 10.

Another important factor is the structure differences. Pebbles used in the PBA experiment have a technical void in the bulk due to production technology (see chapter 3.1.1). In this void large fraction of the gases might be accumulated and can be released sufficiently only if the crack or open porosity have formed connecting this void with the surface. Tritium chemical forms should also have considerable role in its extraction from metallic beryllium. In the pebbles from EXOTIC 8/3 experiment comparably high content of atomic tritium (up to 32%) were found in contrast to PBA pebbles where its content was less than 3% (see chapter 3.1.1). Therefore, from the PBA pebbles tritium starts to release either when molecular tritium starts to dissociate into mobile $T^o$ or molecules have travelled through pores and cracks to the surface.

To explain the role of tritium chemical forms in tritium desorption process the evolution of chemical forms were studied in the samples irradiated in the EXOTIC 8/3 experiment. Pebbles were heated up to temperatures 280°C and 500°C as long as 15-20% of tritium is released (3 and 1 hour, respectively). Distribution of chemical forms of the remaining tritium in the pebbles was measured (Figure 3.12).

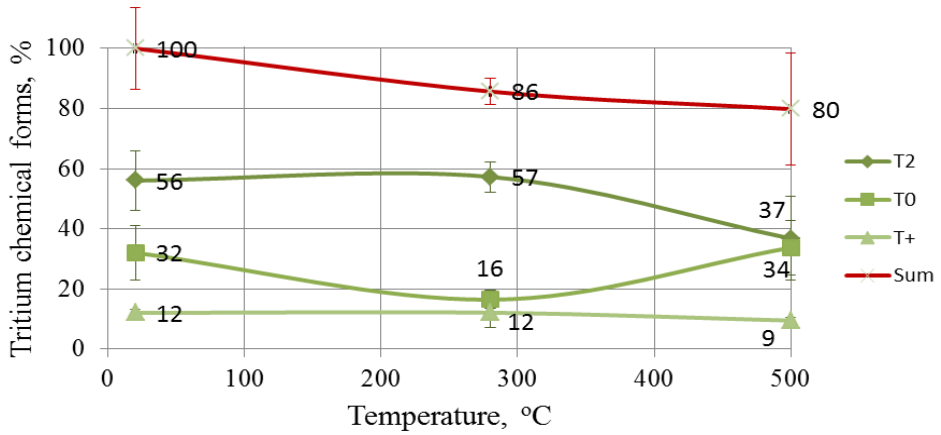


*Figure 3.12* **Evolution of tritium chemical forms remaining after thermo-annealing at different temperatures (first point 20°C refers to storage temperature and describes initial state of tritium in the samples)**

Results show that the amount of chemically bonded tritium changes insignificantly after the thermal treatment of pebbles. At low temperature (280°C) only content of atomic tritium has decreased (32% into 16%), other forms had stayed immobile. Heating at higher temperature 500°C decreases the $T_2$ content due to the molecule dissociation into the mobile $T^o$. Dissociation

of molecular tritium is also the reason the atomic form content has increased (16% back into 34%).

Concentration and size of helium gas inclusions and bubbles are also of great importance. It is believed that most of the tritium is trapped in the helium gas inclusions therefore their behaviour during thermo annealing affects tritium release from the pebbles.

The effective diffusion coefficients have been also calculated from the thermal desorption spectra according to the method described in Chapter 2.2.4.

For the samples from EXOTIC 8/3 experiment effective diffusion coefficient were estimated at the temperatures 720 and 850$^{o}$C, and were $(4.6\pm0.1)\times10^{-14}$ $m^2\cdot s^{-1}$ and $(4.4\pm0.2)\times10^{-14}$ $m^2\cdot s^{-1}$ respectively. As mentioned above these pebbles have different sizes. In calculations the average diameter 0.1 mm has been used. For the samples from PBA experiment effective diffusion coefficient was estimated at 772$^{o}$C and 815$^{o}$C, and were $2.5\times10^{-13}$ $m^2\cdot s^{-1}$ and $(7\pm2)\times10^{-13}$ $m^2\cdot s^{-1}$ respectively. Effective diffusion coefficient in EXOTIC 8/3 pebbles is almost for an order smaller than that for the PBA pebbles. There might be two reasons for that. First, EXOTIC 8/3 pebbles have higher oxide content where tritium diffusion is slower than in pure metal. Second, specific surface of EXOTIC 8/3 is larger by a factor OF 10 than for pebbles from PBA experiment (approximately 32430 $cm^2\cdot g^{-1}$, 3140 $cm^2\cdot g^{-1}$, respectively). One of the limiting factors for tritium desorption is its release from surface where it tends to adsorb. Only when all of the surface is covered by hydrogen atoms (tritium and protium from the purge gas) they start to recombine forming a molecule and release into the purge gas.

To understand tritium behaviour during thermal treatment thermo desorption spectra (TDS) have been studied in more detail for each group of samples.

*EXOTIC 8/3*

In the thermo desorption spectra of tritium from EXOTIC 8/3 pebbles three separate peaks can be distinguished (Figure 3.11) that might indicate presence of three mechanisms of desorption. To study these mechanisms in detail tritium thermo desorption has been performed at different temperatures that are chosen to exclude one or more mechanisms. For example, to study process occurring at the low temperatures, sample was heated up to a temperature that is below the temperature at which the next mechanisms first appears.

After heating sample up to 280$^{o}$C and held for 3 h at this temperature 14±6 % of the total tritium amount is released. A typical spectrum is shown in Figure 3.13.

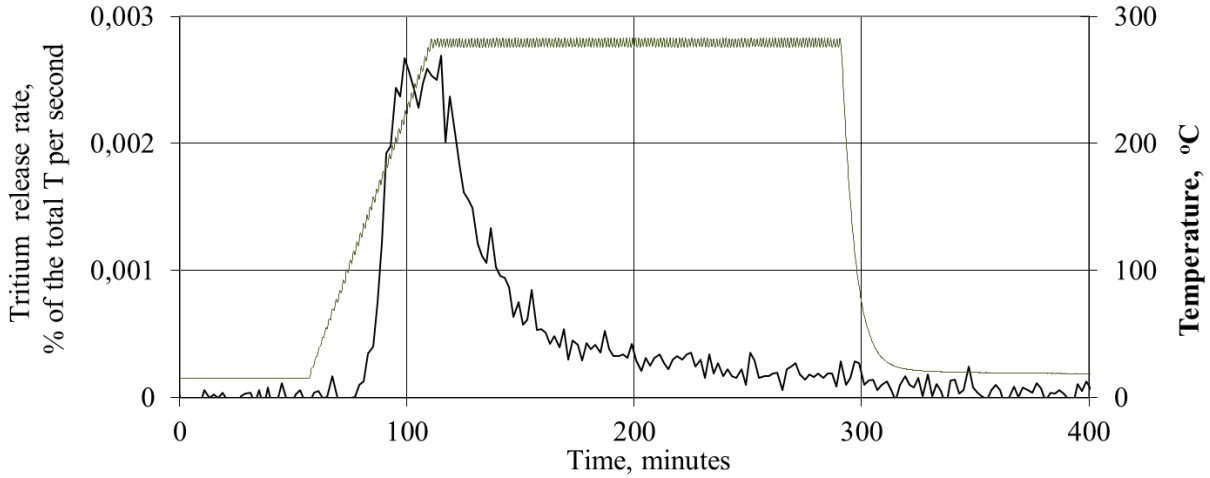


*Figure 3.13* **Tritium thermo desorption from pebbles irradiated in EXOTIC 8/3 experiment (heating rate ~5°C·min$^{-1}$ up to 280°C, held at constant temperature for 3 h)**

Low temperature release might be related to surface processes (isotopic exchange with hydrogen from the purge gas) due to high specific surface area. According to chemical form evolution (considerable decrease of atomic tritium content) it is also related to release of tritium that was accumulated initially as separate interstitial atoms. Increase of the temperature increases the kinetic energy of tritium atoms. Beryllium structure cannot be considered as an ideal crystal – in the diffusion path tritium atom might meet crystal defects such as vacancies or grain boundaries, as well as impurity inclusions. Beryllium like aluminium tends to have thin oxide layer on its surface and this might acts as a barrier - hydrogen diffusion coefficient in beryllium oxide is much smaller than that for the metallic beryllium and it can be also trapped chemically. Therefore not all of atomic tritium is released by this mechanism. No structure changes have been observed after heating at 100°C which corresponds to the initial release temperature.

Tritium desorption has been also studied under action of accelerated electron radiation. During these experiments the temperature has been measured. Accelerated electron irradiation considerably heats the sample, approximately up to 200 - 280°C. To ensure that temperature measurements in these experiments are adequate, appropriate calculations have been done. It was assumed that experiment of heating up to 280°C and experiment of exposing to accelerated electrons are comparable according the temperature. Nevertheless, difference in the temperature increase rate must be noted - in case of radiation heat maximum temperature is reached almost instantly, whereas in thermal heating it takes almost an hour. Comparison of tritium desorption spectra under different conditions is shown in Figure 3.14.

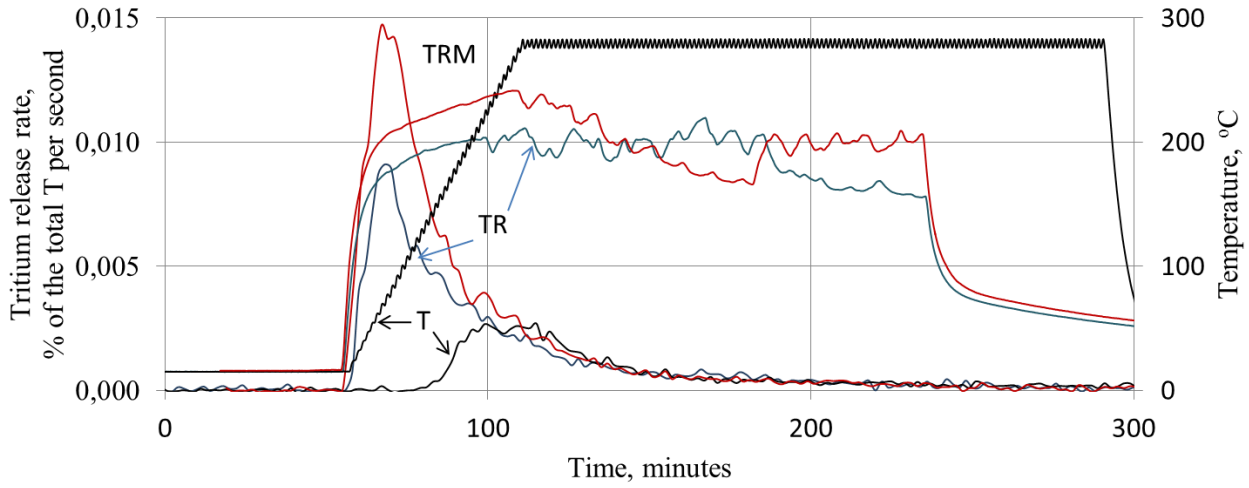


*Figure 3.14* **Tritium desorption from pebbles irradiated in EXOTIC 8/3 experiment, where "T" heated up to 280°C, "TR" exposed to accelerated electrons (5 MeV, 14 MGy·h$^{-1}$), "TRM"– simultaneously exposed to accelerated electrons and magnetic field**

If one compares tritium release by thermal and radiation heating it is noticeable that in the case of radiation heat tritium release starts in a few minutes with a sharp peak, whereas at thermal heating release starts after a longer period of time and peak is flatter. This might be related to the temperature increase rate differences - if one compares temperatures of release start it should be noted that these temperatures are more of less similar (about 100°C). At electron radiation heating also higher fraction of tritium is released 20±4 %. Therefore radiation facilitated diffusion might be considered. This might be explained by several ways of impact. First is the high kinetic energy that can be transferred from the fast electron in case of collision. Second is effects based on radiation chemistry - molecular tritium localized somewhere in lattice defects can be dissociated into two atoms that might migrate away from each other (and also recombine with a high probability). Tritium chemically bonded in beryllium hydroxide in the surface oxide layer might be also released if the hydroxide molecule is split as a result of encounter with fast electron. Fast electrons might cause also some short lived structure damages that would facilitate transport of gaseous species.

In case of tritium radiolysis driven dissociation it must be magnetic field sensitive since magnetic field changes electron spins and therefore probability of recombination back to immobile molecule. However, the desorption process can be delayed by a magnetic field since it decreases the probability of tritium atom recombination into a molecule that can leave the surface

Experiments of thermal and accelerated electron heating have been performed also under action of high magnetic field (up to 1.7 T). At this point it must be noted that beryllium has very low magnetic susceptibility, therefore magnetic field within beryllium material stays almost unchanged. Results shows that simultaneous action of radiation and magnetic field has a synergetic facilitating effect on tritium desorption. To see the role the evolution of chemical forms of tritium during annealing at these conditions remaining tritium measurements has been done and compared (Figure 3.15). It is obvious that accelerated electrons considerably decreases amount of molecular tritium (57 to 43%) that hasn't change in case of thermal heating at similar temperature. At the simultaneous action of accelerated electrons and magnetic field fraction of molecular tritium has decreased even more (57 to 36%). These results prove the hypothesis about radiation and magnetic field effects stated above.

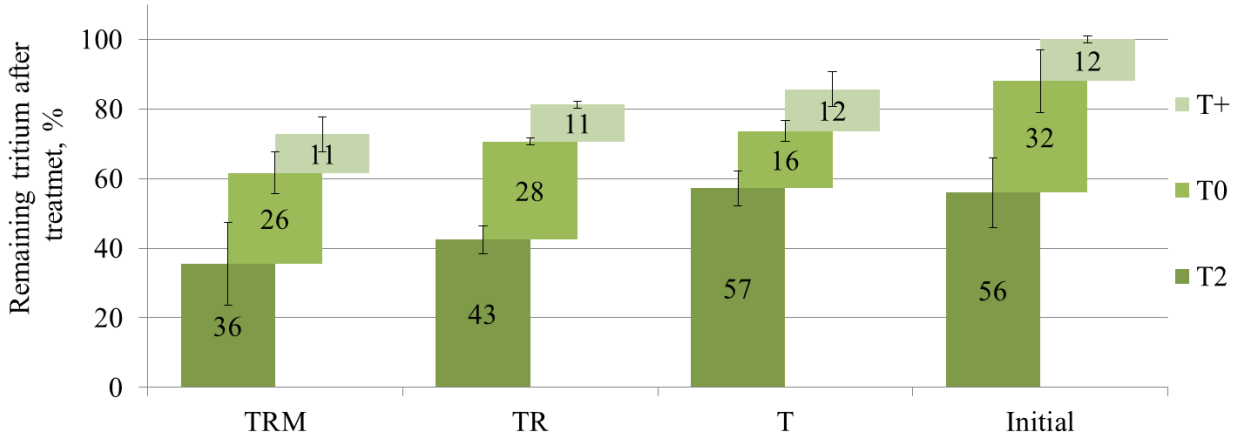


*Figure 3.15* **Distribution of the chemical forms of tritium in beryllium pebbles after thermo-annealing experiments, where "T" heated up to 280$^{o}$C, "TR" exposed to accelerated electrons (5 MeV, 14 MGy·h$^{-1}$), "TRM"– simultaneously exposed to accelerated electrons and magnetic field**

As temperature is increased second desorption peak appears (Figure 3.16). At higher temperatures gas trapped in the inclusions and bubbles according to the gas law gains its pressure (at this temperature pressure is increased by factor ~2.5) that at some point starts to force tritium gas to move into the lattice. Since tritium molecule is too large to migrate through the beryllium lattice it dissociates into atomic tritium (re-dissolution) that afterwards follows the same mechanism as described above. This process starts at temperatures above 300$^{o}$C in these particular samples. In thermo desorption experiments where temperature has been raised up to 500$^{o}$C and then held for 1 h tritium release was (21±4) % from total.

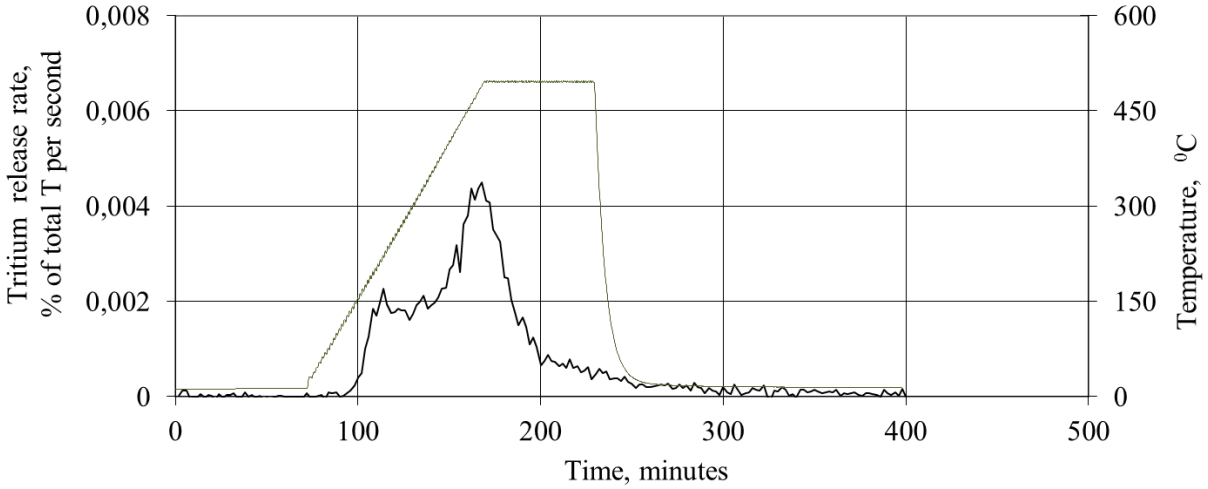


*Figure 3.16* **Tritium thermo desorption from pebbles irradiated in EXOTIC 8/3 experiment (heating rate ~5°C·min$^{-1}$ up to 500°C, held at constant temperature for 1 h)**

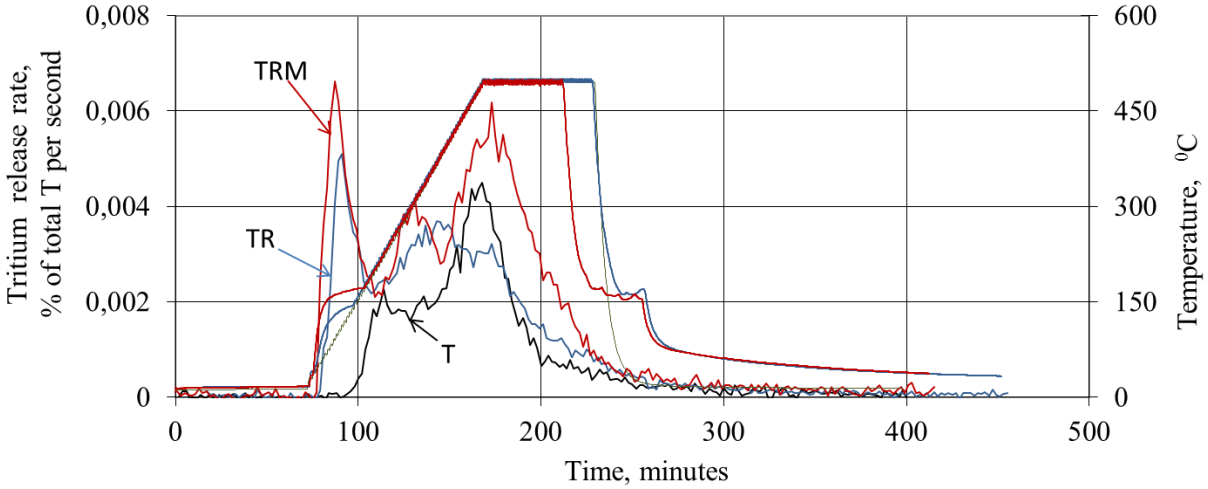


*Figure 3.17* **Tritium thermo desorption from pebbles irradiated in EXOTIC 8/3 experiment where "T" heated up to 500°C, "TR" exposed to accelerated electrons (5 MeV, 14 MGy·h$^{-1}$), "TRM"– simultaneously exposed to accelerated electrons and magnetic field**

If an accelerated electron radiation is added to the thermal heating second peak starts to appear already at lower temperatures (Figure 3.17) and total tritium release reaches (27±6) %. It could be assumed that tritium re-dissolution in beryllium lattice from gas inclusions starts at lower temperature as a result radiation induced radiolysis of tritium molecule. If the magnetic field is also added tritium release is even more efficient ((34±3)% ).

As the temperature is further raised beryllium structure starts to change. SEM images have been taken of pebbles after thermal treatment at 650°C (Figure 3.18). At this temperature so called burst release starts (Figure 3.19).

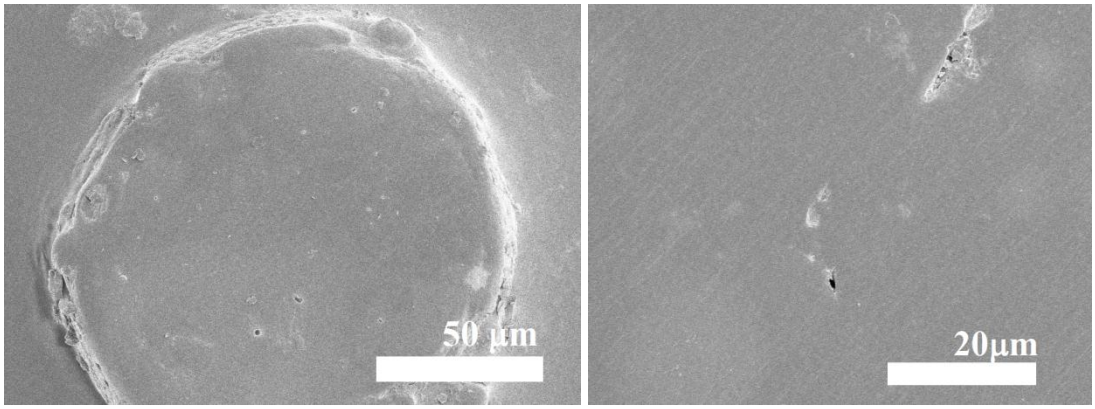


*Figure 3.18* **SEM images of EXOTIC 8/3 pebbles after treatment in He+0.1H2 at 650°C (heating rate ~5°C·min$^{-1}$ up to 650°C, held at constant temperature for 1 h) when rapid tritium release is started**

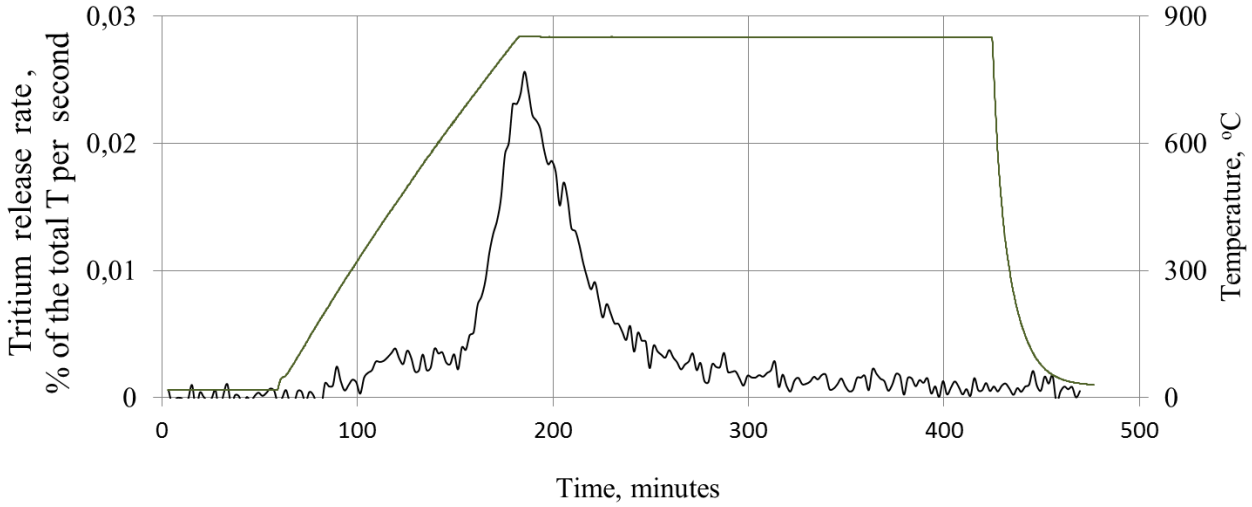


*Figure 3.19* **Tritium thermo desorption from pebbles irradiated in EXOTIC 8/3 experiment (heating rate ~5°C·min$^{-1}$ up to 850°C, held at constant temperature for 3h)**

Increasing pressure in the gas inclusion starts to deform beryllium lattice until coalescence of bubbles forms the interlinked network porosities connected to the surface where gas might freely migrate without penetration into tight lattice of beryllium. In the code ANFIBE that describes tritium and helium behaviour in the neutron irradiated beryllium it is assumed that these networks are formed only along the grain boundaries and gas migration within the interlinked pore system is considered to be the only mechanism of the release of gaseous products [162]. Nevertheless, pebbles used in EXOTIC 8/3 experiment is so small that they might consist of only one grain. Therefore, there are no grain boundaries and these networks are supposed to be formed also within the grain. Beryllium become also more brittle in the high temperature therefore formation of cracks also can occur that acts similar to the open porosity (Figure 3.20).

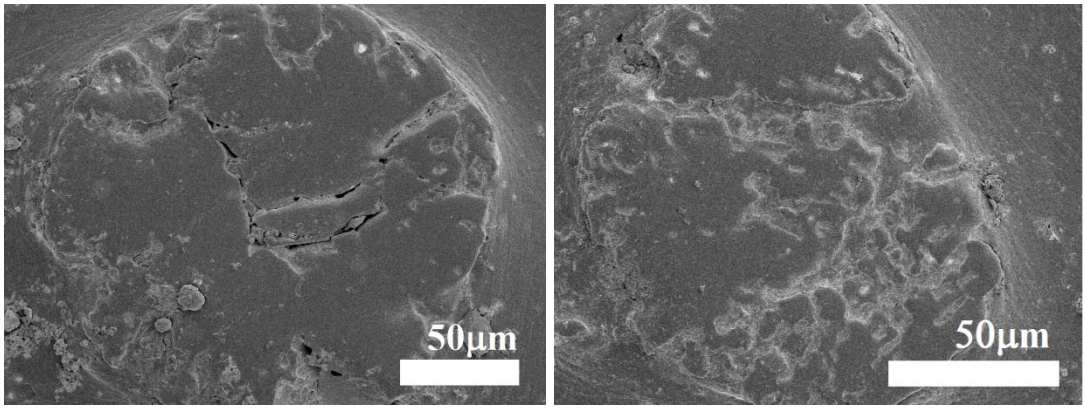


*Figure 3.20* **SEM images of EXOTIC 8/3 pebbles after treatment in He+0.1$H_2$ at 850$^o$C (heating rate ~5$^o$C·min$^{-1}$ up to 850$^o$C, held at constant temperature for 1 h) when rest of the tritium is released**

By this the rest of the tritium is released. Gas migration through open porosity and cracks formed due to the temperature and gas inclusion pressure governed structure changes of beryllium itself could be assumed to be the main tritium release mechanism. Therefore it might be concluded that for detrititation process temperature supposed to be at least 620$^o$C. Chemically bonded tritium (in hydroxide) could be released as a result of isotope exchange process with the hydrogen in the purge gas.

In Table 3.1 summary of tritium release under different condition is given.

Table 3.1 **Tritium desorption from EXOTIC 8/3 pebbles under different conditions**

| Tritium desorption conditions | | Tritium release, % from total |
|---|---|---|
| Abbrev. | Experiment details | |
| T1 | 5$^o$C ·min$^{-1}$ up to 280$^o$C, 3 h constant | 14±6 |
| R | Accelerated electron beam, 5 MeV, 14 MGy·h$^{-1}$ (200-280$^o$C) | 20±4 |
| RM | Accelerated electron beam, 5 MeV, 14 MGy·h$^{-1}$ (200-280$^o$C), magnetic field, 1.7 T | 29±10 |
| T2 | 5$^o$C ·min$^{-1}$ up to 500$^o$C, 1 h constant | 20±5 |
| TR | 5$^o$C ·min$^{-1}$ up to 500$^o$C, 1 h constant, Accelerated electron beam, 5 MeV, 14 MGy·h$^{-1}$ | 29±11 |
| TRM | 5$^o$C·min$^{-1}$ up to 500$^o$C, 1 h constant, Accelerated electron beam, 5 MeV, 14 MGy·h$^{-1}$ , magnetic field, 1.7 T | 35±2 |
| T3 | 5$^o$C·min$^{-1}$ up to 850$^o$C, 3 h constant | 100 |

*PBA*

PBA pebbles have been heated at temperatures up to 850°C - 1250°C with a temperature increase rate ~ 2.5 and ~5 $^{o}C \cdot min^{-1}$. Typical thermo desorption spectra are demonstrated in Figure 3.21. In the experiments at high temperature 100% of tritium has released.

From PBA pebbles tritium desorption starts at much higher temperatures and spectra are having different shape than that for EXOTIC 8/3. This is due to the fact that there is almost no atomic tritium in the lattice that might release at low temperature and fraction of the gas is accumulated in the technical void.

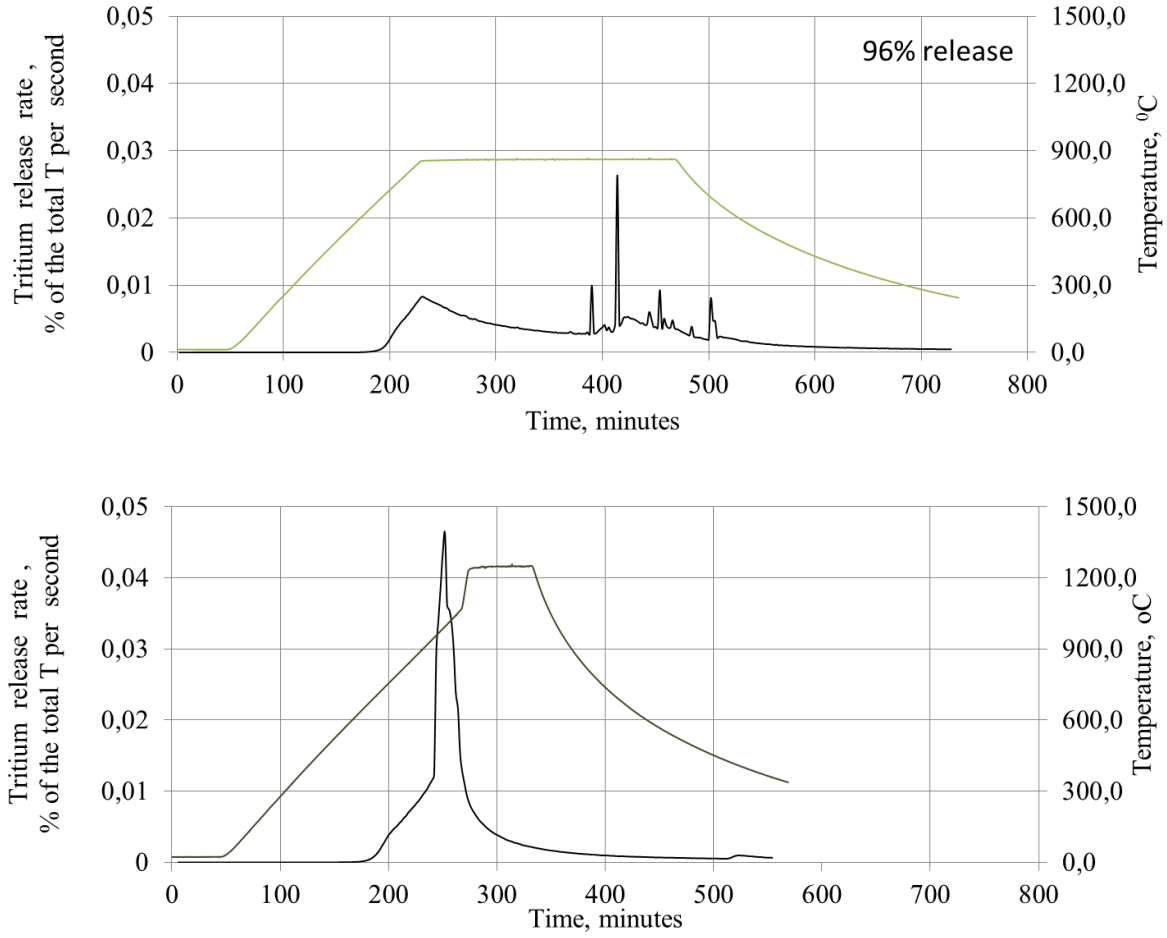


*Figure 3.21* **Tritium thermo desorption from PBA pebbles at 867°C and 1258°C (temperature increase rate 2.5°C·min$^{-1}$)**

An important issue that should be mentioned is the pressure in the technical void. According to the pebble fabrication method this void is generated during the solidification phase of melted beryllium droplet. Since droplet is cooled from the outside (cold inert gas atmosphere) solidification is starting from the outer surface and due to shrinkage of material volume (density

of liquid beryllium at the melting temperature is about 10% lower than that for a solid material, 1.69 and 1.85 $g \cdot cm^{-3}$, respectively) the void is formed in a centre of solid pebble. Therefore the initial pressure (before irradiation) could be assumed to be lower than an atmospheric one. After neutron irradiation it has been estimated to contain 300-600 appm He that corresponds to roughly 0.00075-0.0015 $cm^{-3}$ volume of the helium gas in 1mg pebble. According to these rough calculations it might be assumed that gaseous species formed as a result of neutron induced transmutation cannot fill more that about 10% of the void volume and therefore it could be concluded that even after irradiation gas pressure in the void is negative relative to atmospheric pressure.

Thermo-annealing experiment at the temperature of 650$^{o}$C that correspond to the release start has been performed and SEM images of the inner structure of the pebbles taken. At this temperature visible porosity starts to appear. Pores up to 500 nm can be distinguished and indicates the start of the migration of gaseous species within the lattice of beryllium (Figure 3.22).

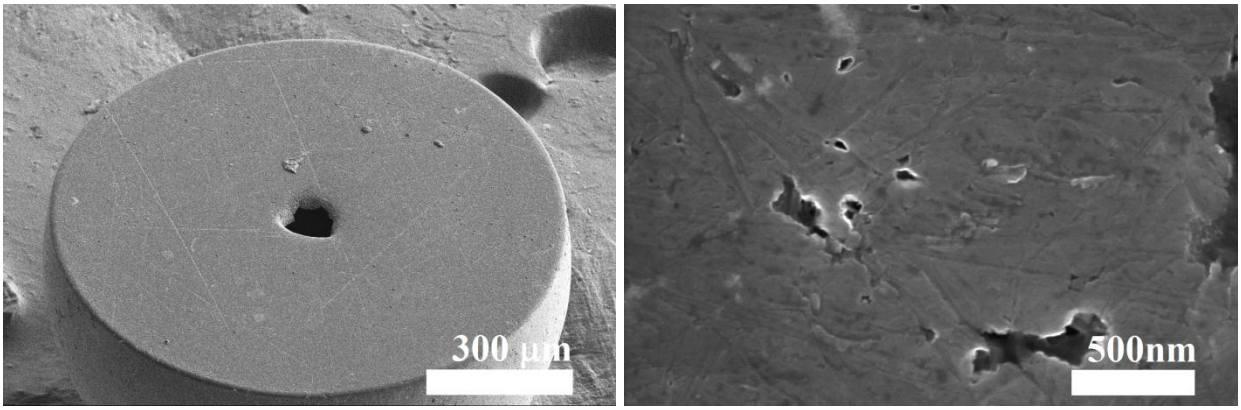


*Figure 3.22* **SEM image of PBA pebble after treatment in He + 0.1%$H_2$ at 650$^{o}$C (5$^{o}$C/min and 2h at constant temperature) that corresponds to the tritium release start temperature**

Another important issue is the fact that due to the accumulation of gases in the void instead of lattice, beryllium itself is less damaged and formation of open porosity and cracks might appear later than that for the samples where swelling had taken place. Burst release typical for the transport through the cracks connecting the void and surface starts at a temperature 933±4$^{o}$C and a considerable fraction of tritium is released at this stage.

In SEM images taken after thermal treatment at 950$^{o}$C it is obvious that structure has changed considerably – there are large cracks connecting the technical void with a surface and

also the connected pore system has been formed. Moreover, the size of the pores has increased up to several tens of micrometres.

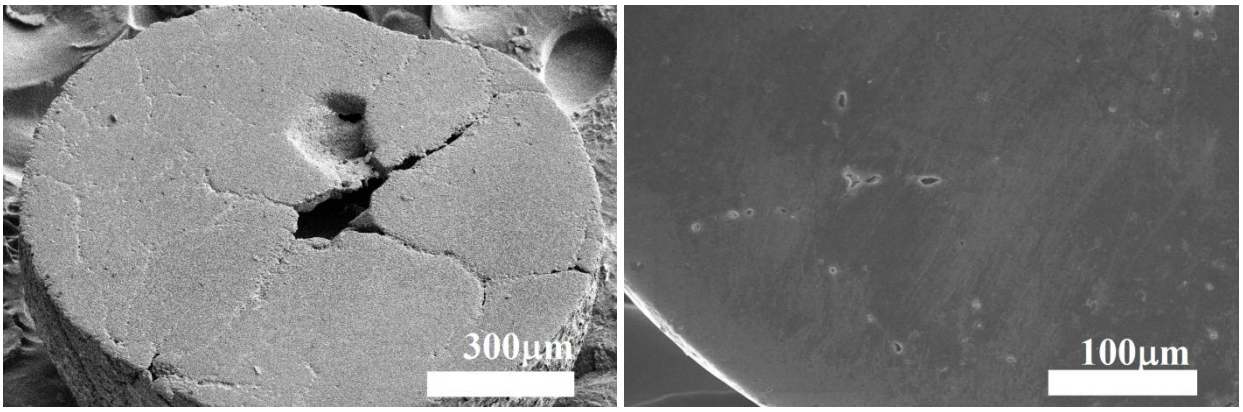


*Figure 3.23* **SEM image of PBA pebble after treatment in He + 0.1%$H_2$ at 950°C (5°C/min and 2 h at constant temperature) that corresponds to the tritium burst release start temperature**

Therefore it might be concluded that for detritiation of this type of pebbles required temperature is at least 935°C. It is about 300°C more than that for EXOTIC 8/3 pebbles.

After heating of the sample at high temperature (up to 1260°C) when all tritium is released structure had been changed drastically – large radial cracks and high porosity can be observed (Figure 3.24). The pebble was very brittle and broke into pieces instead of being polished.

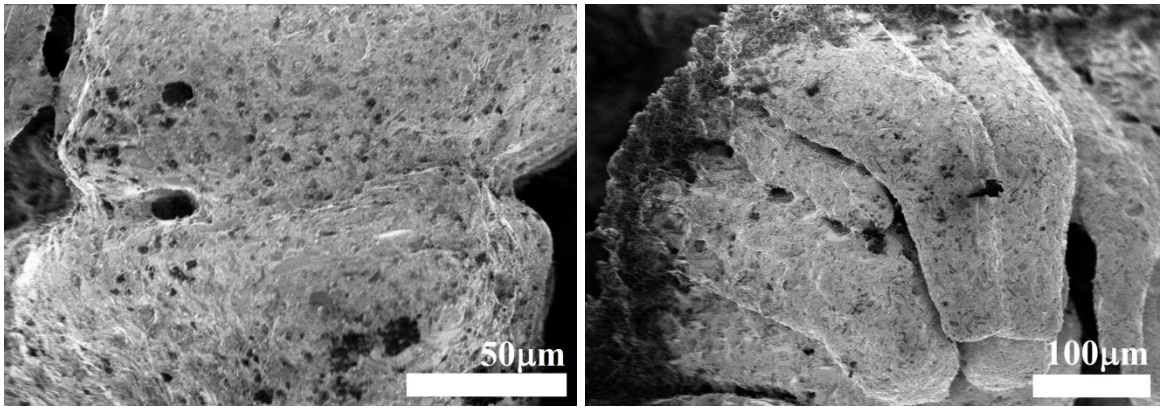


*Figure 3.24* **SEM images of PBA pebble after treatment in in He + 0.1%$H_2$ at 1260°C when all tritium is released**

In the experiment where sample has been heated up to ~850°C ~90% of total tritium content was released, whereas at temperature close to the melting point of beryllium 100% of tritium was released. Contribution of each mechanism, dissolution into lattice followed by diffusion to surface and molecule transport through cracks connecting void with a surface, in both experiments are quite similar. Main difference is in a time required for desorption - in high temperature (>930°C) burst release starts due to intense crack and pore formation in the pebble

and tritium release peak is very sharp and narrow. Whereas at lower temperatures this release is slow, that might indicate formation of few small cracks that are not sufficient for efficient gas transport.

### 3.1.3 Tritium behaviour model in neutron irradiated beryllium pebbles

According to the results described above and literature data a simplified model of tritium behaviour can be built (Figure 3.25).

After its production by nuclear transmutation of beryllium tritium atom is situated in a lattice vacancy or in an interstitial space. For approximation vacancy will not be considered. Further tritium diffuses as interstitial through the beryllium lattice (I) until it reaches one of the following: grain boundary, helium gas inclusion (helium production in beryllium is significantly higher than that for tritium), beryllium oxide layer, other tritium atom. According to the results about tritium chemical forms - most of the tritium is accumulated in a molecular form, therefore it can be concluded that tritium is trapped by helium inclusions. Probability to meet another tritium atom is small due to its low concentration and even if two atoms have met they will not form the molecule since in the metal lattice it is not energetically favourable. Further each situation will be discussed in more detail:

Tritium diffusion in beryllium lattice (process I in Figure 3.25) depends on the diffusion coefficient, activation energy and temperature. Diffusion coefficient and activation energy have been measured by number of authors, therefore literature data can be used. Only variable is temperature.

Tritium diffusion in beryllium oxide layer is unavoidable since this layer is always present on the surfaces. For tritium to release from the pebble it must get through this layer. Besides diffusion process as such tritium might chemically react with the BeO to form $Be(OT)_2$. Beryllium oxide effect on tritium effective diffusion is obvious if to compare EXOTIC 8/3 and PBA pebbles – in EXOTIC 8/3 that has higher oxide content tritium diffusion coefficient is considerably smaller. The overall process therefore depends on the following parameters: diffusion coefficient, activation energy, temperature, reaction probability of tritium with BeO.

After diffusion through oxide layer tritium has reached the surface. To release into the purge gas tritium has to form a molecule either with another tritium atom or protium atom (0.1% of $H_2$ is present in the purge gas). Energetically it is more favourable to stay on the surface as adsorbed atom. The recombination occurs only if the whole surface is covered with tritium and

protium atoms (protium atoms comes from the purge gas) or/and the temperature is high enough to cross the desorption energy barrier (III). This process might be influenced by the magnetic field - in the presence of magnetic field recombination yield must be decreased due to spin transformations.

Tritium diffusion along grain boundaries (process IV) might be faster that in the lattice according to the literature data on other materials. However, grain boundaries might contain also trapping sites for tritium. Therefore this process depends on the following variables: total surface of grain boundaries, diffusion coefficient along grain boundaries, number of trapping sites.

Another possibility for tritium is to reach helium gas inclusions and to be trapped there (VI). This process depends mainly on the sizes and concentration of the helium bubbles. It can be either modelled (helium formation, behaviour etc) or can be estimated from the available literature data. To release from the pebbles this tritium should either re-dissolve into the beryllium lattice (V) or follow the helium gas through the open porosity network to the surface (IX). Tritium re-dissolution into the lattice might be facilitated by the ionizing radiation since it would cause an intensified dissociation of tritium molecules into atoms, whereas IX process might be predicted according to the experimental data. According to the results on beryllium structure evolution during thermo annealing obtained in this study, process IX starts to evolve above 600$^{o}$C and does not depend on the size and production method of the pebbles.

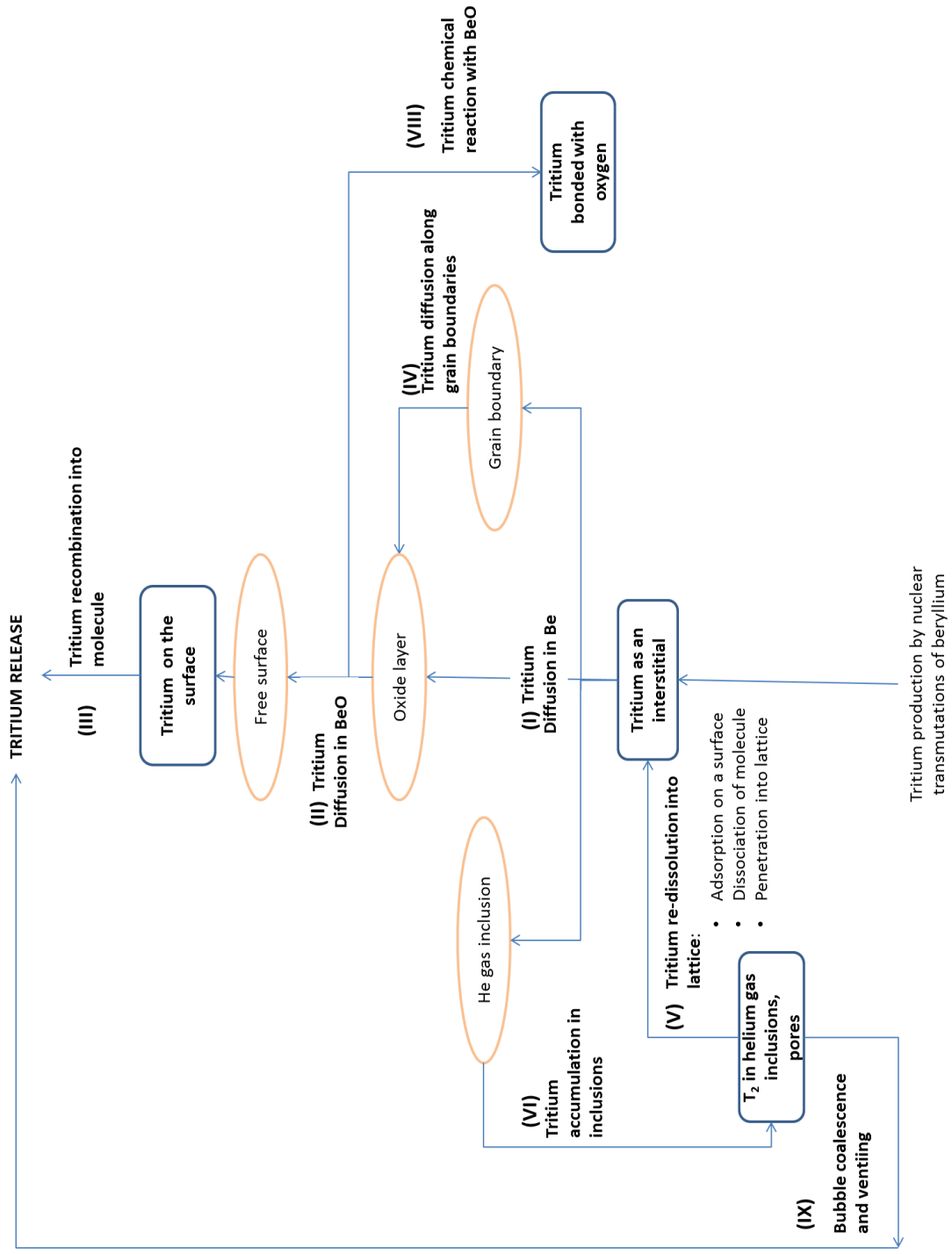


*Figure 3.25* **Schematic view of tritium behaviour in neutron irradiated beryllium**

## *3.2 Plasma facing materials – beryllium and carbon fibre tiles exposed in JET plasma chamber*

Metallic beryllium and carbon fibre composites are materials of different properties but similar application in the fusion devices – protection of other components from direct impact of plasma.

### 3.2.1 Preliminary examination

- *Structure and chemical composition*

During the exploitation in the plasma chamber both beryllium and carbon materials change their structure due to neutron irradiation and plasma exposure. Pre-eroded particles and other impurities from the plasma deposit on the surfaces of these materials and form so called deposition layers of a complex chemical composition and structure. These deposition layers are crucial regarding the tritium inventory.

*Beryllium*

Surface of the beryllium tiles is either coated by the deposition layer (up to 40μm) or it is melted as a result of the interaction with plasma (Figure 3.26). Analysis revealed that deposition layer itself consist of several layers with different structure and chemical composition. XRD analysis performed at the Department of Chemistry showed beryllium oxide presence in the plasma facing surface, whereas EDX analysis gave possibility to see heavier impurities. According to literature the deposition on the Be tiles is predominantly carbon [174]. Main impurity besides carbon and oxygen that was found on the surface of the beryllium tiles was nickel. It has come from the *Inconel* used in the plasma chamber. Such elements as Al, Si, Fe, S were also present (Figure 3.27).

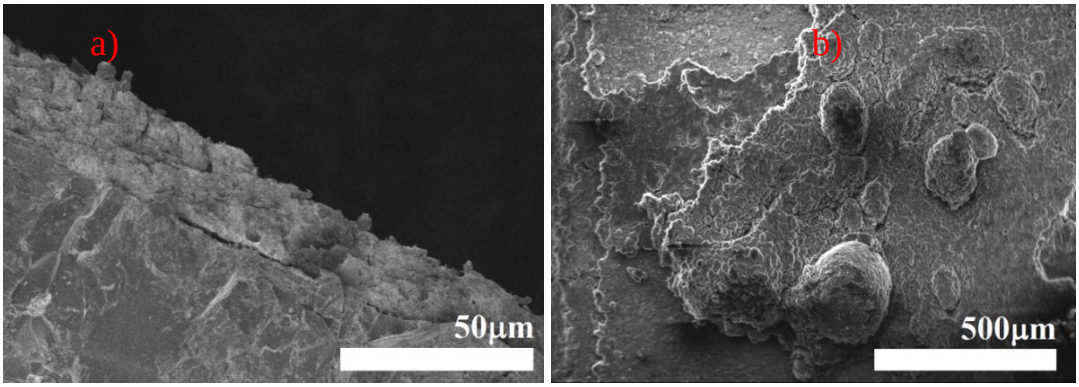


*Figure 3.26* **SEM images of beryllium tiles: a) of the cross-section of the beryllium tile with a deposition layer, b) structure of the deposition layer**

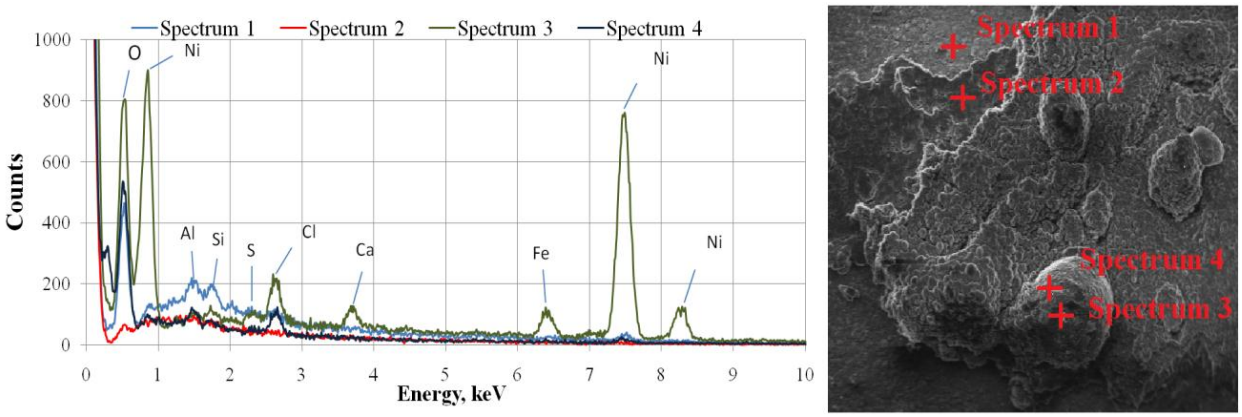


*Figure 3.27* **EDX spectra of the plasma facing surface of beryllium tiles and SEM image showing the locations spectra have been obtained from**

According to the literature beryllium material used in production of the tiles has significantly smaller grain sizes than that for pebbles [162]. No significant pores and cracks were observed.

*Carbon fibre composite*

Surface of divertor tiles are also coated with a deposition layer that is in fact thicker than that for the limiter tiles. In some positions of the divertor deposition layer could reach up to 300 μm of thickness [165]. Properties of these layers have been described widely in literature [145, 165, 175]. Therefore in this study structure of the tile material itself has been analysed. The structure analysis of the carbon fibre material was performed in different positions- both close to the surface and in the bulk of the tile. The fibres deep in the bulk of the tile were assumed not to have any modification and were used as a reference. The structure of the separate individual fibres corresponds to the core-sheath type of fibre [176] and has a diameter of (31.1±0.1) μm (Figure 3.28). On the erosion dominated areas of the plasma facing surface (some areas in the SRP part) the bending or complete destruction of the fibres was observed.

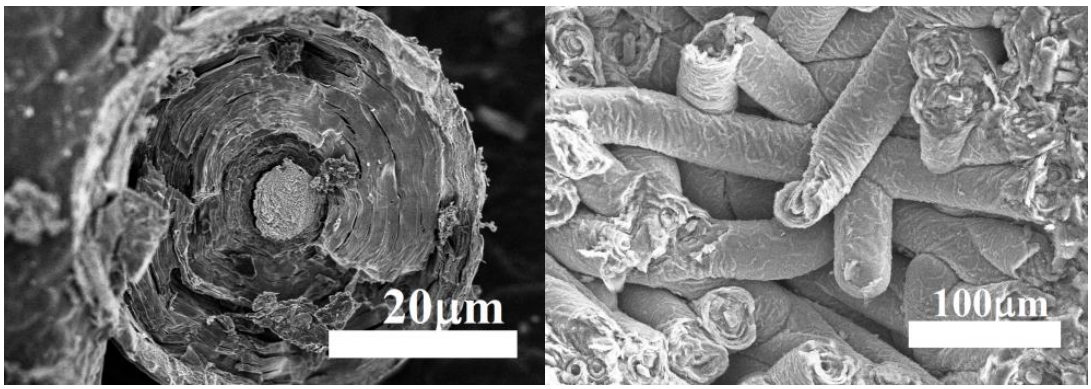


*Figure 3.28* **SEM images of carbon fibres in the bulk of JET divertor tile (on the right) and separate fibre cross-section**

To estimate the changes of the material structure the carbon fibre modifications were analysed. An increase of the fibre diameter close to the backside surface was observed to be up to 30% (in the sloping part), see Figure 3.29

There was also a small increase near the plasma facing surface of the SRP part. Increase of fibre diameter can be caused by neutron irradiation as a result of formation of extra graphite planes [177] or interplanar voids [178]. However, the neutron flux in the JET is not sufficient to cause such changes ($3.60 \cdot 10^{14} n \cdot cm^{-2}$ for the 2001-2004 operation period [179]) and neutron damage would be uniform through the tile: the largest modification was observed at the backside of the tile. This might mean that fibre modifications have been caused by some other reason, e.g. mechanical forces due to the method of mounting the tile in the divertor. The tile is mounted by pulling down on a central bolt from the backside with the tile supported at the corners, so that the backside is in tension. Therefore, there are no extra graphite planes but existing planes have separated as a result of the deformation, and extra space for tritium to migrate has appeared.

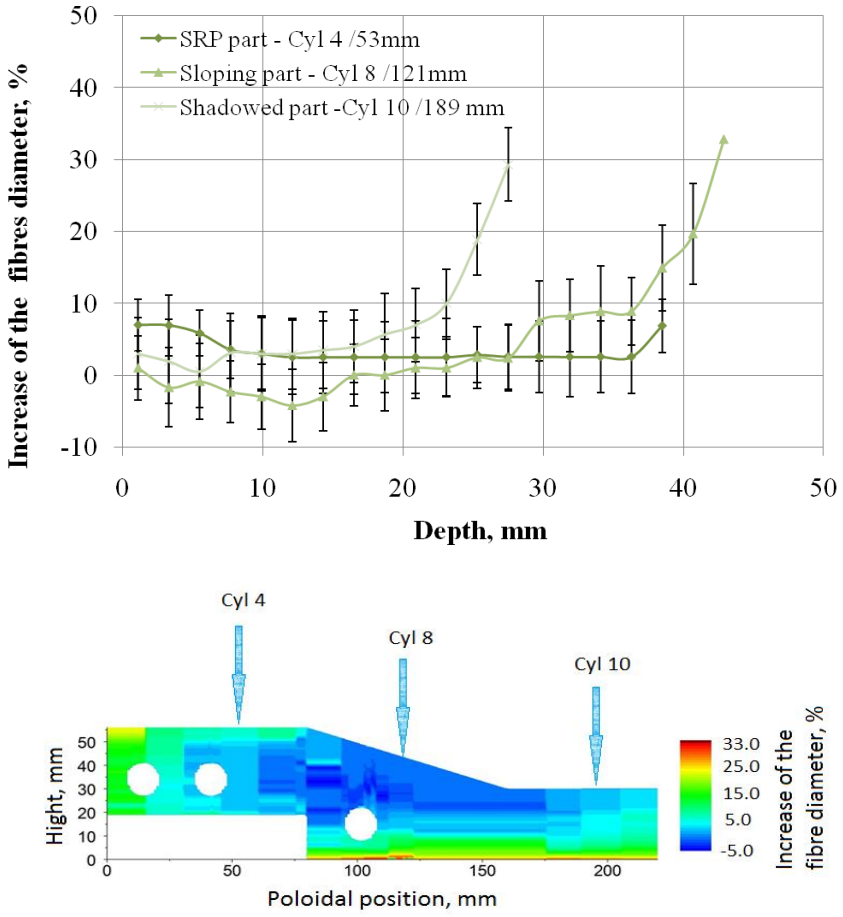


*Figure 3.29* **Increase of the fibre diameter in the tile 14BWG4B: a plot showing the increase of the fibre diameter with depth through the tile and distribution of the fibre swelling within the tile**

Another process that might have an effect on the structure is CFC interactions with oxygen during the storage in air. Whereas the plasma facing surface could be protected from an action of atmospheric oxygen by the deposition layer, it might explain small changes of the fibres in the SRP part where the deposition layer is relatively thin. Note, however, these interactions are at room temperature so would be expected to have a small effect. Increase of specific surface area and concentration of trapping sites resulting from destruction of fibres that follows from the 30% radial growth could lead to increased tritium retention [135].

Chemical composition analysis was done for unexposed carbon fibre tiles that were found to be comparably pure- XRF spectra showed just small amounts of impurities, such as Fe.

- *Initial tritium content, chemical forms and distribution*

*Beryllium*

Tritium content and chemical forms varies a lot depending on the location on tile and interaction with plasma. Because of the differences in exposure conditions, the tile was divided virtually in three parts of analysed areas: 1 plasma facing surface or operating surface of a "tooth" of beryllium tile, 2 lateral surfaces and 3 lateral surfaces between "teeth" of beryllium tile. Melted areas were also distinguished separately (Figure 3.30). Differences of tritium content in these separate parts are significant (

Figure *3.31*). The highest content was found to be in the plasma facing surface except for the melted areas where tritium is likely to be released as a result of exposure to high temperature.

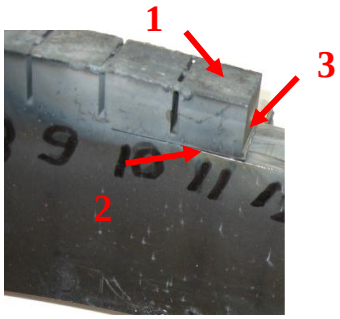


*Figure 3.30* **Fragment of a beryllium tile showing different parts studied: 1 - plasma facing surface, 2- lateral surface, 3- lateral surface between castellation**

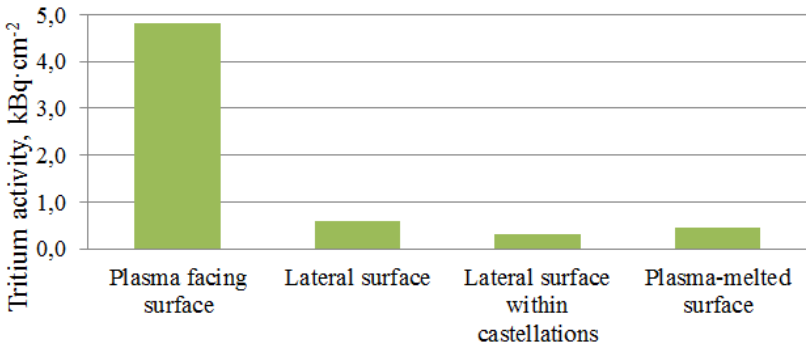


*Figure 3.31* **Tritium content in different parts of a beryllium tile**

Distribution of tritium chemical forms differs in these parts. The largest differences were observed in melted areas of a beryllium tile surface (Figure 3.32). In the melted areas only chemically bonded tritium was found, it might remain in the surface of tile after heat exposure in contrast to the molecular and atomic tritium.

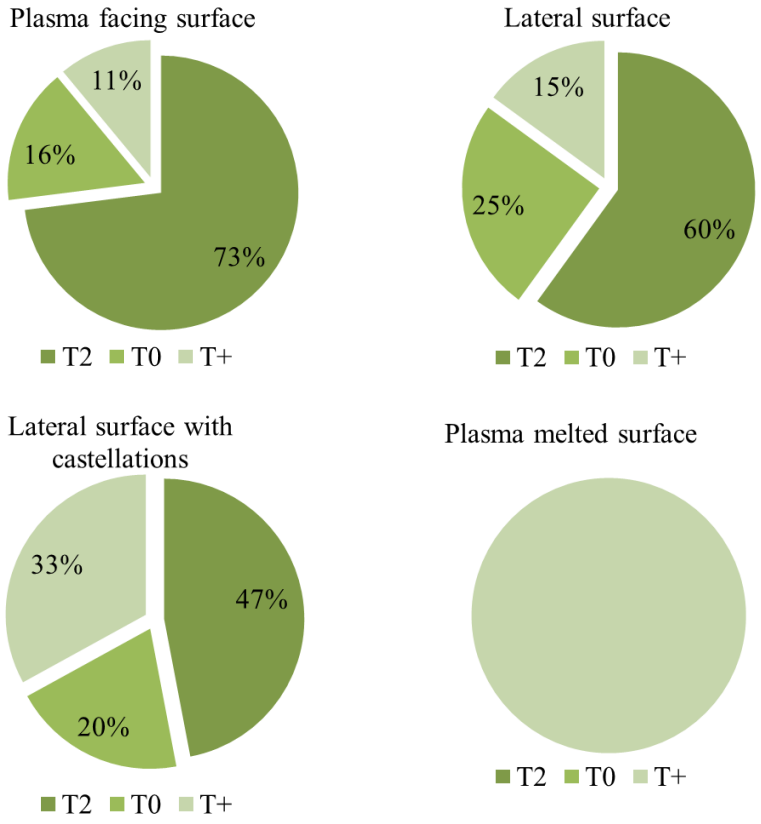


*Figure 3.32* **Distribution of tritium chemical forms in different parts of a beryllium tile**

Tritium bulk measurement in beryllium tiles revealed that the highest content of tritium is in the depth of about 10 -50 μm from the surface and then it decreases roughly exponentially until it is not detectable at the depth of about 150 μm (Figure 3.33). It must be emphasized that

tritium distribution has been measured only in metallic beryllium since method is based on chemical reactions between acid and metal. Tritium in deposition layer is most likely chemically bonded with carbon and therefore remains in the solution.

To estimate tritium accumulation mechanisms tritium sorption experiments have been performed on non-exposed beryllium tile. Sample has been exposed to tritium gas in 500$^{o}$C temperature for three hours and then tritium distribution measured.

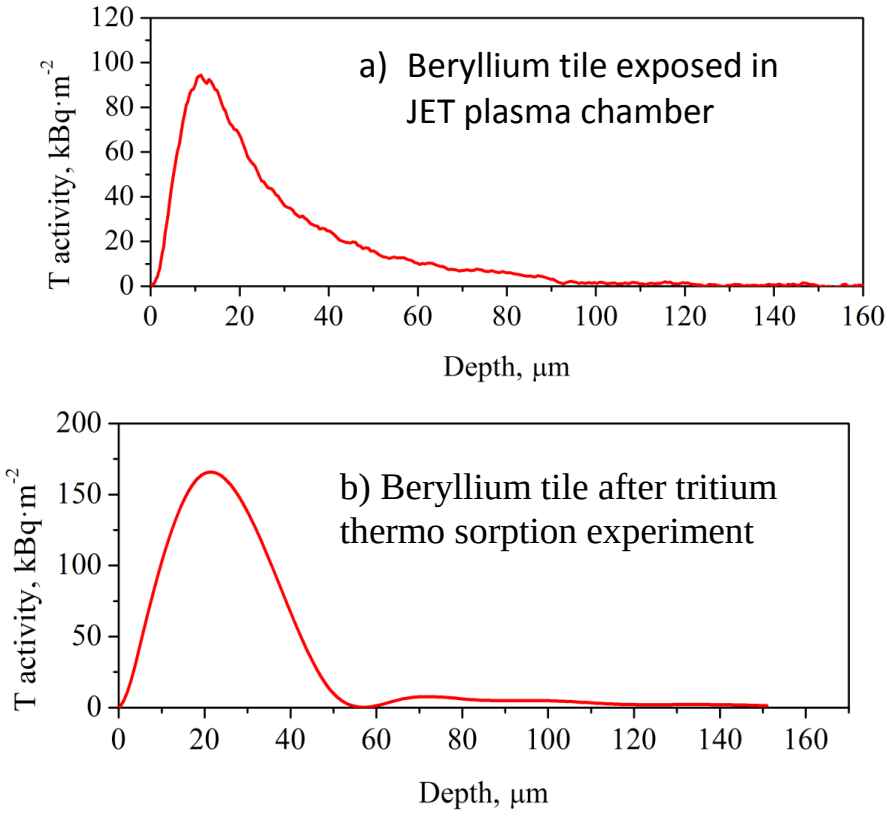


*Figure 3.33* **Tritium distribution in the surface layer of beryllium tile (0 corresponds to surface): a) tile exposed in JET plasma chamber and b) tile after thermo sorption experiment**

It was found that tritium distribution in beryllium tile after thermo sorption experiments is quite similar. Differences in distribution are related to the exposure time - in tile from plasma chamber tritium has been diffused deeper into the surface, whereas deposition layer on the surface delays tritium desorption from the surface, in contrast to the tile from sorption experiment that has a clean surface where tritium might freely release. This proves that tritium diffusion from the environment (in case of tiles exposed in plasma chamber term “environment” includes also the tritium containing deposition layer on the surface of the tile) into bulk of beryllium had been the main mechanism of accumulation, whereas energetic ion implantation from plasma has insignificant contribution. In real fusion reactor conditions where in contrast to JET high neutron

flux will be present tritium will be produced also as a result of neutron induced transmutation of beryllium and this tritium will be distributed more of less evenly.

*Carbon fibre composites*

Depth profiles of tritium trapped in the CFC tile were determined. In contrast to beryllium samples in CFC tiles tritium distribution was not measured continuously but by separate data point due to different methods. Tritium mass activity of the plasma surface layers (within the depth of 1mm), the bulk and the backside layers have been compared in the cylinders from different parts of the tile. Data points of the tritium mass activity of a typical cylinders cut from each of the three areas of the tile 14BWG4B are shown in logarithmic scale in Figure 3.34, the x-axis shows the depth position in millimetres and the last point of each figure represents the backside surface (cylinders from sloping part were also cut perpendicular to the plasma facing surface).

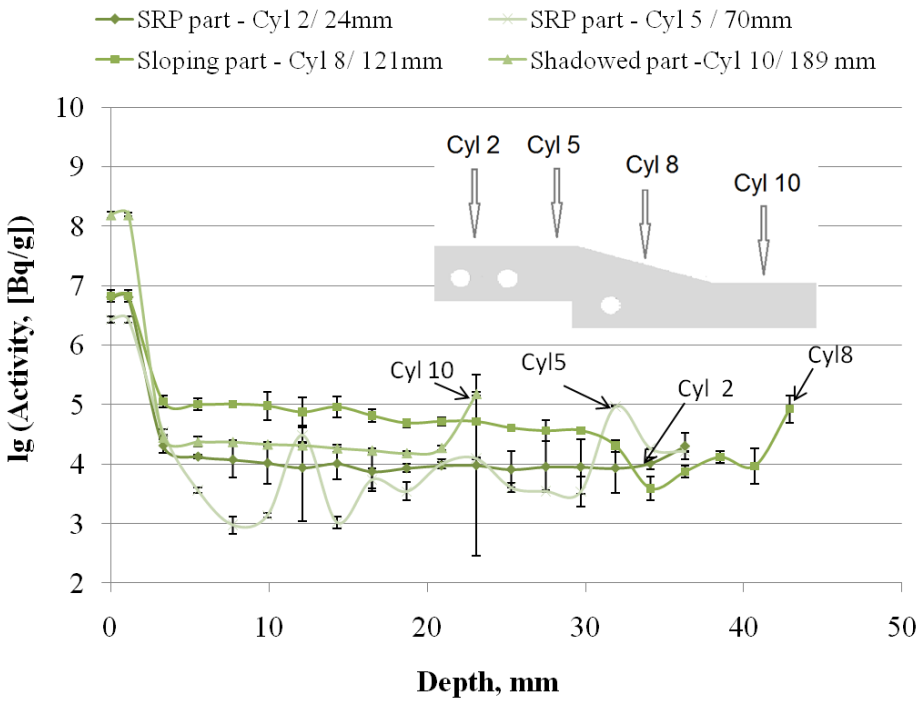


*Figure 3.34* **Tritium depth profiles in selected cylinders representing SRP, Sloping and Shadowed parts of the tile (in logarithmic scale)**

A common feature for all the cylinders investigated is that a large fraction of the tritium is localized in the plasma-facing surface slices of 1mm. This is due to the co-deposition of tritium in the thick deposition layers that are present on the tile 4 and also the implantation of the high energy tritons coming from the plasma could have some contribution. There is then a sharp decrease by 2-4 orders of magnitude to a bulk tritium activity which is at a more or less uniform

level until it reaches the backside layers where the activity increases again by about one order of magnitude. The phenomenon of increasing tritium content in the backside layer has been observed also by other authors [137] and no explanation has been given yet.

The highest surface activities of tritium were found in the shadowed part of the tile. For instance, the mass activity of the surface slice of Cyl10 was 0.156 $GBq \cdot g^{-1}$, while in Cyl 2 representing the SRP part it was only 0.006 $GBq \cdot g^{-1}$. Tritium activity in the surface layer can be described as a variable proportional to the thickness of deposition layer and inversely proportional to the energy deposited on a tile since tritium accumulated in the co-deposition layer and the hydrocarbon species would be released at a high temperature [134]. The shadowed area has both a thick deposition layer and no contact with plasma, in contrast to other parts of the tile. The sloping part of the tile has the thickest deposition layer (up to 300 μm), but at the same time it has been subjected to high temperature due to the plasma striking the surface and ELMs. Therefore tritium surface activity has similar values to that in the SRP part where the deposition layer is only 10 μm or less.

Migration of tritium into the bulk of a tile may be expected at high temperatures [170]. The surface of the sloping part of the tile may reach $1000^{o}C$ during plasma exposure: this is clearly reflected in the results from the sloping part in figure 3 where the tritium mass activity of the bulk was found to be about an order of magnitude higher than in other parts of the tile.

Chemical forms of tritium in carbon based tiles were not measured due to reasons mentioned above.

- *Summary*

In plasma facing material main tritium accumulation source is its co-deposition on the surface and subsequent diffusion into the bulk of material. To prove this mechanism tritium thermo sorption experiments have been performed with unexposed beryllium tiles and it was found that spatial distribution of diffused tritium is similar to that from plasma facing tiles. If one compares beryllium and carbon fibre composition tiles it is obvious that tritium accumulation in CFC tiles is much higher - in beryllium tiles tritium were found only in the surface layer of about 150 μm, whereas in CFC it was found to be distributed through all the bulk.

### 3.2.2 Tritium desorption

*Beryllium*

Tritium release from beryllium tiles must be considered to consist of several mechanisms. Major fraction of tritium is accumulated in the co-deposition layer where it is more likely chemically bonded with carbon [138]. Therefore, from this part tritium can be released as a tritium gas or as a tritium containing gaseous hydrocarbons. In beryllium itself it can be a molecule, atom or chemically bonded with impurities, mainly oxygen. At the same time deposition layer might work as physical barrier for tritium to release from the tile surface. Due to complicity of this system interpretation of the tritium desorption spectra is quite intricate. Tritium release starts at about 250$^{o}$C which is remarkably high for considering that tritium is accumulated so close to the surface.

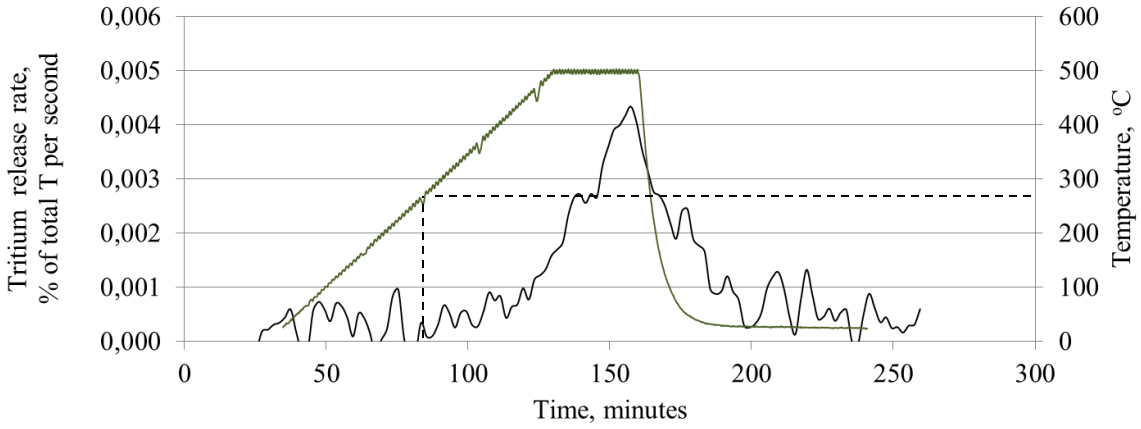


*Figure 3.35* **Tritium thermo desorption from sample of beryllium tile exposed in JET plasma chamber**

Tritium desorption has also been studied under action of such factors as accelerated electron radiation and magnetic field (Figure 3.35). It is obvious that these samples are more sensitive to the external factors if one compares with the beryllium pebbles. This phenomenon could have several explanations. Firstly, tritium accumulated in the deposition layer could be more sensitive to these external fields. In case of tritium chemically bonded in hydrocarbon radiolysis might have large contribution to its release; therefore also the processes during radiolysis in magnetic field could have significant impact. Secondly, tritium is located in a thin surface layer of the beryllium in contrast to pebbles where it is distributed in all the bulk.

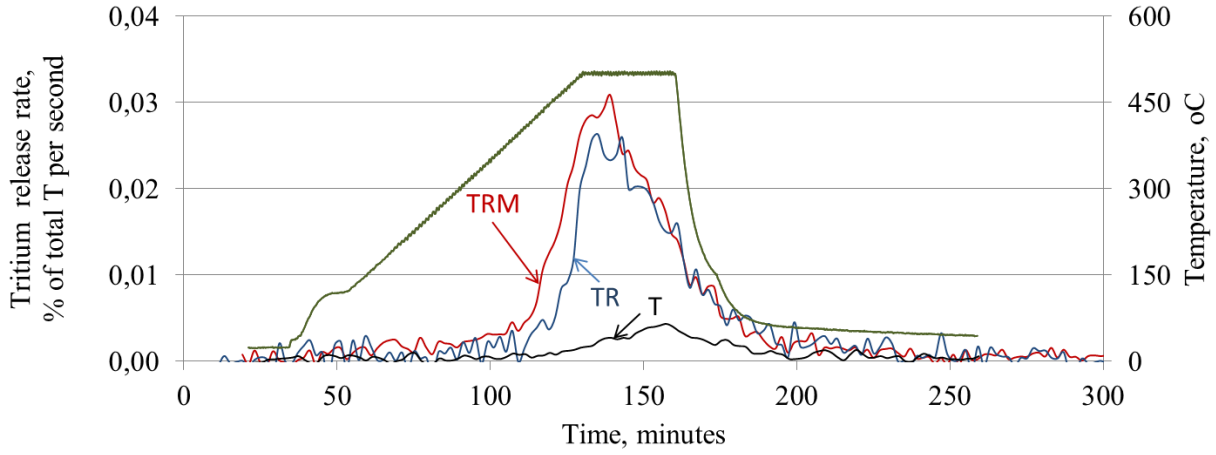


Figure 3.36 **Tritium thermo desorption from beryllium tiles (heating rate ~5°C·min$^{-1}$ up to 500°C, held at constant temperature for 1 h) under action of accelerated electrons (5 MeV, 14 MGy·h$^{-1}$) and magnetic field (1.7 T)**

Fractions of released tritium during thermo annealing for 1 hour at 500°C at different conditions are compared in Table 3.2

*Table 3.2* **Tritium desorption from beryllium tiles under different conditions**

| Tritium desorption conditions | | Tritium release, % from total |
|---|---|---|
| Abbrev. | Experiment details | |
| T | 5°C ·min$^{-1}$ up to 500°C, 2 h 40 min constant | 9±3 |
| TR | 5°C ·min$^{-1}$ up to 500°C, 2 h 40 min constant, accelerated electron beam, 5 MeV, 14 MGy·h$^{-1}$ | 45±13 |
| TRM | 5°C ·min$^{-1}$ up to 500°C, 2h 40 min constant, accelerated electron beam, 5 MeV, 14 MGy·h$^{-1}$ (200-280°C), magnetic field, 1.7 T | 63±11 |

*Carbon fibre composite*

Tritium desorption experiments has been performed with surface disks of cylinders from different parts of the divertor tile. Samples were heated up to 1100°C. It is obvious that desorption process depends a lot on a position on a tile (Figure 3.37).

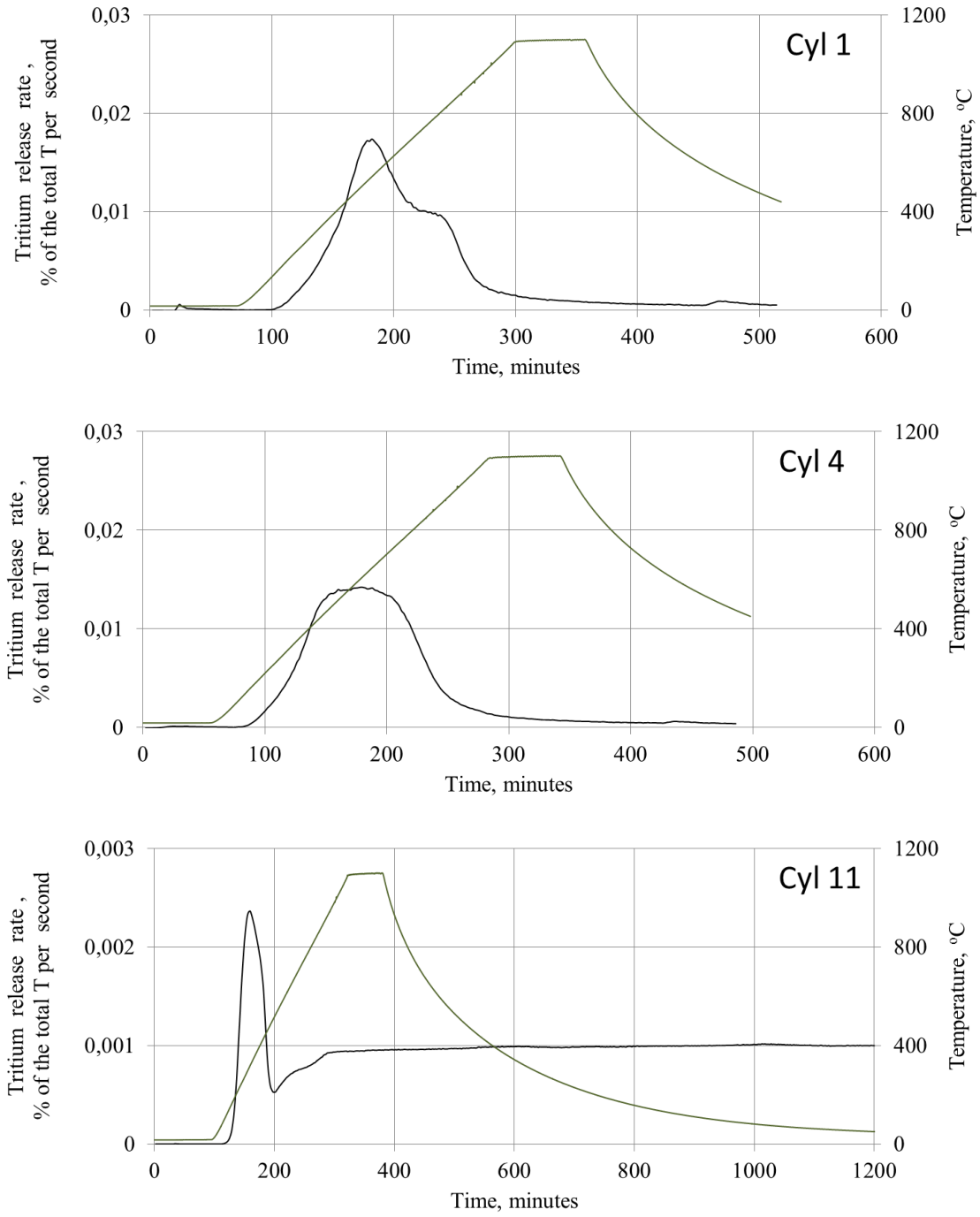


*Figure 3.37* **Tritium release by thermal desorption from the surface disks of cylinders 1, 4 and 11 of tile 14BWG4B**

It might be assumed that all desorption curves are combination of similar processes, but in different contribution ratios. As mentioned above - surface of the plasma facing materials consist of two different parts – deposition layer and substrate, in this particular case, the carbon fibre composite. According to the work of Kanashenko et al, there are three types of tritium

adsorption/trapping sites in a carbon structure: relaxed and un-relaxed dangling bonds on the edges of interstitial carbon clusters and grain surfaces, respectively, and adsorption on a basal planes (true solution) (see chapter 1.6.2), whereas deposition layers mostly consist of hydrogenated amorphous carbon where tritium is chemically bonded to the carbon either in $sp^3$ or $sp^2$ hybridization. Therefore we may consider tritium to be bonded with at least 5 different energies. Also the tritium containing species might be of different composition, such as $T_2$ (TH, TD), $CH_xQ_y$ (where Q is D and/or T, x + y = 4) and longer tritium containing hydrocarbon chains. With the method used in this study it was not possible to distinguish these different chemical forms as it is based on tritium radioactivity measurements in a purge gas.

Cylinder 1 is from horizontal part of tile nearest the Septum Replacement Plate that has some shadowing from SRP tile. Desorbed tritium reached 1.2 $MBq \cdot cm^{-2}$ and release started at ≤ 200°C. Cylinder 4 is also from horizontal part of tile nearest the Septum Replacement Plate but has some exposure to plasma (deposition layer about 10 μm). Amount of desorbed tritium 2.1 $MBq \cdot cm^{-2}$ and release started at ≤ 100°C. Cylinder 11 is from horizontal part of the tile shadowed from the plasma by tile 3 with thick deposition layer (smooth, dense film with high H/C ratio). Desorbed tritium: ~10 MBq/cm2 (due to the "tail" of the TDS no precise value can be calculated), release started at ≤ 50°C. Deposition layer is a very complex material and its composition and properties might differ a lot depending on a position in the vessel or even on a single tile. Cylinder 11 represents the shadowed area of a tile that is not subjected to a plasma impact; therefore tritium could be also trapped by a weak interactions that in cases of other cylinders has been released already during exposure in the plasma chamber. That could also explain the fast start of the release of tritium from cylinder 11 in the temperature programmed desorption experiment.

### 3.2.3 Tritium behaviour model in plasma facing materials

In general, plasma facing material might be considered as a dual system consisting of a substrate and a deposition layer. These two parts have significant differences regarding tritium transport and accumulation mechanisms.

Dominant mechanism of tritium accumulation is its co-deposition with eroded particles form plasma facing materials (process I in scheme, see Figure 3.38). It is well known that carbon erosions are considerably higher than that for beryllium or other metallic materials, therefore in JET plasma chamber this deposition layer mostly consist of carbon and hydrogen. Tritium release

from this layer occurs as a result of C-H or C-C bond breaking where tritium molecule of short chain hydrocarbon molecule is produced. Exposure to accelerator electron radiation must be facilitating this process considerably. Magnetic field could have two opposite effects – formation of tritium molecules would be slowed down, whereas short chain hydrocarbon segregation would be facilitated.

Another tritium accumulation mechanism is its implantation as an energetic ion (II). As a result of this process tritium is trapped in the first nanometers of the material. In carbon based materials it is trapped on the trapping sites, whereas in beryllium it is most likely as an interstitial. From beryllium samples tritium will released by diffusion to the surface and then recombination into molecule, whereas from carbon based – by trapping – detrapping process and then recombination into molecules (IV, V).

According to the results on tritium bulk distribution it is clear that tritium has diffused also into the bulk of the materials. Especially in CFC tiles where it was found to be accumulation throughout all the bulk. In carbon based material tiritum is most likely bonded on trapping sites of different energies (see chapter 1.6.2) and might be release by trapping-detrapping mechanism or by diffusion through the pore channels (CFC material is very porous) (IV). In beryllium tritium could be accumulated as interstitial or chemically bonded with oxygen impurities. From bulk of beryllium tiles it releases by diffusion (through lattice or along grain boundaries) to the surface and recombination into molecules (IV).

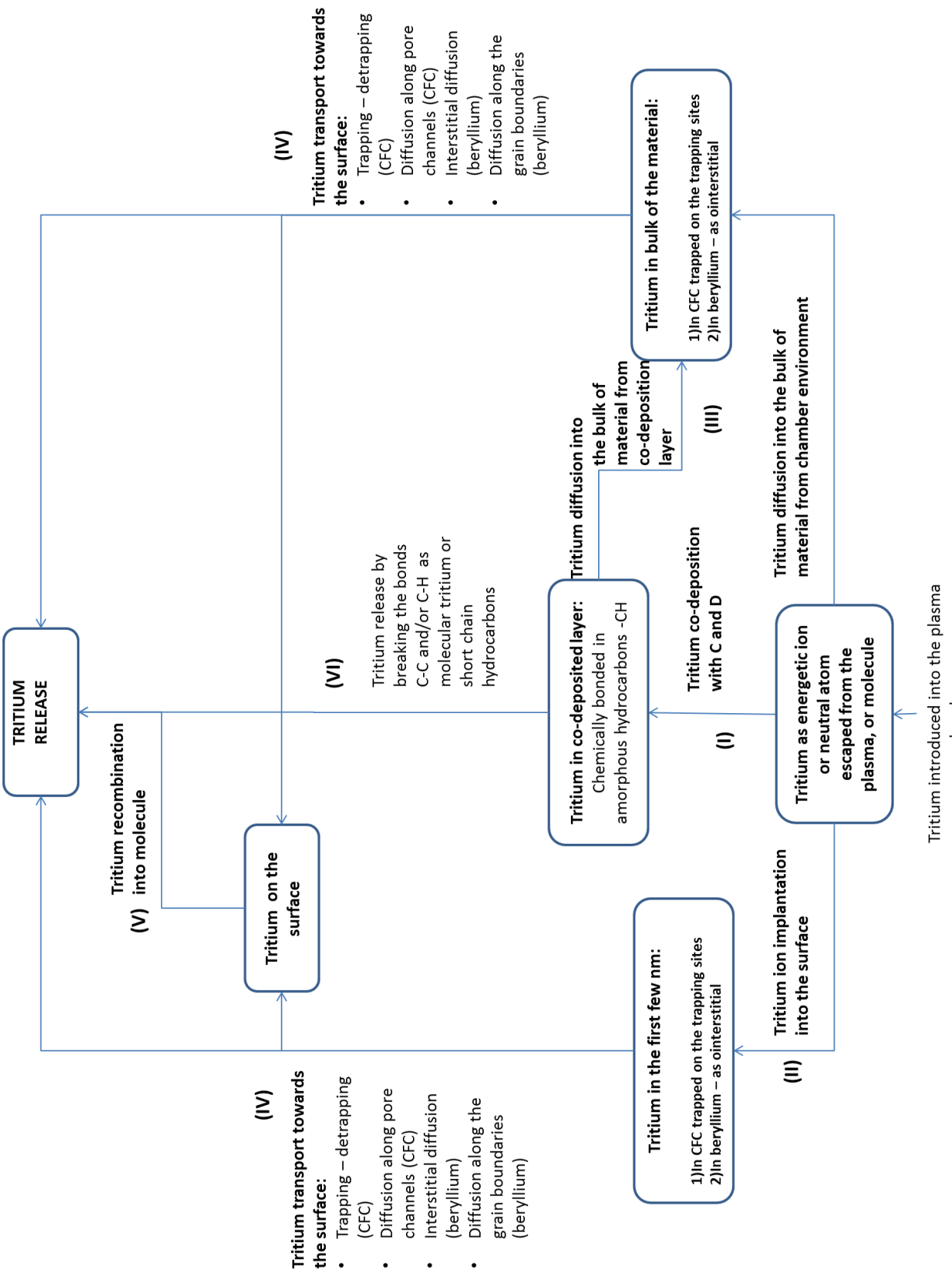


*Figure 3.38* **Schematic view of tritium behaviour in plasma facing materials**

**Summary**

Tritium thermodesorption is governed by two main mechanisms – desorption from the substrate material and a deposition layer. Substrate material (either CFC or beryllium) might be expected to have similar properties all over the plasma vessel, except for eroded or melted areas. Properties of deposition layer vary a lot depending on the position in a plasma chamber. Facilitating effect of ionizing radiation on tritium desorption has been observed and might be assumed to occur due to hydrocarbon radiolysis for deposition layer of plasma exposed samples. If the magnetic field is added in the process the synergetic effect can be observed.

### *3.3 Role of high magnetic field and ionizing radiation in tritium behaviour in fusion reactor materials*

In post irradiation/exposure tritium desorption studies performed within this work it has been found that simultaneous action of ionizing radiation and high magnetic field facilitates tritium release. However, up to now in situ measurements of tritium desorption rates under conditions similar to reactor no magnetic field has been used. Therefore it might be concluded that at least for beryllium materials situation in real reactor conditions where high magnetic field is present situation could be more optimistic as it is predicted based on in situ experiments with no magnetic field.

Mechanisms of the facilitating effect of irradiation and magnetic field on tritium desorption from beryllium could be explained by radiation chemistry of gases in the presence of high magnetic field.

As a result of interaction with fast electrons molecular tritium dissociates into atoms. Though, the recombination back to molecule probability is very high. However, in the presence of magnetic field the electron spins of tritium might be changed to parallel due to the Zeeman effect and atoms do not react and therefore move away from each other (Figure 3.39). Furthermore atomic tritium can diffuse through the lattice.

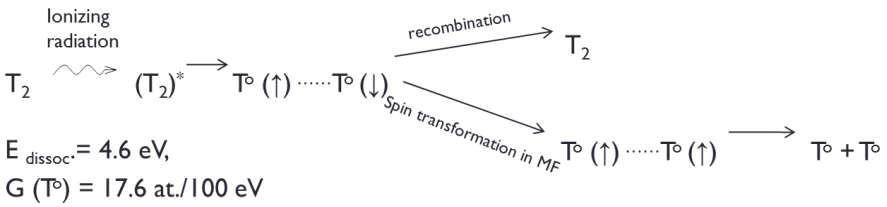


*Figure 3.39* **Mechanism of tritium radiolysis in presence of magnetic field**

That might be the dominant process responsible for the magnetic field effect in the irradiated beryllium pebbles - *beryllium/tritium/helium* system.

### *3.4 Recommendations regarding nuclear waste reduction*

Fusion reactor materials after exploitation can be classified as nuclear wastes due to radioactive tritium inventory. Recommendations regarding the nuclear waste reduction could be developed based on the results obtained in this work.

(1) Contribution of synergetic magnetic field and irradiation effect must be taken into account when estimating tritium inventory in materials according to in-pile desorption rates. Presence of magnetic field increases tritium release by 5-10% for neutron multiplier beryllium pebbles.

(2) Detritiation methods based on material thermo-annealing could be improved by introduction of an extra factor - simultaneous irradiation and exposure to magnetic field, since it could decrease temperature of thermal treatment, and therefore there would be no need to handle liquid beryllium (melted).

### *3.5 Summary*

The objective of this dissertation was to develop the knowledge base for fusion applications of beryllium and carbon fibre composites (CFC). This has been achieved by

- collating the mass of data from fission experiments relevant for future fusion requirements, particularly on beryllium pebbles
- using metallurgical techniques to increase the understanding of neutron damage in the materials
- developing the Chemical Scavenger method in UL Laboratory of Radiation Chemistry of Solids for analysis of radioactive samples for fusion application
- determining the degree of tritium accumulation that may occur in neutron irradiated materials
- demonstrating that accelerated electrons can improve the detritiation process, and that the presence of a strong magnetic field has a beneficial synergism for detritiation

# CONCLUSIONS

1. The structure of neutron irradiated beryllium materials and presence of impurities have been shown to have a significant role in tritium accumulation process. In neutron irradiated beryllium tritium can be accumulated as an interstitial atom ($T^o$), a molecule in gas inclusions ($T_2$) or it can be chemically bonded to impurities ($T^+$). Main chemical form of the tritium localized in the irradiated beryllium pebbles is $T_2$ (up to 96%). High content of this immobile form might significantly extend the time and therefore increase the cost of detritiation method based on thermo-annealing processes.

2. If one compares beryllium and carbon fibre composition tiles it is obvious that tritium accumulation in CFC tiles is much higher - in beryllium tiles tritium was found only in a surface layer of about 150 μm, whereas in CFC it was found to be distributed through all the bulk.

3. The increase of the specific surface area and concentration of the hydrogen traps in the CFC material as a result of deformations and destruction of the fibres was shown to increase total tritium accumulation.

4. The chemical forms of tritium before and after thermal treatment under different conditions have been determined, from which the processes occurring during the thermo-annealing have been estimated. Several stages of tritium transport process in neutron irradiated beryllium have been distinguished (interstitial diffusion and diffusion along grain boundaries at low temperature, transport along open pore network system and cracks as temperature is raised).

5. Tritium release is much faster and requires lower temperature from 0.1 mm pebbles produced by Inert Gas Atomization (IGA) method than that for pebbles of 1.0 mm pebbles produced by Rotating Electrode Process (REP) method. It can be explained by both smaller diffusion length in IGA pebbles and the existence of voids in REP methods, where molecular tritium is trapped.

6. Desorption of tritium from plasma exposed samples strongly depends of the location on the plasma facing sample within the torus and hence the extent of direct interaction of the surface with the plasma. The pathways for tritium introduction into the sample have been estimated from the thermal desorption spectra.

7. Accelerated electron radiation has been demonstrated to facilitate tritium desorption from materials. This phenomenon is postulated to be related to molecular tritium radiolysis in case of neutron irradiated beryllium and hydrocarbon radiolysis for deposition layer

of plasma exposed samples. However, the synergetic effect of accelerated electron irradiation and magnetic field has been shown to considerably increase tritium release. Presence of magnetic field increases tritium release by 5-10% for neutron multiplier beryllium pebbles, and by up to 50% for plasma facing materials – beryllium tiles. Thus detritiation methods based on material thermo-annealing could be improved by the introduction of an extra factor - simultaneous irradiation and exposure to magnetic field.

# List of author's scientific publications

***Original research articles***

1. **E. Pajuste, A. Vitins, G. Kizane, V. Zubkovs and P. Birjukovs** Tritium distribution and chemical forms in the irradiated beryllium pebbles before and after thermoannealing. *Fusion Engineering and Design*, 2011. *86* (9-11), 2125-2128.

2. **E. Pajuste, G. Kizane, J.P. Coad, A. Vitins, A. Kirillova, M. Halitovs and JET-EFDA Contributors** Structural changes and distribution of accumulated tritium in the carbon based JET tiles**.** *Journal of Nuclear Materials*, 2011. *415* (1), S765-S768.

3. **A. Vītiņš, V. Zubkovs, G. Ķizāne, E. Pajuste and V. Kinerte** Tritium release characteristics of neutron-irradiated reference beryllium pebbles for the helium cooled pebble bed (HCPB) blanket. *Fusion Science and Technology*, October 2011. *60* (3), 1143-1146.

*4.* **Juris Tīliks, Aigars Vītiņš, Gunta Ķizāne, Vija Tīlika, Elīna Kolodinska, Sarmīte Kalēja, Broņislavs Leščinskis** Effects of external energetic factors on tritium release from the EXOTIC 8-3/13 neutron-irradiated beryllium pebbles *Fusion Engineering and Design*, 2009. *84* (7-11), 1842-1846.

*5.* **J. Tīliks, G. Ķizāne, A. Vītiņš, E. Kolodinska, J. Tīliks Jr., I. Reinholds** Tritium release from beryllium articles for use in fusion devices *Journal of Nuclear Materials,* 2009. *386-388,* 874-877.

6. **Juris Tīliks, Gunta Ķizāne, Aigars Vītiņš, Elīna Kolodinska, Vija Tīlika and Broņislavs Leščinskis** Tritium sorption and desorption from JET beryllium tiles under temperature, electron radiation and magnetic field, *Fusion Engineering and Design,* 2008. *83,* (10-12), 1388-1391.

7. **Vītiņš, G. Ķizāne, J. Tīliks, J. Tīliks Jr., E. Kolodinska** Tritium release from breeding materials in high magnetic field, *Fusion Engineering and Design*, 2007. *82*(15-24), 2341-2346.

8. **Juris Tīliks, Gunta Ķizāne, Aigars Vītiņs, Elīna Kolodinska, Elisa Rabaglino** Magnetic Field Effect on the Tritium Release from Neutron – Irradiated Beryllium Pebbles, *Nuclear Technology*, 2007. *159* ( 3), 245-249.

***Conference proceedings with editors***

1. **J. Tiliks, G. Kizane, A. Vitins, E. Kolodinska, V. Tilika, S. Kaleja** Chemical forms of tritium in Be pebbles after different treatments, – **In:** *22nd IAEA Fusion Energy Conference (IAEA FEC 2008)* held in Geneva, Switzerland, October 13-18, 2008. Preprint FT/P2-14G. (Edit. G. Mank, A. Malaquias), 2008, Pages 1 – 5, Available online at: http://www-pub.iaea.org/MTCD/Meetings/FEC2008/ft_p2-14.pdf

2. **G. Ķizāne, J. Tīliks, A. Vītiņš, E. Kolodinska** Influence of High Magnetic Field on Fusion Reactor Blanket Processes,- **In:** *21st IAEA Fusion Energy Conference*, held in Chengdu, China, October 16-22, 2006, ISBN 92-0-100907-0/ISSN 0074-1884, 2007, Preprint FT/P5-17 (Edit. G. Mank, A. Malaquias), Pages 1 – 8. Available online at: http://www-pub.iaea.org/MTCD/Meetings/FEC2006/ft_p5-17.pdf

3. **E. Kolodinska, G. Ķizāne, J. Tīliks, A. Vītiņš, I. Reinholds** Tritium release from fusion reactor beryllium materials,- **In:** *International conference Radiation interaction with material and its use in technologies* held in Kaunas, Lithuania September 28-30, 2006, Program and Materials (Edit. A. Grigonis), 2006, Pages142 – 144

# Participation in international conferences

1. **E. Pajuste, A. Vitins, G. Kizane, V. Zubkovs, P. Birjukovs** Tritium distribution and chemical forms in the irradiated beryllium pebbles before and after thermo-annealing. In: 26th International Sypmphosium on Fusion Technology (SOFT-26) held in Porto, Portugal, September 28 - October 1, 2010.

2. **E. Pajuste, G. Ķizāne, J.P. Coad, A. Vītiņš, A. Kirilliova, M. Halitovs and EFDA JET Contributors** Structural changes and distribution of accumulated tritium in the carbon based JET tiles. **In:** *19th International Conference on Plasma Surface Interaction (PSI-19)* held in San Diego, USA, May 24 - 28, 2010, Page 168.

3. **E. Pajuste, G. Ķizāne, J.P. Coad, A. Vītiņš, M. Halitovs and EFDA JET Contributors** Thermal desorption of tritium from carbon based tiles **In:** 10th International Workshop on Hydrogen Isotopes in Fusion Reactor Materials held in Pleasanton, USA, May 31 - June 1, 2010.

4. **E. Kolodinska, G. Ķizāne, J.P. Coad, A. Vītiņš, V. Tīlika, I. Dušenkova** Behavior of tritium accumulated in the surface layer of beryllium tiles,- **In:** *9$^{th}$ International Workshop on Hydrogen Isotopes in Fusion Reactor Materials*, held in Salamanca, Spain, June 2 - 3, 2008. Abstract Book. Page 35.

5. **E. Kolodinska, G. Ķizāne, A. Vītiņš, J. Tīliks, P. Coad and G. Piazza**, Tritium localization and release from surfaces of beryllium tiles,-**In:** *11$^{th}$ International Workshop on Plasma Facing Materials and Components for Fusion Application*, held in Greifswald, Germany, October 10 - 12, 2006, Abstracts, Page79.

# REFERENCES


1. **McCracken, G. and Stott, P.**, Fusion, The Energy of the Universe. *Complementary Science* 2005, Burlington: Accademic Press. 224.
2. **de Laeter, J.R.,Böhlke, J.K.,De Bièvre, P., *et al.*** Atomic weights of the elements. Review 2000 (IUPAC Technical Report). *Pure and Applied Chemistry*, 2003. *75*(6), 683-800.
3. **Sublette, C.** Nuclear Weapons Frequently Asked Questions. *Nuclear Weapons Archive* 2006; Available from: http://nuclearweaponarchive.org/Nwfaq/Nfaq12.html.
4. **Lawson, J.D.** Some Criteria for a Power Producing Thermonuclear Reactor. *Proceedings of the Physical Society. Section B*, 1957. *70*(1), 6.
5. **Boozer, A.H.** Physics of magnetically confined plasmas. *Reviews of Modern Physics*, 2005. *76*(4), 1071.
6. **Smirnov, V.P.** Tokamak foundation in USSR/Russia 1950–1990. *Nuclear Fusion*, 2010. *50*(1), 014003.
7. **JET-EFDA**. European Fusion Development Agreement (EFDA) – Joint European Toros (JET). [cited 2011 19.03.2011]; Available from: http://www.jet.efda.org/.
8. **Spitzer, L.J.**, Theory of Confinement in the Stellarator. 1958, Ptinceton University: New Jersey.
9. **Schauer, F.** Status of Wendelstein 7-X construction. *Fusion Engineering and Design*, 2007. *82*(5-14), 443-453.
10. **Federici, G. and et al.** Plasma-material interactions in current tokamaks and their implications for next step fusion reactors. *Nuclear Fusion*, 2001. *41*(12), 1967.
11. **Laboratory, L.L.N.** National Ignition Facility & Photon Science. [cited 2011 19.03.2011]; Available from: https://lasers.llnl.gov/.
12. **(F4F), F.f.E.** Fusion For Energy. 2007 [cited 2011 19.03.2011]; Available from: www.fusionforenergy.europa.eu.
13. **Brumfiel, G. and Cyranonski, D.** Quake sparks nuclear crisis. *Nature*, 2011. *471*(7338), 273-275.
14. **Brodén, K.,Edwards, R.,Lindberg, M., *et al.*** Waste from fusion reactor: A comparison with other energy producing systems. *Fusion Engineering and Design*, 1998. *42*(1-4), 1-6.
15. **Gruber, J.** High-level radioactive waste from fusion reactors. *Environmental Science & Technology*, 1983. *17*(7), 425-431.
16. **McBride, J.P.,Moore, R.E.,Witherspoon, J.P., *et al.*** Radiological Impact of Airborne Effluents of Coal and Nuclear Plants. *Science*, 1978. *202*(4372), 1045-1050.
17. **Konishi, S.,Glugla, M. and Hayashi, T.** Fuel cycle design for ITER and its extrapolation to DEMO. *Fusion Engineering and Design*, 2008. *83*(7-9), 954-958.
18. **Holtkamp, N.** An overview of the ITER project. *Fusion Engineering and Design*, 2007. *82*(5-14), 427-434.
19. **Organization, I.** ITER. 2011 [cited 2011 19.03.2011]; Available from: http://www.iter.org.
20. **Ihli, T.,Basu, T.K.,Giancarli, L.M., *et al.*** Review of blanket designs for advanced fusion reactors. *Fusion Engineering and Design*, 2008. *83*(7-9), 912-919.

21. **Boccaccini, L.V.,Salavy, J.F.,Bede, O., *et al.*** The EU TBM systems: Design and development programme. *Fusion Engineering and Design*, 2009. *84*(2-6), 333-337.
22. **Boccaccini, L.V.,Salavy, J.F.,Lässer, R., *et al.*** The European test blanket module systems: Design and integration in ITER. *Fusion Engineering and Design*, 2006. *81*(1-7), 407-414.
23. **Cardella, A.,Rigal, E.,Bedel, L., *et al.*** The manufacturing technologies of the European breeding blankets. *Journal of Nuclear Materials*, 2004. *329–333*, 133–140.
24. **Gasparotto, M.,Boccaccini, L.V.,Giancarli, L., *et al.*** Demo blanket technology R&D results in EU. *Fusion Engineering and Design*, 2002. *61-62*, 263-271.
25. **Poitevin, Y.,Boccaccini, L.V.,Cardella, A., *et al.*** The European breeding blankets development and the test strategy in ITER. *Fusion Engineering and Design*, 2005. *75-79*, 741-749.
26. **Nishitani, T.,Tanigawa, H.,Jitsukawa, S., *et al.*** Fusion materials development program in the broader approach activities. *Journal of Nuclear Materials*, 2009. *386-388*, 405-410.
27. **Zmitko, M.,Poitevin, Y.,Boccaccini, L., *et al.*** Development and qualification of functional materials for the EU Test Blanket Modules: Strategy and R&D activities. *Journal of Nuclear Materials*. *In Press, Corrected Proof*.
28. **Lindau, R.,Möslang, A.,Rieth, M., *et al.*** Present development status of EUROFER and ODS-EUROFER for application in blanket concepts. *Fusion Engineering and Design*, 2005. *75-79*, 989-996.
29. **Akiba, M.,Enoeda, M. and Tanaka, S.** Overview of the TBM R&D activities in Japan. *Fusion Engineering and Design*, 2010. *85*(10-12), 1766-1771.
30. **Cismondi, F.,Rey, J.,von der Weth, A., *et al.*** Design update and mock-up test strategy for the validation of the EU-HCPB-TBM

concept. . *Fusion Science and Technology*, 2009. *56*(1), 221-226.
31. **Rubel, M.** Structure Materials in Fusion Reactors: Issues Related to Tritium, Radioactivity and Radiation-Induced Effects. *Fusion Science and Technology*, 2010. *57*(2T), 474-482.
32. **Taylor, N.P.,Forty, C.B.A.,Petti, D.A., *et al.*** The impact of materials selection on long-term activation in fusion power plants. *Journal of Nuclear Materials*, 2000. *283-287*(Part 1), 28-34.
33. **Fedorov, A.V.,Peeters, M.M. and van der Laan, J.G.**, EXOTIC-8: Tritium Release Measurements in Ceramic Tritium Breeder Materials, A.J.Magielsen, Editor. 2008, NRG: Petten. p. 109.
34. **van der Laan, J.G.,Boccaccini, L.V.,Conrad, R., *et al.*** Test-element assembly and loading parameters for the in-pile test of HCPB ceramic pebble beds. *Fusion Engineering and Design*, 2002. *61-62*, 383-390.
35. **Hegeman, J.B.J.,van Essen, E.D.L.,Jong, M., *et al.*** Thermomechanical behaviour of ceramic breeder pebble stacks for HICU. *Fusion Engineering and Design*, 2003. *69*(1-4), 425-429.
36. **Hegeman, J.B.J.,Laan, J.G.v.d.,Kawamura, H., *et al.*** The HFR Petten high dose irradiation programme of beryllium for blanket application. *Fusion Engineering and Design*, 2005. *75-79*, 769-773.
37. **van Til, S.,Hegeman, J.B.J.,Cobussen, H.L., *et al.*** Evolution of beryllium pebbles (HIDOBE) in long term, high flux irradiation in the high flux reactor. *Fusion Engineering and Design*. *In Press, Corrected Proof*.

38. **Fedorov, A.V. and Magielsen, L.** Analysis of in-pile operation and modeling of tritium transport in lead-lithium irradiation experiments Libretto 4/1, 4/2 and 5. *Fusion Engineering and Design*. *In Press, Corrected Proof*.
39. **Merola, M.,Dänner, W.,Palmer, J., *et al.*** European contribution to the development of the ITER divertor. *Fusion Engineering and Design*, 2003. *66-68*, 211-217.
40. **Rabaglino, E.,Ronchi, C. and Cardella, A.** Recent progress in the modelling of helium and tritium behaviour in irradiated beryllium pebbles. *Fusion Engineering and Design*, 2003. *69*, 455-461.
41. **Möslang, A.,Pieritz, R.A.,Boller, E., *et al.*** Gas bubble network formation in irradiated beryllium pebbles monitored by X-ray microtomography. *Journal of Nuclear Materials*, 2009. *386–388*, 1052–1055.
42. **Kurinskiy, P.,Cardella, A.,Klimiankou, M., *et al.*** Production and thermal stability of beryllium with fine grain structure to improve tritium release during neutron irradiation. *Fusion Engineering and Design*, 2005. *75–79*(Proceedings of the 23rd Symposium of Fusion Technology - SOFT 23), 709–713.
43. **Verzilov, Y.,Sato, S.,Ochiai, K., *et al.*** The integral experiment on beryllium with D-T neutrons for verification of tritium breeding. *Fusion Engineering and Design*, 2007. *82*(1), 1-9.
44. **Lee, Y.-K.** Analysis of the tritium breeding ratio benchmark experiments using the Monte Carlo code TRIPOLI-4. *Fusion Engineering and Design*, 2010. *85*(7-9), 1125-1128.
45. **Pereslavtsev, P.,Cismondi, F.,Fischer, U., *et al.*** Neutronic analysis of the HCPB TBM in ITER utilizing an advanced integral approach. *Fusion Engineering and Design*, 2010. *85*(7-9), 1653-1658.
46. **Paméla, J.,Romanelli, F.,Watkins, M.L., *et al.*** The JET programme in support of ITER. *Fusion Engineering and Design*, 2007. *82*(5-14), 590-602.
47. **Keilhacker, M. and Watkins, M.L.** D-T experiments in the JET tokamak. *Journal of Nuclear Materials*, 1999. *266-269*, 1-13.
48. **Rebut, P.-H.** The JET preliminary tritium experiment. *Plasma Physics and Controlled Fusion*, 1992. *34*(13), 1749.
49. **JONES, T.T.C. and Contributors, J.E.** Technical and Scientific Aspects of the JET Trace-Tritium Experimental Campaign. *Fusion Science and Technology*, 2005. *48*(1), 250-257.
50. **Pospieszczyk, A.,Brezinsek, S.,Meigs, A., *et al.*** Molecular (H/D/T) sources in JET. *Journal of Nuclear Materials*, 2007. *363-365*, 811-815.
51. **Zastrow), J.T.p.b.K.-D.** Trace tritium transport in JET. *Nuclear Fusion*, 1999. *39*(11Y), 1891.
52. **Rimini), J.T.p.b.F.G.** DT fusion power production in ELM free H modes in JET. *Nuclear Fusion*, 1999. *39*(11Y), 1897.
53. **Mironov, M.I. and et al.** Tritium transport studies with use of the ISEP NPA during tritium trace experimental campaign on JET. *Plasma Physics and Controlled Fusion*, 2010. *52*(10), 105008.
54. **Matthews, G.F. and et al.** Overview of the ITER-like wall project. *Physica Scripta*, 2007. *2007*(T128), 137.
55. **Paméla, J.,Matthews, G.F.,Philipps, V., *et al.*** An ITER-like wall for JET. *Journal of Nuclear Materials*, 2007. *363-365*, 1-11.
56. **Riccardo, V.** Engineering challenges of the JET ITER-like Wall. *Journal of Nuclear Materials*, 2009. *390-391*, 895-899.

57. **Cristescu, I.R. and et al.** Tritium inventories and tritium safety design principles for the fuel cycle of ITER. *Nuclear Fusion*, 2007. *47*(7), S458.
58. **Chen, Y.,Fisher, U.,Pereslavtsev, P., *et al.***, The EU Power Plant Conceptual Study - Neutronic Design Analysis for Near Term and Advanced Reactor Models. 2003, Forschungszentrum Karlsruhe: Karslruhe. p. 61.
59. **Murdoch, D.K.,Day, C.,Gierszewski, P., *et al.*** Tritium inventory issues for future reactors: choices,
parameters, limits. *Fusion Engineering and Design*, 1999. *46*(2-4), 255–271.
60. **Scaffidi-Argentina, F.,Dalle Donne, M.,Ferrero, C., *et al.*** Helium induced swelling and tritium trapping mechanisms in
irradiated beryllium: a comprehensive approach. *Fusion Engineering and Design*, 1995. *27*, 275 282.
61. **Chakin, V.P.,Posevin, A.O.,Obukhov, A.V., *et al.*** Radiation growth of beryllium. *Journal of Nuclear Materials*, 2009. *386-388*, 206-209.
62. **Snead, L.L.** Low-temperature low-dose neutron irradiation effects on beryllium. *Journal of Nuclear Materials*, 2004. *326*(2-3), 114–124.
63. **Chakin, V.P.,Kazakov, V.A.,Melder, R.R., *et al.*** Effects of neutron irradiation at 70-200 °C in beryllium. *Journal of Nuclear Materials*, 2002. *307-311*(Part 1), 647-652.
64. **Sernyaev, G.A.,Pokrovskiy, A.S.,Bagautdinov, R.M., *et al.*** Swelling, strengthening and embrittlement of beryllium under neutron irradiation to a fluence of 1.72 × 1021 n/cm 2 ( E > 0.85 MeV) at a temperature of 330-350°C. The role of main structure factors. *Journal of Nuclear Materials*, 1996. *233-237*, 891-897.
65. **Tomberlin, T.A.** Beryllium—A Unique Material in Nuclear Applications. in *36th SAMPE International Technical Conference*. 2004. San Diego, California: Society for the Advancement of Material and Process Engineering.
66. **Van Renterghem, W.,Leenaers, A. and Van denBerghe, S.** TEM investigation of long-term annealed highly irradiated beryllium. *Journal of Nuclear Materials*, 2008. *374*(1-2), 54-60.
67. **Kupriyanov, I.B.,Melder, R.R. and Gorokhov, V.A.** The effect of neutron irradiation on beryllium performance. *Fusion Engineering and Design*, 2000. *51-52*, 135–143.
68. **Leenaers, A.,Verpoucke, G.,Pellettieri, A., *et al.*** Microstructure of long-term annealed highly irradiated beryllium. *Journal of Nuclear Materials*, 2008. *372*(2-3), 256-262.
69. **Beeston, J.M.,Longhurst, G.R. and Wallace, R.S.** Mechanical properties of irradiated beryllium. *Journal of Nuclear Materials*, 1992. *195*(1-2), 102-108.
70. **Kaur, R. and Prakash, S.** Isotope effect for hydrogen diffusion in metals. *Journal of Physics F: Metal Physics*, 1982. *12*(7), 1383.
71. **Jones, P.M.S. and Gibson, R.** Hydrogen in beryllium. *Journal of Nuclear Materials*, 1967. *21*(3), 353-354.
72. **Causey, R.A.** Hydrogen isotope retention and recycling in fusion reactor plasma-facing components. *Journal of Nuclear Materials*, 2002. *300*(2-3), 91-117.
73. **Abramov, E.,Riehm, M.P.,Thompson, D.A., *et al.*** Deuterium permeation and diffusion in high-purity beryllium. *Journal of Nuclear Materials*, 1990. *175*(1-2), 90-95.
74. **Cho, S.,Raffray, A.R. and Abdou, M.A.** Modeling of tritium release from beryllium in fusion
blanket applications. *Journal of Nuclear Materials*, 1994. *212-215*, 961-965.
75. **Baldwin, D.L. and Billone, M.C.** Diffusion/ desorption of tritium from irradiated beryllium. *Journal of Nuclear Materials*, 1994. *212-215*, 948-953.

76. **Oberkofler, M.,Reinelt, M. and Linsmeier, C.** Retention and release mechanisms of deuterium implanted into beryllium. *Nuclear Instruments and Methods in Physics Research Section B: Beam Interactions with Materials and Atoms*. *In Press, Corrected Proof*.
77. **Kéroack, D. and Terreault, B.** Laser desorption study of deuterium implanted in beryllium. *Journal of Nuclear Materials*, 1994. *212-215*(Part 2), 1443-1447.
78. **Ganchenkova, M.G.,Borodin, V.A. and Nieminen, R.M.** Hydrogen in beryllium: Solubility, transport, and trapping. *Physical Review B*, 2009. *79*(13), 134101.
79. **Macaulay-Newcombe, R.G.,Thompson, D.A. and Smeltzer, W.W.** Thermal absorption and desorption of deuterium in beryllium and beryllium oxide. *Journal of Nuclear Materials*, 1992. *191-194*(Part 1), 263-267.
80. **Cho, S. and Abdou, M.A.** Analysis of tritium transport in irradiated beryllium. *Fusion Engineering and Design*, 1995. *28*, 265-270
81. **Palmer, A.R.,Roman, D. and Whitfield, H.J.** The diffusion of tritium from irradiated beryllium oxide powders. *Journal of Nuclear Materials*, 1964. *14*, 141-146.
82. **Shimakawa, S.,Sagawa, H.,Kuroda, T., *et al.*** Estimation of the tritium production and inventory in beryllium. *Fusion Engineering and Design*, 1995. *28*(Proceedings of the Third International Symposium on Fusion Nuclear Technolog), 215-219.
83. **Chakin, V.,Moeslang, A.,Kurinskiy, P., *et al.*** Tritium permeation, retention and release properties of beryllium pebbles. *Fusion Engineering and Design*. *In Press, Corrected Proof*.
84. **Tazhibaeva, I.L.,Shestakov, V.P. and Chikhray, E.V.** in *18th Symphosium on Fusion Technology*. 1994. Germany, Karlsruhe.
85. **Ishitsuka, E.,Kawamura, H.,Terai, T., *et al.*** Effects of helium production and radiation damage on tritium release behavior of neutron-irradiated beryllium pebbles. *Journal of Nuclear Materials*, 2000. *283-287*(2), 1401-1404.
86. **Kupriyanov, I.B.,Gorokhov, V.A.,Vlasov, V.V., *et al.*** The effect of helium generation and irradiation temperature

on tritium release from neutron irradiated beryllium. *Journal of Nuclear Materials*, 2004. *329–333*, 809–813.
87. **Scaffidi-Argentina, F.,Dalle Donne, M. and Werle, H.** Tritium and helium release from neutron irradiated beryllium pebbles from the EXOTIC-8 irradiation. *Fusion Engineering and Design*, 2001. *58–59*, 641–645.
88. **Dalle Donne, M.,Scaffidi-Argentina, F.,Ferrero , C., *et al.*** Modelling of swelling and tritium release in irradiated beryllium. *Journal of Nuclear Materials*, 1994. *212-215*, 954-960.
89. **Rabaglino, E.,Hiernaut, J.P.,Ronchi, C., *et al.*** Helium and tritium kinetics in irradiated beryllium pebbles. *Journal of Nuclear Materials*, 2002. *307-311*(Part 2), 1424-1429.
90. **Scaffidi-Argentina, F.,Dalle Donne, M. and Werle, H.** Critical assessment of beryllium pebbles response under neutron irradiation: Mechanical performance and tritium release. *Journal of Nuclear Materials*, 1998. *258-263*, 595-600.
91. **Klepikov, A.K.,Tazhibaeva, I.L.,Shestakov, V.P., *et al.*** Hydrogen release from reactor-irradiated beryllium. *Journal of Nuclear Materials*, 1996. *233-237*(2), 837-840.
92. **Rabaglino, E.,Baruchel, J.,Boller, E., *et al.*** Study by microtomography of 3D porosity networks in irradiated beryllium. *Nuclear Instruments and Methods in Physics Research Section B: Beam Interactions with Materials and Atoms*, 2003. *200*, 352-357.

93. **Pemsler, J.P.,Anderson, R.W. and Rapperport, E.J.**, SOLUBILITY AND DIFFUSION OF GASES IN BERYLLIUM. 1963, TEXTRON INC WEST CONCORD MA NUCLEAR METALS DIV: Ohio.
94. **Patel, B. and Parsons, W.** Operational beryllium handling experience at JET. *Fusion Engineering and Design*, 2003. *69*(1-4), 689-694.
95. **Deksnis, E.B.,Peacock, A.T.,Altmann, H., *et al.*** Beryllium plasma-facing components: JET experience. *Fusion Engineering and Design*, 1997. *37*(4), 515-530.
96. **Thompson, V.,Krivchenkov, Y.,Riccardo, V., *et al.*** Analysis and design of the beryllium tiles for the JET ITER-like wall project. *Fusion Engineering and Design*, 2007. *82*(15-24), 1706-1712.
97. **Loarte, A.,Saibene, G.,Sartori, R., *et al.*** A new look at JET operation with Be as plasma facing material. *Journal of Nuclear Materials*, 2005. *337-339*, 816-820.
98. **Roth, J.,Tsitrone, E.,Loarte, A., *et al.*** Recent analysis of key plasma wall interactions issues for ITER. *Journal of Nuclear Materials*, 2009. *390-391*, 1-9.
99. **Brooks, J.N.,Allain, J.P.,Alman, D.A., *et al.*** Erosion, transport, and tritium codeposition analysis of a beryllium wall tokamak. *Fusion Engineering and Design*, 2005. *72*(4), 363-375.
100. **Pintsuk, G.,Kühnlein, W.,Linke, J., *et al.*** Investigation of tungsten and beryllium behaviour under short transient events. *Fusion Engineering and Design*, 2007. *82*(15-24), 1720-1729.
101. **Pisarev, A.A. and Grachova, M.L.** Plasma-driven accumulation of tritium in beryllium. *Journal of Nuclear Materials*, 1996. *233-237*(Part 2), 1137-1141.
102. **Berardinucci, L.** Modelling of tritium permeation through beryllium as plasma facing material. *Journal of Nuclear Materials*, 1998. *258-263*(1), 777-781.
103. **Gan, Y. and Kamlah, M.** Identification of material parameters of a thermo-mechanical model for pebble beds in fusion blankets. *Fusion Engineering and Design*, 2007. *82*(2), 189-206.
104. **Verzilov, Y.,Ochiai, K.,Klix, A., *et al.*** Non-destructive analysis of impurities in beryllium, affecting evaluation of the tritium breeding ratio. *Journal of Nuclear Materials*, 2004. *329–333*(2), 1337–1341.
105. **Roux, N.,Abassin, J.J.,Briec, M., *et al.*** Compatibility behavior of beryllium with LiAlO2 and Li2ZrO3 ceramics, with 316 L and 1.4914 steels in SIBELIUS. *Journal of Nuclear Materials*, 1992. *191-194*(Part 1), 168-172.
106. **Chakin, V.,Klimenkov, M.,Rolli, R., *et al.*** Microstructural and tritium release examination of titanium beryllides. *Journal of Nuclear Materials*. *In Press, Corrected Proof*.
107. **Haigh, A.D. and Pick, M.A.** Operational aspects of using beryllium—safety and decontamination. *Fusion Engineering and Design*, 1997. *37*, 531–541.
108. **Campbell, D.J.**, Structural Composite Material. 2010, Ohio: ASM International. 612.
109. **Pintsuk, G.,Compan, J.,Koppitz, T., *et al.*** Mechanical and thermo-physical characterization of three-directional carbon fiber composites for W-7X and ITER. *Fusion Engineering and Design*, 2009. *84*(7-11), 1525-1530.
110. **Snead, L.L.,Katoh, Y. and Ozawa, K.** Stability of 3-D carbon fiber composite to high neutron fluence. *Journal of Nuclear Materials*. *In Press, Corrected Proof*.
111. **Snead, L.L.,Burchell, T.D. and Katoh, Y.** Swelling of nuclear graphite and high quality carbon fiber composite under very high irradiation temperature. *Journal of Nuclear Materials*, 2008. *381*(1-2), 55-61.

112. **Wu, C.H.,Bonal, J.P.,Kwast, H., *et al.*** EU results on neutron effects on PFC materials. *Fusion Engineering and Design*, 1998. *39-40*(0), 263-273.
113. **Barabash, V.,Federici, G.,Rödig, M., *et al.*** Neutron irradiation effects on plasma facing materials. *Journal of Nuclear Materials*, 2000. *283-287, Part 1*(0), 138-146.
114. **Tanabe, T.** On the possibility of ITER starting with full carbon. *Fusion Engineering and Design*, 2006. *81*(1-7), 139-147.
115. **Robertson, J.** Diamond-like amorphous carbon. *Materials Science and Engineering: R: Reports*, 2002. *37*(4-6), 129-281.
116. **Jacob, W. and Moller, W.** On the structure of thin hydrocarbon films. *Applied Physics Letters*, 1993. *63*(13), 1771-1773.
117. **Serra Díaz-Cano, L. and Jones, A., P.** Carbonaceous dust in interstellar shock waves: hydrogenated amorphous carbon (a-C:H) vs. graphite. *A&A*, 2008. *492*(1), 127-133.
118. **Jacob, W.** Surface reactions during growth and erosion of hydrocarbon films. *Thin Solid Films*, 1998. *326*(1-2), 1-42.
119. **Smith, F.W.** Optical properties and local atomic bonding in hydrogenated amorphous carbon and silicon-carbon alloys. *Materials Science Forum*, 1991. *52-53*, 323-340.
120. **Roth, J. and et al.** Tritium inventory in ITER plasma-facing materials and tritium removal procedures. *Plasma Physics and Controlled Fusion*, 2008. *50*(10), 103001.
121. **Peacock, A.T.,Andrew, P.A.,Brennan, D., *et al.*** Tritium inventory in the first wall of JET. *Fusion Engineering and Design*, 2000. *49-50*(0), 745-752.
122. **Alves, L.C.,Alves, E.,Barradas, N.P., *et al.*** Surface composition and morphology changes of JET tiles under plasma interactions. *Fusion Engineering and Design*, (0).
123. **Petersson, P.,Bergsåker, H.,Possnert, G., *et al.*** Cross sections of deposited layers investigated by micronuclear reaction analysis. *Journal of Nuclear Materials*, (0).
124. **González de Vicente, S.M.,Uytdenhouwen, I.,Coad, J.P., *et al.*** Surface compositional study of Be and T contaminated CFC tiles from JET. *Journal of Nuclear Materials*. *In Press, Corrected Proof*.
125. **Baldwin, M.J.,Schmid, K.,Doerner, R.P., *et al.*** Composition and hydrogen isotope retention analysis of co-deposited C/Be layers. *Journal of Nuclear Materials*, 2005. *337-339*(0), 590-594.
126. **Linsmeier, C.,Reinelt, M. and Schmid, K.** Surface chemistry of first wall materials – From fundamental data to modeling. *Journal of Nuclear Materials*, (0).
127. **Mercadier, L.,Hermann, J.,Grisolia, C., *et al.*** Analysis of deposited layers on plasma facing components by laser-induced breakdown spectroscopy: Towards ITER tritium inventory diagnostics. *Journal of Nuclear Materials*, (0).
128. **Pardanaud, C.,Giacometti, G.,Martin, C., *et al.*** Raman study of CFC tiles extracted from the toroidal pump limiter of Tore Supra. *Journal of Nuclear Materials*, (0).
129. **Buzhinskij, O.I.,Barsuk, V.A.,Otroshchenko, V.G., *et al.*** The investigation of structure, chemical composition, hydrogen isotope trapping and release processes in deposition layers on graphite sample surfaces exposed to DIII-D divertor plasma in extreme conditions. *Fusion Engineering and Design*, 2002. *61-62*(0), 191-195.
130. **Jacob, W.** Redeposition of hydrocarbon layers in fusion devices. *Journal of Nuclear Materials*, 2005. *337-339*(0), 839-846.
131. **Wright, R.B.,Varma, R. and Gruen, D.M.** Raman scattering and SEM studies of graphite and silicon carbide surfaces bombarded with energetic protons, deuterons and helium ions. *Journal of Nuclear Materials*, 1976. *63*(0), 415-421.
132. **Warrier, M.,Schneider, R.,Salonen, E., *et al.*** Effect of the porous structure of graphite on atomic hydrogen diffusion and inventory. *Nuclear Fusion*, 2007. *47*, 1656-1663.

133. **Kanashenko, S.L.,Gorodetsky, A.E.,Chernikov, V.N., *et al.*** Hydrogen adsorption on and solubility in graphites. *Journal of Nuclear Materials*, 1996. *233-237, Part 2*(0), 1207-1212.
134. **Atsumi, H.** Mechanism of Hydrogen Trapping and Transport in Carbon Materials. *Physica Scripta*, 2007. *2003*(T103), 77.
135. **Kolasinski, R.D.,Umstadter, K.R.,Sharpe, J.P., *et al.*** The impact of specific surface area on the retention of deuterium in carbon fiber composite materials. *Fusion Engineering and Design*, 2009. *84*(2-6), 1068-1071.
136. **Penzhorn, R.D.,Coad, J.P.,Bekris, N., *et al.*** Tritium in plasma facing components. *Fusion Engineering and Design*, 2001. *56-57*(0), 105-116.
137. **Bekris, N.,Skinner, C.H.,Berndt, U., *et al.*** Tritium depth profiles in 2D and 4D CFC tiles from JET and TFTR. *Journal of Nuclear Materials*, 2003. *313-316*, 501-506.
138. **Bekris, N.,Coad, J.P.,Skinner, C.H., *et al.*** Thermal release rate of tritium trapped in bulk and plasma exposed surfaces of carbon specimens obtained from JET divertor. *Journal of Nuclear Materials*, 2007. *367-370*(Part 2), 1254-1259.
139. **Pisarev, A.,Gasparyan, Y.,Rusinov, A., *et al.*** Deuterium thermal desorption from carbon based materials: A comparison of plasma exposure, ion implantation, gas loading, and C-D codeposition. *Journal of Nuclear Materials*. *In Press, Corrected Proof*.
140. **Bohmeyer, W.,Tabares, F.L.,Baudach, M., *et al.*** The scavenger effect – Does it work? *Journal of Nuclear Materials*, 2009. *390-391*(0), 560-563.
141. **Tabarés, F.L.,Ferreira, J.A.,Ramos, A., *et al.*** Tritium control techniques in ITER by ammonia injection. *Journal of Nuclear Materials*, (0).
142. **Perevezentsev, A.N.,Bell, A.C.,Rivkis, L.A., *et al.*** Experimental Trials of Methods for Metal Detritiation for JET. *Fusion Science and Technology*, 2007. *52*(1), 84-99.
143. **Skinner, C.H.,Gentile, C.A.,Carpe, A., *et al.*** Tritium removal from codeposits on carbon tiles by a scanning laser. *Journal of Nuclear Materials*, 2002. *301*(2-3), 98-107.
144. **Widdowson, A.,Coad, J.P.,Farcage, D., *et al.*** Detritiation of JET tiles by laser cleaning. *Fusion Science and Technology*, 2008. *54*(1), 51-54.
145. **Widdowson, A.,Coad, J.P.,Bekris, N., *et al.*** Efficacy of photon cleaning of JET divertor tiles. *Journal of Nuclear Materials*, 2007. *363-365*, 341-345.
146. **Wong, K.Y.,Hircq, B.,Jalbert, R.A., *et al.*** Tritium decontamination of machine components and walls. *Fusion Engineering and Design*, 1991. *16*, 159-172.
147. **Ghirelli, N.,Blet, V. and Gastaldi, O.** Pre-study of a detritiation process for plasma facing components in the ITER hot cells. *Fusion Engineering and Design*, 2009. *84*(2-6), 821-824.
148. **Bekris, N.,Coad, J.P.,Grisolia, C., *et al.*** 555 Fusion Technology related studies at JET: Post-mortem tile analysis with MKII-HD geometry, In situ laser detritiation and Molecular Sieve Bed detritiation. *Journal of Nuclear Materials*. *In Press, Corrected Proof*.
149. **Dinescu, G.,Ionita, E.R.,Luciu, I., *et al.*** Flexible small size radiofrequency plasma torch for Tokamak wall cleaning. *Fusion Engineering and Design*, 2007. *82*(15-24), 2311-2317.
150. **Bekris, N.,Coad, J.P.,Sugiyama, K., *et al.*** Ex-situ tritium removal from JET tiles using RF inductive heating. *Fusion Engineering and Design*, 2008. *83*(7-9), 1137-1141.
151. **Bekris, N.,Skinner, C.H.,Berndt, U., *et al.*** Assessment of the heating technique as a possible ex situ detritiation method for carbon wall materials from fusion machines. *Journal of Nuclear Materials*, 2004. *329-333*(Part 1), 814-819.

152. Fundamentals of Magnetic Field Effects, in *Magneto-Science*, M. Yamaguchi and Tanimoto, Y., Editors. 2006, Springer Berlin Heidelberg. p. 1-40.
153. **Steiner, U.E. and Ulrich, T.** Magnetic field effects in chemical kinetics and related phenomena. *Chemical Reviews*, 1989. *89*(1), 51-147.
154. **Parkinson, J.**, An Introduction to Quantum Spin State, D.J.J. Farnell, Editor. 2010, Springer Link: Berlin, Heidelberg.
155. **Hayashi, H.**, Introduction to Dynamic Spin Chemistry: Magnetic Field Effects upon Chemical and Biochemical Reactions (World Scientific Lecture and Course Notes in Chemistry, Vol. 8). 2004: World Scientific Publishing Company. 268.
156. **Atkins, P.W. and Lambert, T.P.**, The effect of a magnetic field on chemical reactions, in *Annual reports on the progress of chemistry*. 1976. p. 67-88.
157. **Till, U. and Hore, P.J.** Radical pair kinetics in a magnetic field. *Molecular Physics: An International Journal at the Interface Between Chemistry and Physics*, 1997. *90*(2), 289 - 296.
158. **A. Walsh, K.**, Beryllium chemistry and processing, ed. D. L. Olson, E. Vidal, E., Dalder, E., *et al.* 2009, Ohio: ASM International. 575.
159. **Dombrowski, D.E.** Manufacture of beryllium for fusion energy applications. *Fusion Engineering and Design*, 1997. *37*(2), 229-242.
160. **Ishitsuka, E.,Kawamura, H.,Sakamoto, N., *et al.***, Process for preparing metallic beryllium pebbles, U.S. Patent, Editor. 1999, Japan Atomic Energy Research Institute (JP) NGK Insulators, Ltd. (JP) United States. p. 10.
161. **Nishida, K. and Sakamoto, N.**, Metallic Beryllium Pebble, J. Patent, Editor. 1994, NGK INSULATORS LTD Japan.
162. **Rabaglino, E.**, Helium and tritium in neutron-irradiated beryllium, in *Fakultat fur Maschinenbau*. 2004, Univeritat Karlsruhe: Karlsruhe. p. 127.
163. **Fedorov, A.V.,Peeters, M.M. and van der Laan, J.G.**, EXOTIC-8: Tritium Release Measurements in Ceramic Tritium Breeder Materials, A.J.Magielsen, Editor. 2008, NRG: Petten. p. 109.
164. **Rebut, P.-H.** The JET preliminary tritium experiment *Plasma Physics and Controlled Fusion*, 1992. *34*(13), 1749-1758.
165. **Coad, J.P.,Likonen, J.,Rubel, M., *et al.*** Overview of material re-deposition and fuel retention studies at JET with the Gas Box divertor *Nuclear Fusion*, 2006. *46*(2), 350-366.
166. **Tanabe, T.,Sugiyama, K.,Renvall, T., *et al.*** Tritium distribution measurement of JET Mk II SRP divertor tiles. *Journal of Nuclear Materials*, 2007. *363-365*, 960-965.
167. **Jones, T.T.,Brennan, D.,Pearce, R.J.H., *et al.*** Technical and scientific aspects of the JET trace-tritium experimental campaign. *Fusion Science and Technology*, 2005. *48*(1), 250-257.
168. **Webster, D. and Crooks, D.** Creep mechanisms in beryllium. *Metallurgical and Materials Transactions A*, 1976. *7*(8), 1307-1315.
169. **Tiliks, J.,Kizane, G.,Vitins, A., *et al.*** Magnetic Field Effects on Tritium Release from Neutron-Irradiated Beryllium Pebbles. *Nuclear Technology* 2007. *159*(3), 245-249.
170. **Vance, D.E.**, in *Report LA-7716 UC-4*. 1979, University of California, Los Alamos Scientific Laboratory,: Los Alamos, New Mexico, USA. p. 5.
171. **Penzhorn, R.D.,Bekris, N.,Hellriegel, W., *et al.*** Tritium profiles in tiles from the first wall of fusion machines and techniques for their detritiation. *Journal of Nuclear Materials*, 2000. *279*(2-3), 139-152.
172. **Kleykamp, H.** Chemical interactions in the EXOTIC-7 experiment. *Journal of Nuclear Materials*, 1999. *273*(2), 171-176.

173. **Ganchenkova, M.G.,Vladimirov, P.V. and Borodin, V.A.** Vacancies, interstitials and gas atoms in beryllium. *Journal of Nuclear Materials*, 2009. *386–388*, 79-81.
174. **Coad, J.P. and et al.** Carbon Deposition and Hydrogen Isotope Retention in JET. *Physica Scripta*, 1999. *1999*(T81), 7.
175. **Coad, J.P.,Andrew, P.,Erents, S.K., *et al.*** Erosion and deposition in the JET MkII-SRP divertor. *Journal of Nuclear Materials*, 2007. *363-365*, 287-293.
176. **Pennock, G.M.,Taylor, G.H. and Gerald, J.D.F.** Microstructure in a series of mesophase pitch-based fibers from du pont: zones, folds, and disclinations. *Carbon*, 1993. *31*(4), 591-609.
177. **Timothy, D.B.** Radiation damage in carbon–carbon composites: structure and property effects. *Physica Scripta*, 1996. *1996*(T64), 17.
178. **Munsat, T.**, High-Temperature Carbon-Irradiation Issues for the Sombrero ICF Reactor, in *Other Information: PBD: 1 Oct 1999*. 1999. p. Medium: ED; Size: 521 Kilobytes pages.
179. **Popovichev, S.**, Personal communication. 2010: Culham, EFDA JET Team.

# APPENDIX